Investigation of the expression and immunogenicity of *Mycobacterium tuberculosis* Rv1460

by

Lucinda Baatjies

Dissertation presented for the degree of Doctor of Philosophy (Molecular Biology) in the Faculty of Medicine and Health Sciences at Stellenbosch University

Supervisor: Dr Monique Joy Williams

Co-supervisor: Dr André Gareth Loxton

March 2021

Declaration

By submitting this dissertation electronically, I declare that the entirety of the work contained therein is my own, original work, that I am the sole author thereof (save to the extent explicitly otherwise stated), that reproduction and publication thereof by Stellenbosch University will not infringe any third-party rights and that I have not previously in its entirety or in part submitted it for obtaining any qualification.

Lucinda Baatjies

March 2021

Abstract

A challenge that has plagued humanity for centuries is the intracellular pathogen *Mycobacterium tuberculosis* (Mtb), the causative agent of tuberculosis. In 2018, over 9.6 million individuals fell ill with the disease and 1.5 million lost their lives. Not all infected individuals get sick, 95% remain healthy (asymptomatic) and are said to be latently infected. Only 3-10% of infected individuals develop tuberculosis (TB).

The shortcomings of current immunodiagnostics include the failure to detect progression from latent infection to active tuberculosis disease, and the inability to monitor treatment efficacy. This highlights the need for new tuberculosis biomarkers. These biomarkers should be highly sensitive and specific diagnosing TB infection, specifically distinguishing between latent infection and active disease. One strategy to identify Mtb antigens with diagnostic potential is to identify genes that are specifically induced during infection or in specific disease stages.

Despite the importance of iron homeostasis during TB infection, the utility of bacterial antigens expressed during the iron limitation experienced by Mtb within the host remains largely unexplored. The *Rv1460* gene encodes a transcriptional regulator of the *Rv1460-Rv1461-Rv1462-Rv1463-csd-Rv1465-Rv1466* mobilization of sulphur (SUF) operon, which encodes the primary iron-sulphur biogenesis system in Mtb. The SUF operon is induced during iron limitation and intracellular growth of Mtb, pointing to its importance during infection.

This study therefore aimed to investigate the level of the Rv1460 protein during intracellular growth of Mtb, and to gain insight into the regulation involved in determining these levels. Furthermore, since Rv1460 levels are predicted to be elevated during intracellular growth and infection, we hypothesize that it is immunogenic and may induce an immune response in individuals infected with Mtb that has diagnostic potential.

To facilitate rapid monitoring of *Rv1460* expression at the single cell level during intracellular growth we sought to develop a fluorescent reporter for monitoring its expression. Two fluorescent reporter vectors were constructed by cloning two *Rv1460* promoter regions (123 bp and 211 bp) upstream of a promoterless *mCherry* gene and transforming Mtb H37Rv with the resulting vector constructs.

The expression of the mCherry protein had no effect on the growth of the fluorescent strains when compared to the wild type (wt) control. Florescence per cell was determined either by dividing fluorescence determined in a plate reader by colony forming units per well i.e., Relative fluorescent units (RFU)/Colony forming units (CFU) or by flow cytometry. The RFU/CFU measurements showed more than a 10x increase between day 4 and 10 for H37Rv *attB*::pMV306 (control strain), H37Rv *attB*::pMV306_123mCherry and H37Rv *attB*::pMV306_211mCherry (fluorescent reporter strains), while values remained constant between day 10 and 14. Flow cytometry showed no increase in fluorescence between day 4, 10 and 14 for the two reporter strains. The high background fluorescence observed in the control strain for the RFU/CFU measurements suggests that the increase observed between day 4 and 10 was due to autofluorescence of the cells or background fluorescence in the media. An increase in the *Rv1460* transcript was observed between day 4 and 10, while between day 10 and 14 the transcript levels decreased. The *mCherry* transcript was significantly lower than the *Rv1460* transcript and the ratio of the two transcripts did not remain constant in either strain over time. This suggests that the mCherry reporters did not accurately reflect changes in *Rv1460* transcript levels over time. Monitoring fluorescence in the reporter strains during intracellular growth suggests that *Rv1460* expression is induced in a subset of bacteria within macrophages, and this population increases over the course of a 72-hour infection.

Rv1460 protein does not seem to be highly immunogenic under the conditions tested. Higher levels of Interleukin (IL)-8 (p = 0.08) and Matrix metallopeptidase (MMP)-9 (p = 0.00) was measured in the active TB group when compared to the Quantiferon (QFN) negative (neg) group for the short-term stimulation (12 hours) with Rv1460 suggestive of an effector or memory response. Short-term stimulation for all stimulation conditions showed significantly lower levels of Regulated and normal T cell expressed and secreted (RANTES) in the active TB group when compared to QFN positive (pos) and QFN neg groups. This cytokine selectively attracts monocyte/macrophages in the airways and strongly induces migration of T cells with the memory phenotype.

Opsomming

‘n Uitdaging wat die mensdom al vir eeue teister is die intrasellulêre patogeen *Mycobacterium tuberculosis*, die bakterieë wat tuberkulose (TB) veroorsaak. In 2018 het meer as 9.6 miljoen individue tuberkulose opgedoen en 1.5 miljoen het hulle lewens as gevolg daarvan verloor. Nie alle individue wat met met die bakterium besmet is raak siek nie, 95% van besmette individue bly gesond (asimptomaties) en word beskryf as latente infeksie. Slegs 3-10% van die wat met die bakterium besmet is ontwikkel TB.

Die tekortkominge van huidige immunodiagnostieke tegnieke sluit in mislukte pogings om vordering van latente infeksie na aktiewe TB siekte te voorspel en die onvermoeë om die doeltreffenheid van behandeling vastestel. Hierdie gebreke beklemtoon die behoefte aan nuwe TB biomerkers. Hierdie biomerkers moet hoog sensitief en baie spesifiek vir die diagnosering van TB infeksie wees, en moet spesifiek tussen latente infeksie en aktiewe siekte kan onderskei. Een strategie wat gebruik kan word is om *M. tuberculosis* antigene met diagnostiese potensiaal te identifiseer. Die wat tydens die uitdrukking van spefieke gene gedurende infeksie en spesifieke siekte fases uitgedruk word. Ondanks die belangrikheid van yster homeostase tydens TB-infeksie, is die gebruik van bakteriële antigene wat die bakterium tydens yster beperkings in die gasheer ervaar grootliks onder bestudeer. Die *Rv1460* geen kodeer ‘n transkripsionele reguleerder van die *Rv1460-Rv1461-Rv1462-Rv1463-csd-Rv1465-Rv1466* (*SUF*) operon, wat die primêre yster-swawel (Fe-S) biogenese stelsel in *M. tuberculosis* is. Die SUF-operon word geïnduseer tydens yster beperkings en intrasellulêre groei van *M. tuberculosis*, wat daarop dui dat dit belangrik is tydens infeksie.

Met hierdie studie het ons be-oog om die vlakke van Rv1460 proteïen tydens intrasellulêre groei van *M. tuberculosis* te ondersoek, en om insig te verkry van die regulering van die proteïen en bepaling van proteïen vlakke. Aangesien daar voorpel word day die Rv1460-vlakke verhoog sal word tydens intrasellulêre groeie en infeksie, reken ons dat dit immunogenies is en ‘n immuunrespons kan veroorsaak by individue wat met *M. tuberculosis* besmet is, end dat dit diagnostiese potensiaal het.

In ‘n poging om die Rv1460-uitdrukking op enkel sel vlak tydens intrasellulêre groei vastestel, het ons ‘n fluoressensie verslaggewende proteïen ontwikkel om uitdrukking vas te stel. Twee fluoressensie vektore is gekonstrueer deur twee Rv1460-promotor gebiede (123 en 211 bp) stroomop van ‘n promotorlose mCherry geen te kloon en *M. tuberculosis* H37Rv met die resulterende vektore konstrukte te transformeer.

Die uitdrukking van die mCherry proteïen in die fluoresserende stamme het geen effek op die groei van die fluoresserende bakteriële stamme gehad nie in vergelyking met die wt-kontrole stamme Fluoressensie per sel is bepaal deur die fluoressensie wat deur ‘n plaatleser of vloei-sitometrie bepaal was deur die kolonie vormerende eenhede per putjie (RFU/CFU) te deel. Die RFU/CFU lesings het meer as ‘n 10x toename getoon tussen dag 4 en 10 vir for H37Rv *attB*::pMV306 (kontrole stam), H37Rv *attB*::pMV306_123mCherry and H37Rv *attB*::pMV306_211mCherry (fluoresserende stamme), terwyl die waardes konstant gebly het tuseen dag 10 en 14. Vloei-sitometrie het geen toename in fluoressensie getoon tussen dag 4, 10 en 14 vir die twee fluoresserende stamme nie. Die hoë agterground fluoressensie (RFU/CFU lesings) wat waargeneem is tussen dag 4 en 10 in die kontrole stamme kan toegeskryf word aan die outofluoresensie van die sel of agterground fluoressensie van die media. ‘n Toename in die *Rv1460*-transkripsie vlakke was waargeneem tussen dag 4 en 10, terwyl ‘n afname tussen dag 10 en 14 waargeneem was. Die *mCherry* transkripsie vlakke was aansienlik laer as die *Rv1460* transkripsie vlakke en die verhouding van die twee transkripsie vlakke het gewissel met tyd. Dit dui daarop dat die mCherry verslaggewende proteïen nie die *Rv1460* veranderinge oortyd akkuraat weerspieël nie. Fluoressensie bepalings tydens intrasellulêre groeie dui daarop dat ‘n seker populasie bakterieë in die makrofage *Rv1460* uitdruk en dat hierdie populasie toeneem oor die 72-uur infeksie periode.

Rv1460 proteiën blyk nie om hoogs immunogenies te wees onder die toestande waarin dit getoets was nie. Hoër vlakke van IL-8 (p = 0.08) and MMP-9 (p = 0.00) was gemeet in die aktiewe TB group in vergelyking met die QFN negatiewe groep vir die kortermyn Rv1460 stimulasie (12 ure). Kortemyn stimulaie, vir al die stimulaie kondisies gee aansienlike laer vlakke van RANTES in die aktiewe TB groep in vergelyking met die QFN positiewe en QFN negatiewe groepe. RANTES het ‘n selektiese aksie as monosiet/makrofaag lokmiddel in die lugweë wat die migrasie van T selle met ‘n geheue fenotiepe induseer.

Acknowledgements

I like would like to extend humbly and sincerely a big thank you to the following persons:

First and foremost, my Lord and Saviour, Jesus Christ without whom I can do nothing.

My supervisor, Dr Monique Williams, who has patiently equipped me in preparation for this PhD journey. When the preparation was over, you guided me on this journey, pursuing my PhD. Thank you.

My co-supervisor, Dr Andrè Loxton for all your help and support, who without wavering accepted the challenge of helping to steer me on this path.

Dr Danicke Willemse, for all your help, you are such a selfless person. May you enrich the lives of all those life puts on your path.

The Fe-S cluster group: Monique Williams, Danicke Willemse, Jessie Arries, Nandi Niemand, Tsaone Tamuhla, Magongwane Ndlozi, and Mischke Nicolaai, thank you for being a part of my journey.

Dr Nasiema Allie, Dr Danicke Willemse, and Dr Monique Williams for helping me with my Biosafety level-3 training and competency.

All the participants in this PhD project, a heartfelt thank you.

All the participant recruiters of SCREEN TB and BARTB and clinical staff for helping me get the clinical samples, without which the immunological arm of the project would not have been possible.

Dr Fanie Malherbe, Dr Andriette Hiemstra, Dr Elouise Kroon, Sr Shirley McAnda and Sr Charmaine Abrahams, thank you.

Prof Grant Theron, for your willingness to help me when I needed your help.

Zaida Palmer for going out of your way to help me getting the clinical samples. Raymond Fredericks, thank you.

Andrea Gutschmidt, you were such a great help, cutting no corners with your flow cytometry training.

Candice Snyders, thank you for your help with my Luminex results, not forgetting Ilana van Rensburg for your help.

Devon Allies, Vinzeigh Leukes, Kennedy Zvinairo and Thandokazi May for training me to work in the SUN-IRG labs.

Ray-Dean Petersen thank you for your support and help with the LightCycler 96.

Dr Jomien Mouton, for your help with the THP-1 infection study and providing me with the *Mycobacterim smegmatis* pCherry plasmid and your advice.

Dr Sven Parsons for transporting my RNA samples to CPGR.

Prof Paul van Helden, whom without refrain allowed me to do this PhD.

Prof Rob Warren who further supported me and developed me during this PhD period.

Candice Minnaar, Tienie Petersen Shahied Taliep, Porchè Fortuin and Leilani Abrahams, for sharing your space and those much-needed small talks.

My Christian brothers and sisters who kept me in your prayers.

My mother for your love and prayers, you are indeed a pillar of strength.

My husband Gerreth, for all your love. For never complaining, but always supporting me. My two sons, Ronin and Caleb, you are and always will be my inspiration. It is in leading you that my every move becomes calculated steps.

Trudy Snyders, Dr Liezel Smith, Dr Jennifer Jackson and Rika van Dyk for your administrative help.

Finally, The SAMRC and DST/NRF Centre of Excellence for Biomedical Tuberculosis Research without whom this PhD would not have been possible.

Table of Content

List of Figures

List of Tables

List of Abbreviations

AFB:	Acid-fast bacilli
AIDS:	Acquired immunodeficiency syndrome
Amp:	Ampicillin
A2M:	Alpha-2-Macroglobulin
ApoA1:	Apolipoprotein-A1
AUCS:	Areas under the curve
BCG:	Bacillus Calmette-Guèrin
bfrA:	Bacterioferritin
bfrB:	Ferritin like protein
BSA:	Bovine serum albumin fraction V
BTLA:	B- and T-lymphocyte attenuator
CAF:	Central Analytical Facilities
CFH:	Complement factor H
CI:	Confidence interval
COPD:	Chronic obstructive pulmonary disease
COR:	Correlate of risk
Covid-19:	Coronavirus disease 2019
CoVs:	Coronavirus
CFP-10:	Culture filtrate protein 10 kDa
CFUs:	Colony forming units
CRP:	C reactive protein
CTLA-4:	Cytotoxic T-lymphocyte-associated protein 4
DM:	Diabetes mellitus
DM2:	Diabetes mellitus 2
DMSO:	Dimethyl sulfoxide

DosR:	dormancy survival regulator
ELISA:	Enzyme-linked immunosorbent assay
EPTB:	Extrapulmonary TB
ESAT-6:	Early secreted antigenic target 6 kDa
EtBr:	Ethidium bromide
FASLG:	Fas ligand
FBS:	Fetal Bovine Serum
Fe-S:	Iron-sulphur cluster
FI:	Fluorescence intensity
HBC:	High burden countries
HBHA:	Heparin-binding hemagglutinin
HHCs:	Household contacts
HIV:	Human immunodeficiency virus
HREC:	Human Research Ethics Committee
Hyg:	Hygromycin
IdeR:	Iron-dependant regulator
IFN-g:	Interferon-gamma
IP-10:	Interferon-inducible protein-10
IGRA:	Interferon gamma release assay
IL-1Ra:	Interleukin-1 receptor antagonist
IL5RA:	Interleukin 5 Receptor Subunit Alpha
IL-6:	Interleukin-6
IL-8:	Interleukin-8
IL-10:	Interleukin-10
IL-12(p40)	Interleukin-12(p40)
IL-12(p70)	Interleukin-12(p70)

ISGAM:	Iron-starved growth-arrested Mtb
LAG-3:	Lymphocyte-activation gene 3
LPA:	Lymphocyte proliferation assay
LTBI:	Latent TB infection
MCP-1:	Monocyte chemotactic protein-1
MDR-TB:	Multi-drug resistant TB
MERS-CoV:	Middle East respiratory syndrome coronavirus
MFI:	Median fluorescent intensity
MIP-1b:	Macrophage inflammatory protein-1b
MOI:	Multiplicity of infection
MMP-9:	Matrix metallopeptidase-9
Mtb*:*	*Mycobacterium tuberculosis*
NaCl:	Sodium chloride
NaHep:	Sodium Heparin
NIC:	not infected controls
NTMs:	Non-tuberculous mycobacteria
OD_{600}:	Optical density at 600nm
PBMCs:	Peripheral blood mononuclear cell
PBS:	Phosphate buffered saline
PCR:	polymerase chain reaction
PD-1:	Programmed cell death protein 1
PHA:	Phytohaemagglutinin
PMA:	Phorbol 12-myristate 13-acetate
PPD:	Intradermal purified protein derivative
QFN neg:	QuantiFERON negative

QFN pos:	QuantiFERON positive
RANTES:	Regulated and normal T cell expressed and secreted
RD-1:	Region of difference-1
RFU:	Relative fluorescence units
Rpfs:	Resuscitation promoting factors
RT-PCR:	Real-time polymerase chain reaction
RT-qPCR:	Quantitative reverse transcriptase PCR
ROC:	Receiver operating characteristics
RT:	Room temperature
SAA:	Serum amyloid A
SARS:	Severe acute respiratory syndrome
SARS-CoV-1:	Severe acute respiratory syndrome coronavirus 1
SARS-CoV-2:	Severe acute respiratory syndrome coronavirus 2
SDS-PAGE:	Sodium dodecyl sulfate polyacrylamide gel electrophoresis
SUF:	Mobilization of sulphur
TB:	Tuberculosis
TBDM:	Tuberculosis and diabetes mellitus
TIM-3:	T-cell immunoglobulin and mucin domain-3
TNF-a:	Tumor necrosis factor-alpha
TST:	Tuberculin test
TPA:	Tissue plasminogen activator
U:	Units
Un:	Unstimulated
VEGF:	Vascular endothelial growth factor
WB:	Whole blood
WBA:	Whole blood assay

WCL:	Whole cell lysates
WHO:	World Health Organization
Wt:	wild type
XDR:	extensive drug resistance

Chapter 1: Literature review

The current tuberculosis diagnostic paradigm

A significant event in the history of medicine and a major event in our understanding of the deadly disease tuberculosis (TB), was the discovery of the tubercle bacillus by Robert Koch in 1882 (1). Killing 1.2 billion people over the last 200 years, TB is ranked as one of the high ranking causes of death from a single infectious microorganism (above human immunodeficiency virus (HIV)/ acquired immunodeficiency syndrome (AIDS)) (2, 3). Tuberculosis is a major cause of poor health even in the 20th century. In 2018, an estimate of 9.6 million people fell ill with TB and 1.5 million people died from the disease according to the World Health Organization (WHO) (3). The causative agent of the disease is an obligate pathogen called *Mycobacterium tuberculosis* (Mtb) (4). Mtb is a member of the slow growing (12 to 24 hour doubling rate) pathogenic Mycobacteria (*Mycobacteriaceae)*, which are rod-shaped, gram-positive, acid-fast bacteria with G-C rich (62–70%) genomes (4–6). This intracellular pathogen has been successful in plaguing humanity over centuries spreading through infected individuals with active TB, who transmit the bacilli by generating aerosolized droplets through coughing, sneezing or speaking (7, 8). Although, the infectious dose is still unclear, reports range between 1 and 200 bacilli, with a single aerosol droplet containing anywhere from 1 to 400 bacilli (5). These droplets are inhaled by close contacts and reach alveolar spaces, where they infect alveolar macrophages (2, 8).

The asymptomatic nature of TB infection and the fact that it does not always progress towards disease contribute to its elusiveness (2). In individuals in whom the host immune response contains the infection, Mtb has the ability to establish a latent TB infection (LTBI) allowing long persistence of viable bacilli in the host (9, 10). Ninety to ninety-five percent of infected individuals remain healthy (asymptomatic) and are said to be latently infected (8). The WHO defines LTBI as a state of persistent immune response to stimulation by Mtb antigens without evidence of clinically manifested active TB (11). Over 2 billion people are estimated to be latently infected with Mtb whereby between 3-10% of all LTBI individuals develop disease during their lifespan (12). LTBI individuals is represent a long-lived pool from which active TB disease will continue to develop (13, 14). The risk of developing active disease decreases exponentially overtime, the first 2 years after infection being crucial with 80% chance of developing TB (2).

A further urgent and difficult challenge facing global TB control was the onset and continuing spread of multi drug resistant Mtb strains. Multi-drug resistant TB (MDR-TB) is defined as infection with an Mtb strain that is resistance to, at least, rifampicin and isoniazid (recommended first-line therapeutic regimen). While, extensive drug resistance (XDR) is resistance to rifampicin and isoniazid, any fluoroquinolone, and at least one of three second-line injectable drugs (capreomycin, kanamycin, and amikacin), in addition to multidrug resistance (15). In 2017, drug-resistant TB accounted for an estimated 558 000 cases and 230 000 deaths of which 82% of these were multidrug-resistant cases (16). Alarmingly, more than a third of the MDR cases were not enrolled for MDR treatment, with this percentage approaching two-thirds in some areas in Asia and Africa (2). The American Lung association, Research and Health Education reported in April 2013 that in Africa and South-East Asia TB deaths, prevalence and incidence are two times higher than other world regions, with the exception of the Eastern Mediterranean (17).

The first sign of TB infection is clinical symptoms, which are often non-specific and misleading (18, 19). The innocuous or asymptomatic nature of TB infection delays diagnosis, which greatly contributes to TB morbidity and mortality (2). Failure to recognise the symptoms may delay TB patients seeking medical care, delaying diagnosis and treatment, and increasing the risk of infecting others (20). More than 60% of patients delay their first visit to a medical provider for more than 30 days following becoming symptomatic (21). Delay in diagnosis and treatment of active TB may lead to transmission and increase the morbidity and mortality of the disease (22). An untreated infectious person can spread the disease by infecting between 10 and 15 people every year (23).

The most important and common criteria for confirming TB diagnosis are acid-fast bacilli (AFB) in sputum smears, radiographic signs, physiological symptoms and risk factors or a combination of these (19). The current diagnostic tools for TB have several limitations. The gold standard for the diagnosis of TB is the detection of Mtb in human specimens by microbiological culture. Microbiological culture has a high sensitivity for detecting Mtb but analysis is lengthy, with up to 2 to 6 weeks for interpretation. Sputum smear microscopy is an inexpensive tool, which is rapid and simple for diagnosing pulmonary TB, however it has low and variable sensitivity when the bacillary load is low. Chest x-rays are also used in diagnosis, but can present with atypical radiological findings that are indistinguishable from community –acquired pneumonia (22). The intradermal purified protein derivative (PPD) test or tuberculin test (TST), which detects an immune response to bacterial proteins, is limited by

the fact that it is not Mtb-specific, since it shares Mtb antigens with other mycobacterial strains (24). In TB endemic settings, new-borns are vaccinated with Bacillus Calmette-Guèrin (BCG) to protect children from developing severe disseminated TB (miliary TB), and this complicates TST interpretation since BCG-vaccinated individuals can give false positive results (25). Another logistical limitation of the TST test is that a second patient visit is required to evaluate the test results (26). The interferon gamma release assay (IGRA) measures the levels of interferon-gamma (IFN-g) released from T-lymphocytes after *in vitro* stimulation with the Mtb-specific antigens, early secreted antigenic target 6 kDa (ESAT-6; Rv3875), and culture filtrate protein 10 kDa (CFP-10; Rv3874) (26,27). It has the advantage over TST in that uses antigens in the region of difference-1 (RD-1), found only in Mtb, thereby erasing cross-reactivity with the BCG vaccine strain. IGRA as diagnostic tool however fails to differentiate between LTBI and active TB and has limited predictive value, failing to identify individuals at risk of progressing to active TB (11, 28, 29).

Sputum-based TB diagnostic tests are limited when the mycobacterial load is low, when the site of infection is not easily accessible, or when patients fail to produce a sputum sample (7). These limitations result in reduced success in identifying individuals at risk for developing extrapulmonary TB (EPTB), pediatric TB and people living with HIV, and therefore non-sputum-based test are important for diagnosing TB in these populations (30). The most recent and widely implemented new diagnostic test, namely the GeneXpert MTB/RIF, has revolutionised the diagnosis of TB. GeneXpert detects 75% of smear negative pulmonary TB cases, as well as rifampicin resistance with results within 2 hours. Although GeneXpert MTB/RIF improves TB case detection, two recent randomised trials in Southern Africa suggest that on its own, GeneXpert may not be able to significantly reduce tuberculosis-related morbidity and mortality (31). Xpert MTB/RIF is an automated molecular test, using real-time polymerase chain reaction (PCR) to amplify the rpoB gene (Mtb specific sequence), and probe it with molecular beacons for mutations within the rifampicin resistance determining region of the gene (32).

The effect of risk factors and co-morbidities on the TB disease burden

The response of the host immune system to Mtb infection determines the outcome of active TB progression. The infected host may rapidly progress to active TB disease or infection may be contained by host defences, resulting in LTBI (33, 34). There are several risk factors that influence the outcome of Mtb infection, including tobacco smoking, alcohol abuse, vitamin D

deficiency, malnutrition, overcrowding, poor socioeconomic status, immune-suppressive drugs and diabetes mellitus (DM) and HIV infection (35, 36).

The risk factor most associated with developing TB disease in high burden countries (HBC) is HIV infection. Both Mtb and HIV rely on host cellular immunity that is gradually destroyed in HIV infection (36, 37). HIV infection comes with several immunological defects, including depletion of CD4+ T cells, impaired T cell proliferation and cytokine expression, decreased cytolytic T cell ability to kill the virus and impaired ability to kill the intracellular pathogen Mtb (34). The immunocompromised state resulting from HIV infection increases the chance to either development of active TB after infection or reactivation of latent infection. In addition, Mtb can also enhance viral replication (33, 37, 38).

TB patients with DM comorbidity (TBDM) has become a major public health problem as confirmed by various studies conducted worldwide (39). DM does not only increase the risk of TB but also gives rise to unfavourable treatment outcome (40). Type 2 diabetes mellitus (DM2) causes a threefold increased risk to progress to TB disease, and it worsens TB disease outcome and risk for death, as increased failure on standard TB treatment occurs. It is proposed that the ability of DM2 patient's macrophages and lymphocytes to contain Mtb may be affected by hyperglycemia and cellular insulinopenia (23, 28).

Patients with chronic obstructive pulmonary disease (COPD) have a higher risk of developing TB and succumbing to the disease when compared with TB patients without this comorbidity. The likely underlying mechanism linking COPD and TB is altered immune responses (41). Pulmonary TB patients with helminth infections present with severe radiological findings and reduced peripheral T-cell frequencies. Increased Tregs and Th2 responses in asymptomatic helminth infected individuals has shown lower rate of sputum smear positivity (37).

A major cause for recurrent TB disease in hyperendemic settings is reinfection. A study by Verver *et al* (2005) concluded that the individuals that are at higher risk for developing TB from reinfection are those who have been treated successfully rather than the general population (42). Uys *et al* (2015) showed that patients were at great risk of becoming re-infected during the initial months after cure (43). Patients with previously treated TB have a higher risk of harbouring drug-resistant strains, and at times require more complex laboratory investigations to diagnose TB disease. A better understanding of the prevalence of drug-resistant strains in previously treated patients will enhance diagnosis and treatment (44).

Could the contagious novel severe acute respiratory syndrome coronavirus 2 (SARS-CoV-2), be the newest threat against the fight against TB? SARS-CoV-2 virus is responsible for the coronavirus disease 2019 (Covid-19), first identified in Wuhan (Hubei, China) in December of 2019 (45). On January 30th, 2020, the WHO declared COVID-19 a public health emergency of international concern, and on March 11th , WHO Director General referred to COVID-19 as a pandemic (45, 46). (CoVs) belong to the family Coronaviridae, they are enveloped viruses with the largest genome (26 to 32 kilobases (kb)) amongst RNA viruses and have a crown-like morphology (47–49). In the past two decades coronaviruses have caused three epidemics, the severe acute respiratory syndrome (SARS) coronavirus (SARSCoV-1) that led to a global epidemic in 2002, the Middle-East respiratory syndrome coronavirus (MERS-CoV), which was discovered in 2012, and most recently the novel coronavirus (SARS-CoV-2), identified in December 2019 (50). The novel SARS-CoV-2 rapidly spreads among humans through respiratory droplets or contaminated surfaces. Incubation periods vary between 1 to 14 days (45), and a wide spectrum of clinical manifestations have been observed, with high case-fatality rates in the elderly and patients with comorbidities (50, 51). A case-control study done by Lui *et al* (2020) looked at 36 Covid-19 cases from Shenyang, China to study the relationship between Mtb infection and COVID-19 pneumonia. Although validation in a larger study is required, the results suggests that Mtb infection likely increases susceptibility to SARS-CoV-2, and increases COVID-19 severity (47). Associations between TB and SARS-CoV1 and MERS-CoV coinfection were reported during outbreaks in 2003 and 2012, respectively. Some patients contracted TB after recovery from viral infection, where others had pulmonary TB followed by viral infection (52). The evidence of the effect of Covid-19 as risk factor for TB disease seems limited at present. Due to large scale disruptions to health systems during the pandemic, the greatest effect in the short term is likely to be diagnostic delay, increased transmission, and interrupted drug supply (53).

Advances in *Mycobacterium tuberculosis* biomarker research and why they are not good enough

It is evident that new approaches to control TB are desperately needed. There is a need for the development of highly sensitive and specific diagnostic tests for the identification of TB infection, specifically for distinguishing between latent and active disease (54). Biomarkers are unique indicators of biological processes, and in the case of infectious diseases they are

indicators of the immune response that are used as surrogates of infection, disease progression or cure (55). Researchers can now quantify multiple cytokines and chemokines with the simple and rapid bead-based multiplex assay (29). Using multiplex assays, host immune biomarkers have been studied for their use in TB diagnosis in samples that are easy to access, such as peripheral blood, saliva, or urine (56). Differential expression of immunological markers by the host in response to Mtb infection may enable us to distinguish the stages of TB infection and disease (57). The following sections discuss biomarker studies, with a focus on host biomarkers that can differentiate between stages of Mtb infection and monitoring of disease progression, and Mtb antigens with the potential to differentiate between the different stages of TB infection.

The impact of geographical location on diagnostic assay and vaccine development

In host biomarker research a key parameter to be considered is the geographic location of the study cohort, since diverse geographical locations are linked with exposure to distinct microorganisms and BCG vaccination strains (58).

The BCG vaccine is currently the only licensed vaccine to protect against TB which is included in the childhood vaccination program of several countries. The vaccine seems to be highly effective at preventing disseminated disease in childhood, however with controversial efficacies in pulmonary TB ranging from 0 to 80% (59–61). BCG vaccine strains have undergone some genetic changes overtime contributing to divergent vaccine formulations. This evolutionary process has complicated the task of determining the clear difference of protective efficacy between them (62, 63). The vaccine strain and genotype may influence the protective effectiveness of BCG against Mtb (64).

Some studies suggest that exposure to non-tuberculous mycobacteria (NTMs) in the environment may contribute to the variability of BCG efficacy, suggesting that populations where BCG is less effective are exposed to high levels of NTM. (65). Non-tuberculous mycobacteria are a geographically heterogeneous group of environmental bacteria implicated in a broad range of diseases including TB-like pulmonary and extrapulmonary disease, cervical lymphadenitis in young children, and visceral and disseminated disease (66, 67). NTMs are defined as mycobacteria other than the Mtb complex or organisms causing leprosy, and include over 170 different species which vary in their ability to cause disease (67). Species isolated from humans are widely distributed in the environment, and they infect humans through contaminated water, soil, and fomites. NTMs are more prevalent in hot than

cold climates and the distribution of species varies geographically (65, 67, 68). Prior exposure to NTMs may have reduced the effectiveness BCG vaccine and it may contribute to the geographical variation in vaccine efficacy (68).

Host biomarkers that differentiate between the different stages of *Mycobacterium tuberculosis* infection and monitor disease progression

IFN-g, a pro-inflammatory cytokine and key macrophage-activating cytokine, is essential in mediating protection against Mtb infection by coordinating many distinct cellular programs and signalling events (69, 70). Two commercial IGRAs, the QuantiFERON-TB Gold In-Tube (QFT) assay (Cellestis/Qiagen, Carnegie, Australia) and the T-SPOT.TB assay (Oxford Immunotec, Abingdon, United Kingdom), were developed to discriminate between BCG vaccination and Mtb infection by stimulating with peptides from ESAT-6 and CFP-10, which are not present in BCG (71, 72).

Stimulating whole blood with Mtb specific antigens causes the release of several host cytokines and chemokines. Several studies have sought to identify other cytokines and chemokines that might better discriminate between LTBI and active TB disease (73). Chegou *et al* (2012), showed stimulation of whole blood cells from TB patients and household contacts (HHCs) with Mtb infection phase-dependent antigens resulted in an increase in multiple host markers other than IFN-g. The diagnostic candidates that diagnosed TB disease in patients with an accuracy of 100% with 95% confidence interval (CI) for the area under the receiver operating characteristics (AUC) plots were interleukin (IL)-12(p40), interferon-inducible protein (IP)-10, interleukin (IL)-10 and tumor necrosis factor-alpha (TNF-a) following stimulation with Rv0081; a Mtb protein in the dormancy survival regulator (DosR) regulon (73). Using a training sample set (n = 491) Chegou *et al* (2016) identified a seven-serum host protein biosignature (C reactive protein (CRP), transthyretin, IFN-g, complement factor H (CFH), apolipoprotein-A1 (ApoA1), IP-10 and serum amyloid A (SAA)) that could diagnose TB disease. In a test set (n = 210), the signature had a sensitivity of 93.8% (95% CI 84.0% to 98.0%), specificity of 73.3% (95% CI 65.2% to 80.1%), and positive and negative predictive values of 60.6% (95% CI 50.3% to 70.1%) and 96.4% (95% CI 90.5% to 98.8%), respectively, irrespective of HIV infection status or ethnicity. Future prospects include development into a field-friendly point-of-care test for TB using this signature (74). Wang *et al* (2018) identified a six-cytokine biosignature that identified TB infected (both active and LTBI) individuals. In the screening group (n = 88) IFN-g, IP-10, and interleukin-1 receptor

antagonist (IL-1Ra) were identified following stimulation with ESAT-6/CFP-10, while IP-10, vascular endothelial growth factor (VEGF), and interleukin (IL)-12(p70) were measure in unstimulated samples. Validation of the six-cytokine biosignature in a biomarker validation cohort (n = 216) showed a sensitivity of 88.2% and specificity of 92.1% and in a clinical validation cohort (n = 194) a sensitivity of 85.7%, a specificity of 91.3% with an accuracy of 88.7% (75).

Transcriptional profiling of blood cells from TB, healthy uninfected and/or LTBI individuals has also shown promise in identifying TB biomarkers (76). A study by Zak *et al* (2016) identified a 16-gene blood transcriptional correlate of risk (COR) signature. The signature predicted the risk of progression to TB in HIV-negative South African adolescents with LTBI with a sensitivity and specificity of 66.1% and 80.6% (with a 95% CI 63.2 – 68.9% and 7.2 – 82.0%, respectively), 12 months preceding TB. It was further validated in an untouched group of adolescents and independent South African and Gambian cohorts with a sensitivity of 53.7% (42.6 – 64.3%) and a specificity of 82.8% (76.7–86%) in 12 months preceding TB (77). Using saliva samples from suspected pulmonary TB individuals, Jacobs *et al* (2016) identified a seven-marker biosignature of CRP, ferritin, SAP, monocyte chemotactic protein-1 (MCP-1), alpha-2-Macroglobulin (A2M), fibrinogen and tissue plasminogen activator (TPA), that might be useful in the diagnosis of TB disease. TB disease was diagnosed with a sensitivity of 78.1% (95% CI, 59.6–90.1%) and specificity of 83.3% (95% CI, 72.3–90.7%) after leave-one-out cross validation (78). CAO *et al* (2018) screened for novel serum biomarkers that can discriminate between LTBI and active TB individuals at the systemic level using an Mtb proteome microarray containing 4,262 antigens. Significantly higher levels of 152 Mtb antigen-specific IgG antibodies were seen in the active TB compared to the LTBI group ($p < 0.05$). ELISA analysis of 11 candidate antigens were consistent with the microarray analysis. Rv2031c, Rv1408, and Rv2421c had higher areas under the curve (AUCs) of 0.8520, 0.8152, and 0.7970, respectively. The author's identified several antigens with potential as serum biomarkers for discriminating between active TB and LTBI (27).

Apart from diagnosis, biomarkers can be used for monitoring treatment response in TB patients. It is believed that people with active TB may have a flawed Mtb-specific T cell response due to an increasing bacterial load. One mechanism that gives rise to the inhibition of antigen-specific T cell effector function is the expression of inhibitory receptors such as programmed cell death protein (PD)-1, cytotoxic T-lymphocyte-associated protein 4 **(**CTLA-4), Lymphocyte-activation gene 3 (LAG-3), T-cell immunoglobulin and mucin domain-3

(TIM-3), and B- and T-lymphocyte attenuator (BTLA). Day *et al* (2018) showed the expression of PD-1 on Mtb specific CD4 T cells, but not CD8 T cells. The expression of PD-1 characterizes a population of effector cells, that have engaged their cognate antigen and have the capacity to produce Th1 cytokines. This study has provided novel insight into the function of PD-1 pathway in regulating T cell response during Mtb infection and the expression of PD-1 on antigen specific CD4 T cells as a biomarker for bacterial load and treatment response in human TB (79). A pilot study by Van Rensburg *et al* (2016) evaluating the transcriptome of B-cells showed the downregulation of Fas ligand (*FASLG)* and Interleukin 5 Receptor Subunit Alpha *(IL5RA)* in TB cases at diagnosis compared to healthy controls and the upregulation of these genes in TB cases after month 6 of treatment. These genes have the potential to be used as a biosignature to monitor treatment response but need to be validated in a larger cohorts (80).

Mycobacterium tuberculosis antigens with potential to differentiate between the stages of TB infection

A principle aspect for setting up an immunodiagnostic test is the identification of stimuli or antigens that are uniquely recognized by the immune system of diseased patients or infected individuals (75, 81). A determinant for immunodiagnostic test sensitivity, specificity and predictive potential is the antigen(s) that is used for stimulation (29). New potential immunogenic Mtb antigens (for new diagnostic or vaccine design) should depict the various phases of Mtb infection i.e. antigens that are expressed during early onset, latency/dormancy and resuscitation of the dormancy phase (82). Host-derived stresses, such as nitric oxide and hypoxia are thought to trigger a shift in metabolism from replication to a slow or non-replicating state, which is followed by changes in antigens available to the immune system (83). Antigen sensitisation with specific Mtb antigens would enhance immune response following a second challenge. Researchers are now challenged in finding antigens that will protect the host, (for vaccine development) and those which will give a specific host response, for biomarker development (56, 84, 85).

To date, many Mtb infection phase-dependent antigens with diagnostic potential have been identified, however, none of these antigens, single or in combination have the ability to discriminate active TB or LTBI with 100% accuracy (73). A study done by Chegou *et al* (2012) assessed the diagnostic potential of 118 Mtb infection phase-dependent antigens (classical TB antigens, DosR regulon encoded antigens, TB reactivation antigens,

resuscitation promoting factors (rpfs) and starvation antigens and other stress induced proteins) in TB patients and HHCs in a high-TB burden population. Using a 7-day diluted whole blood assay (WBA) they screened the antigens to assess their diagnostic potential for identifying active TB. The antigens that could distinguishing between active TB were the rpfs (Rv0867c, Rv2389c, Rv2450c, Rv1009 and Rv1884c), with AUCs between 0.72 and 0.80. Combination of Mtb specific ESAT-6/CFP-10 fusion protein, Rv2624c and Rv0867c accurately predicted 73% of the TB patients and 80% of the non-TB cases after cross validation (81). Loxton *et al* (2012) studied the ability of Mtb surface protein, heparin-binding hemagglutinin (HBHA) to induce multiple cytokines in peripheral blood mononuclear cell (PBMCs) and WBA from TB index cases and HHCs. Results shown that HBHA induces multifunctional INF-g-, IL-2-, and IL-17-coexpressing CD4+ T cells in HHCs, but not in active TB cases (86). HBHA is a 28 kD heparin-binding protein produced by Mtb and *Mycobacterium bovis* (87), present at the outermost layer of the cell and mediates the bacteria-epithelial cell interaction (87, 88).

The diagnostic potential of *Mycobacterium tuberculosis* antigens induced by iron limitation in the host

Iron is an essential micronutrient that is important for the host and Mtb metabolic processes (89, 90). The regulation of iron levels by the host plays an essential role in the susceptibility and outcome of Mtb infection (91), since high macrophage iron stores and nutritional iron overload are associated with an higher chance of developing TB and increased severity of the disease (92). Host iron homeostasis is strictly regulated, and a process called nutritional immunity limits the amount of free iron available to pathogens by upregulating iron sequestration proteins to withdraw iron from circulation. This host defence mechanism causes pathogens to compete with the host for iron (89, 92, 93). Macrophages, which contain high levels of cytoplasmic iron provide a favourable environment where Mtb can thrive (94). Macrophages can remove around 30% of the total circulating iron from the blood stream and some intracellular pathogens stimulate uptake by macrophages to have access to this divalent metal and nutrient rich macrophage environment (92, 95). However, even within macrophages iron acquisition is challenging because it is bound to iron-binding host proteins. To overcome this challenge, Mtb synthesizes chelating molecules that strongly binds iron (siderophores), heme-binding proteins, specialised iron transporters, and iron storage proteins, enabling it to acquire iron from the host (92, 96).

The genes encoding the core Mtb siderophore (mycobactins and carboxymycobactins) biosynthetic machinery are organised in two clusters, *mbt-1*, and the *mbt-2* loci. The *mbt-1* locus consists of 10 genes *mbtA* - *mbtJ* and *mbt-2* locus consists of 4 genes *mbtN* – *mbtK* (89, 97). An *mbtB* mutant of Mtb, defective in the first step of mycobactin synthesis, was impaired for growth in low-iron media and macrophages (96, 98), highlighting the essential role of mycobactin and carboxymycobactin in obtaining iron during intracellular growth (97). This is consistent with the induction of *mtbA-J* during growth in IFN-g activated macrophages and increased *mbtB* mRNA levels detected during Mtb infection in mice (99).

The *mbt* operon is downregulated under iron replete conditions because of the interaction of iron with the iron-dependant regulator (IdeR) (100). IdeR functions as a negative regulator of mycobactin biosynthesis under iron-sufficient conditions, while positively regulating the iron storage genes *bfrA* (bacterioferritin) and *bfrB* (ferritin like protein) (89). The transcription of the *mbt* and *bfr* genes are also dependent on HupB, a 28-kDa DNA-binding protein that is induced under iron-limiting conditions. HupB binds to the *mbtB* promoter in an iron-dependent manner and is thought to induce expression in the absence of IdeR binding. A Mtb *hupB* knockout strain, was unable to survive in macrophages, and showed a marked reduction in mycobactin and carboxymycobactin synthesis (100).

A study by Sivakolundu *et al* (2012) showed high levels of anti-HupB antibodies in TB patients from Hyderabad (India) compared with HHC and healthy controls. They showed low serum iron levels, low total iron-binding capacity and lower transferrin saturation in active TB, while higher serum ferritin was shown in the pulmonary TB group when compared with the normal controls. A strong negative correlation between serum iron levels and total iron-binding capacity with the titre of anti-HupB antibodies was observed in the active TB group. Using anti-HupB antibodies was therefore proposed as a diagnostic screening tool for diagnosing pulmonary and EPTB in this endemic region (101). A follow up study by Sritharan *et al* (2014) used an ELISA to screen the serum of TB patients with three antigenic fragments of HupB, namely the recombinant HupB-F1 (aa 1–71), HupB-F2 (aa 63–161) and HupB-F3 (aa 164–214). They reported that serum from pulmonary TB patients (new cases, defaulters, and recurrent cases) and EPTB showed enhanced immunoreactivity with the HupB-F2 fragment. The negative correlation of the anti-(HupB-F2) antibodies with serum iron was maximal, with a Pearson's correlation coefficient value of − 0,415. In this study the diagnostic potential of HupB was highlighted shown by the antigenic performance of HupB-F2 in screening pulmonary and EPTB (99).

Mtb displays a unique gene expression profile in response to iron starvation. In addition to iron-acquisition gene transcripts, iron-starved Mtb also upregulates iron-sulphur (Fe-S) cluster biosynthesis genes and several Fe-S containing proteins. Fe-S biogenesis therefore seems to be prioritized by Mtb in its iron sparing coping strategy, to ensure that essential Fe-S cluster proteins remain functional (92). The Mtb SUF system is the primary iron-sulphur cluster (Fe-S) biogenesis machinery in Mtb (102) and is encoded by a single operon composed of -*Rv1461-Rv1462-Rv1463-csd-Rv1465-Rv1466*. All the genes in the operon, with the exception of *Rv1460*, were predicted to be essential by forward genetic screens (103–105). A study by Willemse *et al* (2018) showed that Rv1460 is a transcriptional regulator of Fe-S biogenesis, which represses its own expression, as well as the expression of the SUF operon (106). Rhode *et al* (2007) investigated the Mtb global gene expression dynamics and cues during macrophage invasion. They found that extended subjection to intracellular stressors also led to up regulation of genes induced *in vitro* by oxidative stress, including the *SUF* operon (107,108). This suggests that induction of Fe-S cluster biogenesis is required during intracellular growth and implicates this system in survival during infection. Kumar *et al* (2011)) detected anti-Rv1460 antibodies in serum of TB patients suggesting that this regulator is expressed in Mtb during growth within the human host (109). This was further supported by the observation that *Rv1460* expression was induced in Mtb in sputum from TB patients, relative to expression in vitro.

Conclusion

TB remains a global problem partly because current standard diagnostic strategies and tools are not good enough. This causes a delay in the start of treatment, which has serious outcomes for global TB control (110). Earlier diagnosis of the disease could reduce the risk of transmission by allowing earlier treatment commencement (111). The shortcomings of current immunodiagnostics for the detection of progression from LTBI to active TB, diagnosis and treatment monitoring of TB highlights the need for new TB biomarkers (29). Several studies have therefore sought to identify new biomarkers for TB diagnosis and treatment response. Understanding the mechanisms employed by Mtb to survive in the host is one strategy for identifying bacterial proteins with diagnostic potential (109). Iron an essential micronutrient is required by most pathogens to survive in their human host. Despite the importance of iron homeostasis during TB infection, the utility of bacterial antigens expressed during the iron limitation experienced by Mtb within the host remains largely unexplored and therefore warrants further investigation.

Chapter 2: Study rational, Hypothesis, Aim and Objectives

Study rational:

The induction of the *Rv1460* gene during intracellular growth suggests that Rv1460 protein levels will be elevated under these conditions. However, in many cases mRNA transcript levels do not correlate directly to protein levels, due to factors such as transcript stability, post-transcriptional and post-translational regulation. This study therefore aims to investigate the level of the Rv1460 protein during intracellular growth, and to gain insight into the regulation involved in determining these levels. Furthermore, since Rv1460 levels are predicted to be elevated during intracellular growth and infection, we hypothesize that it is immunogenic and may induce an immune response in individuals infected with Mtb, and that it has diagnostic potential.

Hypothesis:

Rv1460 is expressed during intracellular growth and human infection and induces an immune response that confers diagnostic potential.

Aim:

To determine the level of Rv1460 protein during intracellular growth of Mtb using an ex vivo macrophage model, and to determine the host immune response to Rv1460 in Mtb infected and uninfected individuals.

Objective 1:

To investigate regulation of Rv1460 protein levels by comparing the amount of *Rv1460* transcript and Rv1460 protein under standard culture conditions. This was undertaken with the laboratory strain H37Rv, aimed to investigate fundamental mechanisms of regulation, which we hypothesize will be universal in clinical isolates.

Objective 2:

To investigate regulation of Rv1460 protein levels during intracellular growth within a macrophage infection model.

Objective 3:

To assess the immunogenicity of Rv1460 by direct *ex vivo* stimulation of blood samples from participants with newly diagnosed and untreated active TB and Mtb exposed/infected community controls.

Objective 4:

To assess the diagnostic potential of Rv1460 in a cross-sectional analysis of newly diagnosed untreated TB cases and healthy community controls. Two control groups were included, one group who are exposed to active TB patients (IGRA positive) and a second unexposed (IGRA negative) group. These assays were performed by short term stimulation (characterised by the production of IFN-g and other cytokines/growth factors) as that is suggestive of an effector or memory response as well as long term stimulation to determine if the protein induces an immune response.

Chapter 3: Material and Methods

3.1 Molecular Biology

3.1.1 Bacterial strains growth and culture conditions

Mycobacterium tuberculosis H37Rv, H37Rv *attB*::pMV306, H37Rv *attB*::pMV306_123mCherry and H37Rv *attB*::pMV306_211mCherry strains (Table: 3.1) were cultured in Middelbrook 7H9 broth (Difco, BD) supplemented with 0.05% Tween 80, 0.2% glycerol and Middelbrook oleic albumin dextrose catalase (OADC, BD) (7H9 OADC) or on 7H10 (Difco, BD) supplemented with 0.5% glycerol and Middelbrook OADC (7H10 OADC). Hygromycin B (hyg) (50 µg/mL) (Inqaba Biotech) was used for selection purposes. Cultures were incubated at 37˚C and growth monitored by Optical Density of 600nm (OD_{600nm}) readings or determined by colony forming units (CFUs) after plating serial dilutions on supplemented Middlebrook 7H10 media.

Table: 3.1 List of plasmids and strains

Plasmids / Strains	Description	Source
Plasmids		
pJET1.2	Linearized blunt end cloning vector (Amp^R)	CloneJet
pJET1.2Rv1460-123mCherry	pJET1.2 vector containing DNA fusion fragment Rv1460 _123mCherry.	This study
pJET1.2 Rv1460-211mCherry	pJET1.2 vector containing DNA fusion fragment Rv1460 _211mCherry.	This study
pMV306	Mycobacterial integrating shuttle vector with an hygromycin resistance gene and an integrase gene which allows the vector to integrate into the *attB*site of the mycobacterial genome.	(Stover *et al.*, 1991)
pMV306_123mCherry	pMV306 vector with 123 bp of *Rv1460* promotor cloned upstream of a promotorless*mcherry* gene.	This study
pMV306_211mCherry	pMV306 vector with 211 bp of *Rv1460* promotor cloned upstream of a promotorless*mcherry* gene.	This study
Strains		
E. coli XL1 Blue	*recA1endA1gyrA96thi-1hsdR17supE44relA1lac*[F´ *proABlacI*^{q}ZΔ*M15* Tn*10*] (Tet^R)	Stratagene
H37Rv	H37RvMA (ATCC: 27294)	Ioerger*et al.*, 2010
H37Rv*attB*::pMV306	Derivative of H37RV containing pMV306 mycobacterial integrating vector.	This study
H37Rv*attB*:: pMV306_123mCherry	Derivative of H37RV containing pMV306_123mCherry mycobacterial integrating vector.	This study
H37Rv*attB*:: pMV306_211mCherry	Derivative of H37RV containing pMV306-211mCherry mycobacterial integrating vector.	This study
M. smegmatis mc^2155 with pSTCHARGE3 plasmid	*hsp60(ribo)-turboFP635* (inducible TurboFP635 under control of theophylline-inducible riboswitch), Kan^R, episomal	Mouton *et al* (2016)

The *Mycobacterium smegmatis* mc^2155 strain containing pCHARGE3 (Table: 3.1) were cultured overnight in Middelbrook 7H9 OADC (Difco, BD) at 37˚C, shaking at 200 rpm (Yihdern LM 530 orbital shaking incubator, Yihder, Taiwan). *E. coli* XL1 Blue strain (Table: 3.1) was cultured in Luria-Bertani (LB) broth at 37˚C shaking at 200 rpm (Yihdern LM 530 orbital shaking incubator, Yihder, Taiwan). Rubidium chloride competent cells was prepared using this *E. coli* strain (112).

3.1.2 Construction of *Mycobacterium tuberculosis* reporter strains

3.1.2.1 Construction of fluorescent reporter vectors

Fluorescent reporter vectors were constructed as detailed in Figure (3.1). Firstly, two regions of *Rv1460* promotor (123 bp and 211 bp) were amplified from H37Rv genomic DNA. Work in our group at the time of this study re-annotated the start-site of Rv1460 +73 bp downstream of the original annotation (Tuberculist). The two constructs therefore reflect these two annotations, with the 211 bp promoter region including 138 bp upstream of the original start site, and the 123 bp promoter region including 123 bp upstream of the new start site. Using the Phusion High-Fidelity PCR Kit (Thermoscientific, Massachusetts, USA), two 25 µl reactions were setup containing 1X Phusion buffer, 1X GC buffer, 0.02mM dNTPs and Phusion DNA polymerase 0.4 Units (U) with primer sets Rv1460Pf and Rv1460Pr or ComplF1 and Rv1460Pr (Table: 3.2) at a final concentration of 0.025µM and 100ng template DNA. The amplification conditions were: initial denaturation at 98˚C for 1 minute (min), followed by 30 cycles of denaturation at 98˚C for 10 seconds (s), annealing at 60˚C for 30 s and extension at 72˚C for 30 s. A final extension at 72˚C was performed for 7 min. Five microliters (µl) of the PCR products (Rv1460_123 and Rv1460_211) were electrophoresed on a 1% agarose gel (SeaKem® LE Agarose, Lonza) with 0,005% of 10 mg/ml Ethidium bromide (EtBr) in TAE buffer (Appendix 1) for visualisation. The remainder of PCR products was purified using the Wizard SV Gel and PCR Clean-Up System (Promega, Wisconsin, USA) according to the manufacturer's instructions.

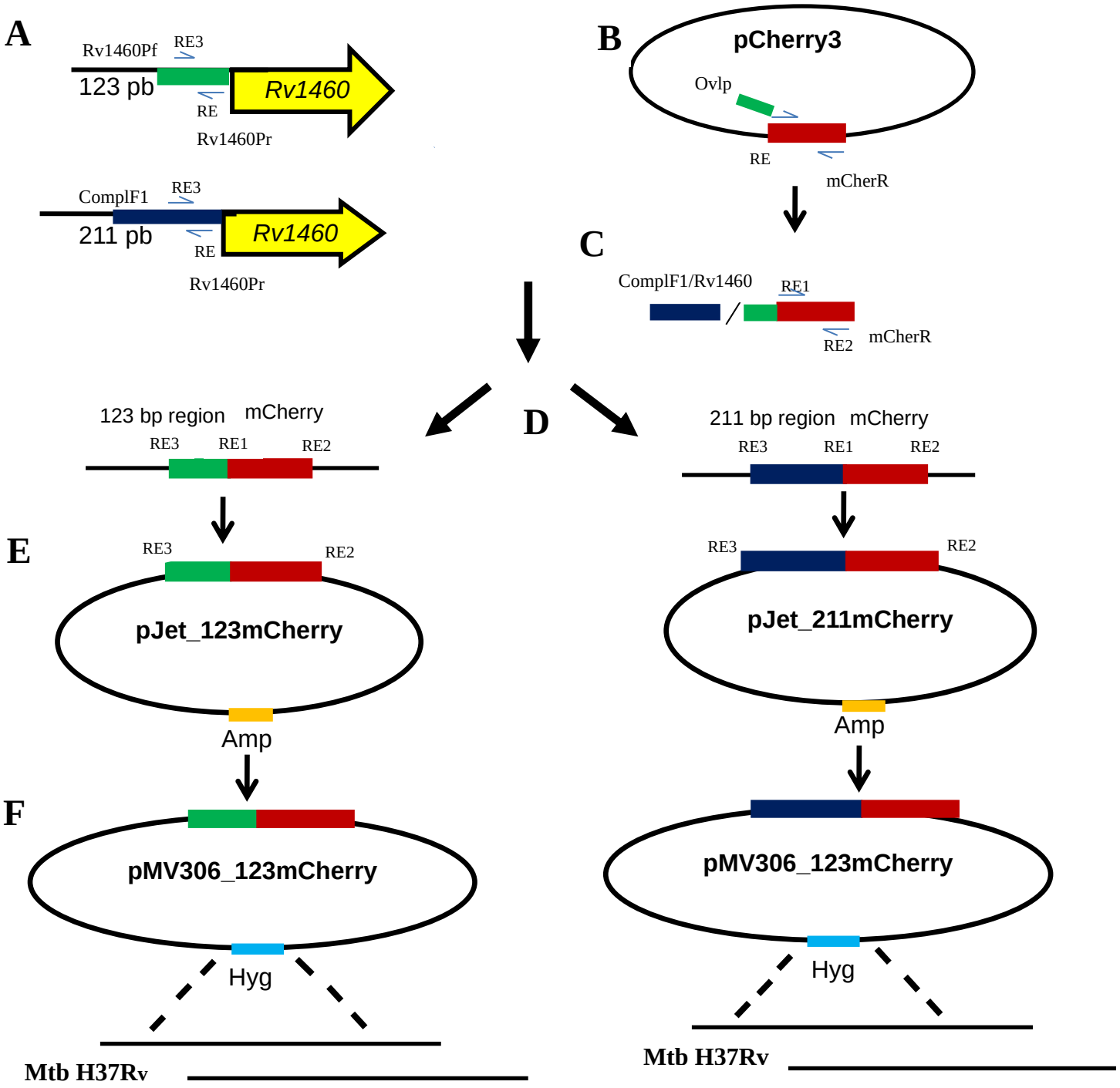

Figure 3.1: Schematic construction of a *Rv1460* promoter mCherry fluorescence reporter. (A) Two regions of *Rv1460* promotor (123 bp and 211 bp) were amplified from H37Rv genomic DNA. (B) Promotorless *mCherry* gene were amplified from pCherry 3 plasmid with an Ovlp primer (containing 20bp of 3' end of *Rv1460* promotor region and 15 bp of 5' end of *mCherry* gene) and mCherR. (C) Two overlap PCR reactions were set up by fusing the overlap *mCherry* gene product to 123 bp and 211 bp Rv1460 promoter regions through amplification with Rv1460Pf/ComplF1 and mCherR, respectively. (D) Rv1460_123 or Rv1460_211 promotorless mCherry fusion products. (E) The fluorescence constructs were cloned into a sequencing vector pJet containing an Ampicillin (Amp) resistance gene. (F) Fragments with correct sequence were subcloned into a Mycobacterial integrating shuttle vector, pMV306 containing a hyg resistance gene. Selected pMV306 constructs were transformed into Mtb H37Rv strain.

Table 3.2: List of primers used for the construction of fluorescent reporter vectors

Primer name	Sequence (5' to 3')	Description
Rv1460Pf	GATATCGCCATTGGTGCAGCCTAAC (EcoRv)	Binds 123 bp upstream of *Rv1460*start site.
ComplF1	GGATATCAGCTCGGTAGTGGTCAGCG (EcoRV)	Binds 211 bp upstream of *Rv1460*start site.
Rv1460Pr	AACATCAGTGTGACAAAATTCCGTTG	Binds 2 bp upstream of *Rv1460*start site
Ovlp	AATTTTGTCACACTGATGTTATGGCGATCATCAAG	Contains20bp of 3' end of *Rv1460* promotor region fused to 15 bp of 5' end of *mCherry* gene 20.
pCherF	ATGGCGATCATCAAGGAGTT	Binds *mCherry* at the start codon.
pCherR	GACGGTATCGATAAGCTTTCAC (Hind III)	Binds 2 bp from the *mCherry*stop codon.

RE sites are underlined and the name of the enzyme is listed in brackets

The promoterless mCherry fluorescent gene was then amplified from pCherry3 plasmid (Addgene plasmid# 24659; http://n2t.net/addgene:24659; RRID: Addgene_24659) with a forward primer (Ovlp) that contained 20 bp of the 3' end of *Rv1460* promoter region and 15 bp of the 5' of *mCherry* gene and reverse primer mCherR (Table: 3.2). Using Phusion High-Fidelity PCR Kit (Thermoscientific, Massachusetts, USA) a 25 µl reaction were setup containing 1X Phusion buffer (5X), 1X GC buffer (5X), 0.02mM and Phusion DNA polymerase 0.4 U with primer set Ovlp and pCherR (Table: 3.2) at a final concentration of 0.025µM and 100 ng template DNA. The amplification conditions were initial denaturation at 98˚C for 1 min, followed by 30 cycles of denaturation at 98˚C for 10 s, annealing at 60˚C for 30 s and extension at 72˚C for 30 s. A final extension at 72˚C was performed for 7 min. Five microliter of the PCR products (OvlpmCherry DNA) was electrophoresed on a 1% agarose gel (SeaKem® LE Agarose, Lonza) with 0,005% of 10 mg/ml EtBr in TAE buffer for visualisation. The remainder of PCR products was purified using the Wizard SV Gel and PCR Clean-Up System (Promega, Wisconsin, USA).

An overlap PCR (Phusion High-Fidelity PCR Kit, Thermoscientific, Massachusetts, USA) was then performed to fuse the Rv1460 promoter fragments Rv1460_123 and Rv1460_211 bp respectively to the amplified promoterless mCherry fragment containing 20 bp overlap. Two 50 µl reactions were setup containing 1X Phusion buffer (5X), 1X GC buffer (5X), 0.04 mM dNTPs, Rv1460_123 or Rv1460_211 DNA fragment (100 ng each) and mCherry DNA fragment (100 ng), dH_2O and Phusion DNA polymerase at 1 U. Reactions were performed in a thermocycler for 98˚C for 1 min and 60˚C for 10 min to melt and anneal the overlapping fragments. Forty microliters from each reaction were removed and 0.1 µM of primers Rv1460Pf and mCherR (Table: 3.2) were added to the reaction mix containing the

Rv1460_123 DNA fragment, while 0.1 µM of ComplF1 and mCherR (Table: 3.2) were added to the reaction mix containing the Rv1460_211 DNA fragment. Reactions were incubated in a thermocycler for 30 cycles at 98˚C for 30 s, 60˚C for 30 s, 72˚C for 30 s and 72˚C for 7 min. Five microliter (µl) PCR products (Rv1460_123mCherry (853 bp) and Rv1460_211mCherry (941 bp) were visualised on 1% agarose gel (SeaKem® LE Agarose, Lonza) with 0,005% of 10 mg/ml EtBr in TAE buffer and the rest of the reaction mixture was purified using the Wizard SV Gel and PCR Clean-Up System (Promega, Wisconsin, USA).

The PCR products (Rv1460_123mCherry and Rv1460_211mCherry) were cloned into the sequencing vector pJET1.2 (Table: 3.1) and transformed into competent *E. coli* cells. Plasmid DNA from selected colonies was isolated and purified using Wizard Plus SV Minipreps DNA Purification System (Promega, Wisconsin, USA). The DNA inserts were Sanger sequenced by Central Analytical Facilities (CAF) using commercially available sequencing primers (pJET1.2For/Rev). The fluorescent reporters were generated by subcloning the fragments with the correct sequences into the HindIII (Roche) and EcoRV (Roche) sites in pMV306 plasmid (Table: 3.2).

3.1.2.2 Transformation of *Mycobacterium tuberculosis*

Competent Mtb H37Rv cells were prepared by inoculating 500 µl frozen stock in 5 ml 7H9 OADC (Difco, BD). The culture was incubated at 37 ˚C for 5 days, and then sub-cultured to an OD_{600nm} of 0.05 in 50 ml 7H9 OADC (Difco, BD). After 7 days (OD_{600nm} of ~ 1) the cells were harvested by centrifugation at 4000 x g for 10 min. The pellet was resuspended and washed 3 times in equal volumes of sterile 10% glycerol, containing 0,05% Tween 80. The final pellet was resuspended in 1,2 ml of 10% glycerol, supplemented with 0,05% Tween 80.

Competent Mtb H37Rv bacterial cells (400 µl) were transformed with (i) pMV306; (ii) pMV306_123mCherry; (iii) pMV306 _211mCherry DNA constructs and (iv) no DNA as a control. Transformed Mtb H37Rv bacterial cultures were incubated at 37˚C overnight to allow bacterial cultures to recover. Dilutions (10^{-1}, 10^{-2}, 10^{-3}) of transformed cultures were plated on 7H10 OADC (Difco, BD) supplemented with 50 µg/ml Hyg. Single colonies obtained for each construct were picked using a sterile loop and used to inoculate 5 ml 7H9 OADC (Difco, BD). Starter cultures were incubated at 37˚C until they reached an OD_{600nm} of approximately 1. Strains were then sub-cultured into 30ml 7H9 OADC (Difco, BD) and incubated at 37˚C until they reached mid-log phase. Aliquots of each strain was stored at -80˚C for subsequent experiments.

3.1.3 *In vitro* fluorescence measurements of fluorescent reporter strains

Frozen stocks (1ml) of each of the following strains: (i) H37Rv *attB*::pMV306 (control strain) (ii) H37Rv *attB*::pMV306_123mCherry and (iii) H37Rv *attB*::pMV306_211mCherry (fluorescent reporter strains) (Table: 3:2) were inoculated in 5 ml 7H9 OADC (Difco, BD). The cultures were incubated at 37˚C for 5 – 6 days. The strains were sub-cultured to an OD_{600nm} of 0.05 in 30 ml. Growth was monitored over time by taking OD_{600nm} readings every second day for 22 days. To measure the fluorescence intensity (FI) over the 22 days, 100 µl of diluted aliquots (triplicate) from each culture was transferred to a black fluorescent 96 well plate. The plate was sealed and FI measured (excitation and emission: 587 and 610 nm) in the BMG LABTECH POLARstar Omega plate reader.

To measure FI per cell via flow cytometry, 1 ml of culture per strain was removed at early log (day 4), mid log (day 10) and early stationary phase (day14). One millilitre of the *Mycobacterium smegmatis* mc^2155 strain containing pCHARGE3 plasmid was used as positive control (Table: 3.1). The samples were sonicated for 12 min at 37˚C and centrifuged (Eppendorf 5810) at 12 500 x g for 5 min. Pellets were resuspended in 200 µl 4% formaldehyde and fixed for 30 min in the dark. The fixed cultures were washed with 800 µl phosphate buffered saline (PBS, Appendix 1) containing 0.05% Tween-80. The pellet was resuspended in 200 µl PBS-0.05% Tween-80 and stored at 4˚C until further processing. Just before flow cytometry analysis samples were centrifuged for 5 min at 12 500 x g, resuspended in 500 µl PBS and filtered through a 40 µm filter (Falcon). Analysis was performed using the FACSJazz (BD) where FI was measured at an excitation of 510 nm and 610/20 filter.

3.1.4 RNA extraction

Frozen stocks (1ml) of control and each fluorescent reporter strains (Table: 3.2) were inoculated in 5 ml 7H9 OADC (Difco, BD). The cultures were incubated at 37˚C for 5 – 6 days. The strains were sub-cultured to an OD_{600nm} of 0.05 in 30 ml. For total RNA extraction, 10 ml of culture per strain were removed at early log, mid log, and early stationary phase. Cells were pelleted by centrifugation (Eppendorf 5810) and resuspended in 2 ml RNA ProBlue solution (Iepsa). A volume of 1 ml of each strain were transferred to a 2 ml tube containing 0.1 mm glass beads (Iepsa) and stored at – 80˚C until RNA extraction was performed.

Before total RNA extraction was performed, the bacterial cultures were thawed on ice and ribolysed in a FastPrep-24 ribolyser (MP Biomedicals) for three 30 s cycles at 4.5 Watts, cooling on ice for 1 min between cycles. Lysates were centrifuged (Eppendorf 5415) at 12 000 x g for 15 min at 4˚C and 700 µl of the cleared lysate transferred to a clean 1.5 ml Eppendorf tube. Phase separation was performed by adding 300 µl chloroform and transferring the aqueous layer to a new tube after centrifugation (mikro 200R centrifuge, Sigma) at 12 000 x g for 10 min. The RNA was precipitated by the addition of 500 µl of ethanol prior to loading on a Nucleospin RNA kit column (Macherey-Nagel). The column was desalted, treated with rDNAse (Nucleospin RNA kit, Macherey-Nagel) for 15 min and washed according to manufacturer's instructions. RNA was eluted in 30 µl nuclease free water by centrifugation at 11, 000 x g for 1 min. The quality of the RNA was assessed by Nanodrop and by Bioanalyser (CPGR/CAF) analysis. The RNA was treated with TURBO DNase provided in the TURBO DNA-free kit (Ambion Thermoscientific) using the rigorous treatment option according to the manufacturer's instruction. DNAse was inactivated with DNAse inactivation reagent TURBO DNA-free kit (Ambion, Thermoscientific) and the DNAse inactivation reagent was removed by centrifugation at 10, 000 x g for 1.5 min. The RNA was aliquoted and stored at – 80˚C.

3.1.5 cDNA synthesis

RNA from both the control and fluorescent reporter strains was reverse transcribed with three reverse transcription (RT) primers: Rv1460RT; SigART and mCherryRTP (Table: 3.3) using the Transcriptor First Strand cDNA Synthesis Kit (Roche) according to manufacturer's instructions. The cDNA synthesis reaction contained 100 ng template RNA, 2 µM of each RT primer (Table: 3.3) and dH_2O made up to a final volume of 13 µl. The reaction was denatured at 65˚C for 10 min, placed on ice for 10 min and 1X transcriptor reverse transcriptase reaction buffer, 20 U protector RNAse inhibitor 1mM dNTPs (1 mM), and 10 U transcriptor reverse transcriptase enzyme added to a final volume of 20 µl. For each reaction, a no reverse transcriptase reaction was also set up as a control. Tubes were briefly mixed and centrifuged to collect the sample in the bottom of the tube, and incubated in a PCR machine (Verity^{TM} 96-Well Thermal Cycler, Thermoscientific) at 55˚C for 30 min. The transcriptor reverse transcriptase was inactivated by heating at 85˚C for 5 min. The cDNA was diluted 10-fold and stored at – 80˚C.until the quantitative reverse transcriptase PCR (RT-qPCR) reactions were performed.

Table:3.3 List of Reverse Transcriptase primers

Primer name	Sequence (5' to 3')	Binding position	Product size
Rv1460RT	TCATCGGGACGCTCCTTCGG	788 bp upstream from start of *Rv1460*	N/A
Rv1460Pf	GATATCGCCATTGGTGCAGCCTAAC	123 bp upstream of *Rv1460*start site	123 bp
ComplF1	GGATATCAGCTCGGTAGTGGTCAGCG	211 bp upstream of *Rv1460* start site	211 bp
Rv1460Pr	AACATCAGTGTGACAAAATTCCGTTG	2 bp upstream of *Rv1460*start site	
mCherryRTP	TGCTTGATCTCGCCCTTCA	503 bp downstream from *mCherry* start site	N/A
pCherF	ATGGCGATCATCAAGGAGTT	*mCherry*starts site	730 bp
pCherR	GACGGTATCGATAAGCTTTCAC	2 bp upstream from *mCherry* stop codon	
SigART	CTGACATGGGGGCCCGCTACGTTG	19 bp downstream of *SigA*	N/A
SigAF	TGCAGTCGGTGCTGGACAC	1379 bp from start of *SigA*	195 bp
SigAR	CGCGCAGGACCTGTGAGCGG	1552 bp from start of *SigA*	

3.1.6 RT-qPCR

The FastStart Essential DNA Green Master mix (Roche) was used to amplify *Rv1460, mCherry* and *sig A* (reference gene) according to manufacturer's instructions. The standard curve method for relative quantification of *Rv1460* and *mCherry* expression relative to the *sigA* gene was used. Reactions were setup containing 1X FastStart Universal SYBR Green Master mix (2X) (Roche), 0.5 µM for each forward and reverse primer sets (Rv1460Pf and Rv1460Pr, ComplF1 and Rv1460Pr, pCherF and pCherR or SigAF/SigAR (see Table: 3.3), 2 µl cDNA and dH_2O to a total of a 20 µl reaction volume. Quantitative PCR was done using the LightCycler 96 machine (Roche) with the following protocol: pre-incubation: 4.4˚C/s ramp rate, for 600 s at 95˚C, 3 step amplification: denaturing at 4.4˚C/s ramp rate for 20 s at 95˚C, amplification at 2.2˚C/s ramp rate for 20 s touchdown from 67˚C to 62˚C with 0.5˚C change per cycle for the first 12 cycles followed by 33 cycles at 62˚C and elongation at 4.4˚C/s ramp rate for 20 s at 72˚C. Melt curve analysis was done at 4.4˚C/s ramp rate for 10 s at 9 ˚C.

Ten-fold dilutions of Mtb genomic DNA (10^6 to 10^1 genome copies per 2 µl) were prepared and qPCR performed as described above in duplicate for each concentration. The log genomic DNA copies were plotted against the Ct values to generate a standard curve for each gene (*Rv1460, mCherry, Sig A*). Each standard curve fit a straight line and the formula of the line was used to determine the log copy number for each Ct value (representing an average of

duplicate Ct readings). The log copy numbers were converted to copy numbers and the expression of *Rv1460* and *mCherry* was standardised by dividing by *sig A* copy numbers for each sample to determine the relative *Rv1460* and *mCherry* expression.

3.1.7 Total protein extraction

To prepare whole cell lysates (WCL) 1 ml frozen stocks of the control and each fluorescent reporter strain was inoculated in 5 ml 7H9 OADC. The cultures were incubated at 37˚C for 5 – 6 days. The strains were sub-cultured to an OD_{600nm} of 0.05 in 30 ml. Ten millilitre of bacterial culture per strain was removed at early log, mid log, and early stationary phase, centrifuged (Eppendorf 5810) at 4, 000 g for 10 min and the pellet washed twice in 10 ml Tris buffer (Appendix 1). The pellet was resuspended in 1 mL Tris-buffer and transferred to a 2 ml screw cap tube containing 0.1 mm glass beads (Biospec Inc). The bacterial cells were lysed using a FastPrep-24 ribolyser (MP Biomedicals) for three 30 s cycles at 4.5 Watts, cooling on ice for 1 min between cycles and centrifuged (Eppendorf 5415) at 16 100 x g for 10 min. Bacterial lysates was filtered twice through a sterile microcentrifuge nylon 0.22 µm filter (Merck) to remove any residual live bacteria. The protein concentration was determined using Bradford protein assay. Bovine Serum Albumin Fraction V (BSA, Roche) was dissolved in Tris-buffer at a concentration of 2 mg/ml, and a dilution series (0-0.4 mg/ml) was prepared. A volume of ten microlitre each of the BSA standard and the bacterial lysates were loaded in triplicate in a 96 well plate. Bradford stock solution (BioRad) was diluted 1:5 and 200 µl of the solution was added to the wells. The absorbance was read in microplate reader (Synergy HT Bio-Tek) at 595 nm within 30 min after the addition of the Bradford reagent. The protein concentrations were determined by using the BSA standard curve. The WCL were aliquoted in and stored at -80 ˚C.

3.1.8 Sodium dodecyl sulfate polyacrylamide gel electrophoresis (SDS-PAGE) and western blotting

The protein levels of Rv1460 within the WCL's of the two fluorescent and wt strains for day 10 and 14 were separated by SDS-PAGE gel electrophoreses. Samples were prepared by adding one part of SDS-PAGE sample loading buffer (6X) (Thermodfisher) to five parts of the WCL samples. Samples were boiled for 5 min at 100˚C in heating block (Accublock™ Digital Dry Bath, Labnet). Three samples, Mtb H37Rv (wt with no plasmid) Mtb H37Rv Rv1460stop mutant, Mtb H37Rv Rv1460stop mutant-complementation. These WCL samples

were donated by Dr Danicke Willemse as part of a control. The protein was expected to be seen in Mtb H37Rv (wt with no plasmid) and Mtb H37Rv Rv1460stop mutant-complementation strains, but not in the Mtb H37Rv Rv1460stop mutant. The full protein was not made in the mutant strain.

The samples were loaded on two gels using a 12% stacking gel (Appendix 1) and concentrated on a 3% resolving gel (Appendix 1). Two gels were loaded with 5 µl molecular marker, PageRuler Plus Prestained Protein Ladder (Thermoscientific) in lane 1 and 12 and 5 µl of the purified Rv1460 protein (1.5 mg/ml) in lane 2. The rest of the samples (5 µg in 25 µl) were loaded as follows: lanes 3 and 4, H37Rv_*attB*::pMV306 day 10 and 14. Lanes 5 and 6, H37Rv_*attB*::pMV306_211mCherry day 10 and 14. Lane 9, 10 and 11 Mtb H37Rv (wt with no plasmid), Mtb H37Rv Rv1460stop mutant and Mtb H37Rv Rv1460stop mutant-complementation strains, respectively. Samples electrophoresed at 150 V for 60 to 75 minutes. One gel was stained for visualization using InstantBlue (Abcam). Proteins on the second gel were transferred to a 0.2 µM nitrocellulose blotting membrane (GE Healthcare, Life science) using cold transfer buffer (Appendix 1) and 100 V was applied for 60 min. Following transfer, the membrane was blocked overnight with blocking buffer (Appendix 1). The blocked membrane was washed 3 times with TBS-T wash buffer and incubated for 60 min with primary custom made anti-Rv1460 antibody (Eurogentec, Belguim). It was incubated with a secondary antibody, goat anti-rabbit IgG-HRP (Santa Cuz) (1: 10 000) for 60 min after a second wash step (3X). After a final wash step (3X), bands were detected with Clarity Western ECL Detection Kit (BioRad) using an autoradiography film in the dark room.

3.1.9 Growth and maintenance of THP-1 cell line for *Mycobacterium tuberculosis* H37Rv infection

THP-1 stocks were taken from -80˚C and thawed in a waterbath (37˚C). The cells were transferred to 5 ml pre-warmed RPMI 1640 with L-Glutamine (Lonza, Sigma), supplemented 10% Fetal Bovine Serum (FBS) (Gibco, Thermoscientific) (culture medium) and centrifuged at 1000 rpm for 5 min, to wash away any dimethyl sulfoxide (DMSO)(Sigma). The pellet was resuspended in 5 ml culture medium, transferred to a 25 cm^2 tissue culture flask (Greiner, Lasec) and incubated at 37˚C in a humidified incubator with 5% CO_2 for 4 days.

Cells were viewed using an inverted phase contrast microscope to confirm the absence of bacterial and fungal contaminants. On day 4 the cell cultures (80% confluency) were transferred to a 15 ml Falcon tube and centrifuged (Eppendorf 5810) at 1000 rpm for 5 min.

The pellet was resuspended in 1 ml culture medium. Cells were sub-cultured by adding 250 µl of the THP-1 culture to 20 ml fresh culture medium in a 250 cm^2 tissue culture flask (Greiner, Lasec) and incubating at 37˚C in a humidified incubator (Class II Biological Safety Cabinets, ESCO Vivid Air) with 5% CO_2 for 4 days.

3.1.9.1 THP-1 differentiation

To count the number of viable cells, cultures were centrifuged (Eppendorf 5810), resuspended in 1 ml culture medium. The number of viable cells was determined by diluting the culture 5-fold by transferring 20 µl of the cell suspension to an Eppendorf tube containing 80 µl of trypan blue. An aliquot of the stained cells was counted using a Neubauer haemocytometer. The cell culture was diluted to a density of 2 $x10^5$ cells/ml. Phorbol 12-myristate 13-acetate (PMA, Sigma) was added to the cell cultures at a final concentration of 50 ng/µl, to differentiate cells. Cells were seeded at 2 x 10^5 cells/per ml (per well) in a 24 well plate. Plates were incubated at 37˚C in a humidified incubator (Class II Biological Safety Cabinets, ESCO Vivid Air) with 5% CO_2 for 3 days. Plates were removed and the spent medium aspirated and washed three times with pre-warmed PBS. Fresh culture media were added to each well and plates incubated overnight at 37˚C in a humidified incubator (Class II Biological Safety Cabinets, ESCO Vivid Air) with 5% CO_2.

3.1.9.2 THP-1 infections

Starter cultures of each strain was prepared in 5 ml 7H9 OADC (Difco, BD) and sub-cultured to an OD_{600nm} of 0.05 in 30 ml. Following incubation at 37˚C for 5 days, 10 ml bacterial culture for each bacterial strain was centrifuged (Eppendorf 5810), at 4000 x g for 10 min. Bacterial cultures were washed 3 times in equal volume of PBS and pellets resuspended in 5 ml cell culture medium. Resuspended cells were sonicated for 12 min at 37˚C to disrupt cell clumps. Bacterial cultures were filtered through a 40 µm filter (Falcon) and OD_{600nm} was measured. An established conversion factor: An OD_{600nm} of 1.0 = 1 X 10^8 bacteria was used to dilute bacterial cultures to obtain a multiplicity of infection (MOI) of 2:1 and 5:1.

THP-1 plates were removed from the 37˚C incubator (Class II Biological Safety Cabinets, ESCO Vivid Air) and the medium were removed. The diluted bacterial culture was added to the THP-1 plates in triplicate (1 ml per well according to plate layout) and incubated at 37˚C in a humidified incubator (Class II Biological Safety Cabinets, ESCO Vivid Air) with 5% CO_2 for 3 hours for bacterial infection of THP-1 cells. After 3 hours the bacterial culture was

removed, and the THP-1 cells treated with 1 ml 1:100 Pen/Strep (10 000 U/ml, Sigma) diluted in RPMI medium. THP-1 plates were incubated at 37˚C in a humidified incubator incubator (Class II Biological Safety Cabinets, ESCO Vivid Air) with 5% $CO_{2\ ()}$ for 40 - 60 min to kill any extracellular bacteria. After the 40 - 60 min incubation Pen/Strep was removed and the plates washed 3 times with PBS. PBS was removed after the final wash step and 500 µl dH_2O was added to the wells (triplicate) to lyse the cells. Dilutions of lysed cells and original cultures were made in PBS with 0.05% Tween-80 and 100 µl of the following dilutions were plated 10^{-4}; 10^{-3}, 10^{-2}, 10^{-1} and incubated at 37˚C to determine the CFU/ml. Uninfected control was plated and no bacterial growth was expected on these plates.

3.2 Immunology

3.2.1 Study participant recruitment

Study participants were recruited in three Cape Town suburbs. Newly diagnosed untreated TB, latently infected (IGRA positive) and healthy uninfected individuals (IGRA negative) were recruited for this study. Since the proportion of healthy uninfected individuals recruited from the abovementioned communities was small this group of individuals were recruited from the Division of Molecular Biology and Human Genetics at the University of Stellenbosch.

3.2.2 Ethics approval

This study was approved by the Human Research Ethics Committee (HREC) of the Faculty of Medicine and Health Science, University of Stellenbosch, S17/02/45. Participant recruitment for the study is covered under studies: N16/05/070 and N14/10/136. The PhD study in which protein were purified for antibody generation was covered by ethics S13/09/159**.**

3.2.3 Sample collection and preparation

3.2.3.1 Sample collection

Blood samples were collected in 9 ml sodium heparin (NaHep) tubes (Lasec) and processed within 2 hours (hrs) of collection. NaHep tubes (Lasec) were inverted 10X and 2.5 ml blood was removed for whole blood assay (WBA, 12-hour assay) and lymphocyte proliferation assay (LPA, 7-day assay).

3.2.3.2 Whole blood assay

Five hundred microliters whole blood were added to four 2 ml screw cap tubes that contained 5 µl anti-CD28 and anti-CD49 (0.5 µg/ml) (BD Biosciences) co-stimulatory antibodies. To each tube (I to IV) the following reagents were added, respectively:

(I) Unstimulated tube – no reagent

(II) *Rv1460* recombinant protein – 1 µg/ml in RPMI 1640 without L-Glutamine (Lonza)

(III) BCG (SSI, Denmark) vaccine final concentration of 1 X 10^6 CFU/ml

(IV) Phytohaemagglutinin (PHA, Bioweb) final concentration of 5 µg/ml in RPMI medium

Tubes were vortexed and incubated at 37˚C in a humidified incubator (Class II Biological Safety Cabinets, ESCO Vivid Air) with 5% CO_2 for 12 hrs. After 7 hrs of incubation 2X 55 µl of supernatant was removed and stored at -80˚C. Brefeldin A (Sigma, 5 µg/ml) was added, vortexed and tubes were incubated in a 37˚C water bath for 5 hrs. Cells were transferred to 15 ml tubes (Falcon) containing 10 ml 1X BD FACS Lysing Solution (BD Biosciences), vortexed and incubated at room temperature (RT) in the dark for 10 min, following centrifugation (Eppendorf 5810) at 400 x g for 10 min. The pellet was resuspended in 500 µl RPMI 1640 without L-Glutamine and 500 µl cryo solution (20% DMSO in FBS (Sigma)) was added drop wise to the cells. Cells were stored overnight in at -80˚C in Nalgene Mr Frosty container, and transferred to -80˚C.

3.2.3.3 Lymphocyte proliferation assay

Whole blood was diluted 1:10 by adding 500 µl of the blood to 4.5 ml pre-warmed RPMI 1640 supplemented with 1% L-Glutamine. Tubes were inverted 10x before adding 1.150 ml of the diluted blood to a 24 well plate containing the following stimulants, plate lay-out as follow (figure 3.2):

Row B and C – Column 1: Unstimulated sample – 100 µl RPMI/L-Glutamine

Row B and C – Column 3: 100 µl *Rv1460* (1 µg/ml in RPMI medium)

Row B and C – Column 4: 100 µl BCG (1.25 x 10^6 CFU/ml)

Row B and C – Column 5: 100 µl PHA (1 µg/ml in RPMI medium, added on day 4). All the other wells were filled with 0.5 ml sterile dH_2O.

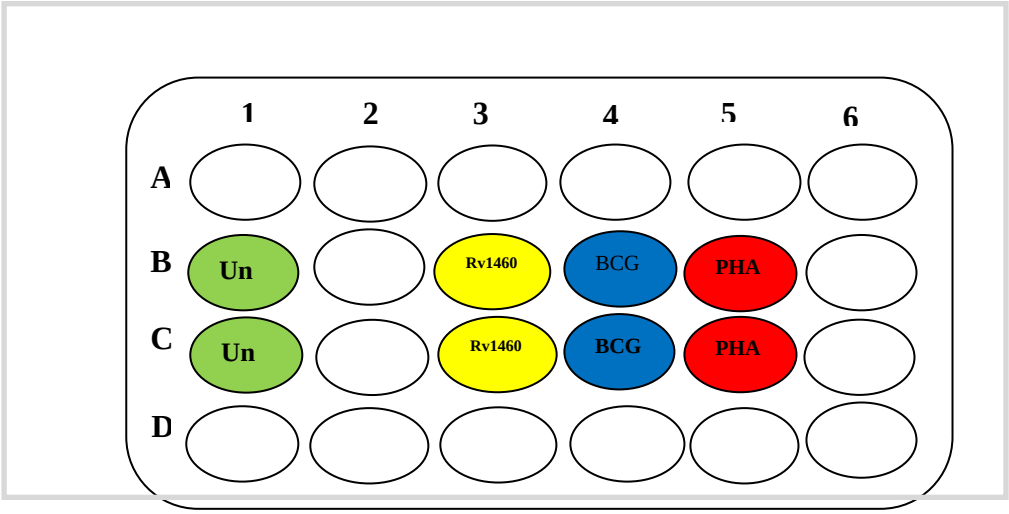

Figure 3.2: Plate lay-out for the LPA assay. Samples were loaded in Rows B and C, Columns 1, 3-5. Column 1, row B and C is unstimulated (Un) whole blood (WB). Column 2, row B and C is Rv1460 stimulated WB. Column 4, row B and C is BCG stimulated WB. Column 5, row B and C is PHA stimulated WB. All other wells were filled with sterile dH_2O.

Plates were incubated at 37˚C in a humidified incubator (Class II Biological Safety Cabinets, ESCO Vivid Air) with 5% CO_2 for 7 days. Plates were removed on day 4 and PHA added to selected well/s. After the 7-day incubation 2X 250 µl supernatant were removed and stored at -80˚C. Brefeldin A (2 µg/ml) was added to all the wells, PMA (Sigma, 20 ng/ml) and ionomycin (Sigma, 2 µg/ml) was added to all the wells except the unstimulated sample. Plates were incubated for a further 4 hours at 37˚C in a humidified incubator (Class II Biological Safety Cabinets, ESCO Vivid Air) with 5% CO_2. Cells were transferred to 15 ml tubes (Falcon) containing 10 ml 1X BD FACS Lysing Solution (BD Biosciences), vortexed and incubated at RT in the dark for 10 min, following centrifugation (Eppendorf 5810) at 400 x g for 10 min. Supernatant was discarded and the pellet resuspended in 1 x BD Pharm Lyse (10 ml), vortexed and incubated at RT in the dark for 10 min, following centrifugation (Eppendorf 5810) at 400 x g for 10 min. Pellet was resuspended in 500 µl RPMI 1640 and 500 µl of cryo solution was added drop wise to the cells. Cells were stored overnight in at -80˚C in Nalgene Mr Frosty container, and transferred to -80˚C.

3.2.4 Luminex Multiplex Immuno Assay

Luminex multiplex immunoassay were used to access the concentration of 8 selected cytokines. Since very little is known about the differential expression of host markers upon *ex vivo* stimulation with Mtb iron associated proteins, we selected host markers that have shown

diagnostic potential in literature. Due to financial constraints the level of only 8 host markers could be measured. An 8-plex analyte-specific antibodies (R&D Systems) were used to measure the concentrations of cytokines in the supernatants of WBA and LPA: IFN-g, MCP-1 (CCL2), Macrophage inflammatory protein (MIP)-1b, Interleukin (IL)-1b, Matrix metallopeptidase (MMP)-9, Interleukin (IL)-6, Interleukin (IL)-8 and Regulated and normal T cell expressed and secreted (RANTES) (CCL5) were precoated onto magnetic microparticles embedded with fluorophores at set ratios for each unique microparticle.

All reagents and samples were brought to RT before use. Samples were briefly vortexed and centrifuged (Eppendorf 5810) for 2 min at 250 x g. Samples were diluted 1:1 with 40 µl Calibrator Diluent RD6-52. Fifty microliters of standard or sample were added to respective wells according to plate lay-out. Fifty microliters of the diluted Microparticle Cocktail were added to each well and the plate was covered with foil and incubated for 2 hrs at RT on a horizontal orbital microplate shaker set at 800 ± 50 rpm. The plate was washed 3X with 100 µl Wash Buffer. Fifty microliters of the diluted Biotin-Antibody Cocktail were added to each well. The plate was covered with foil and incubated for 1 hr at RT on shaker (Orbit^{TM} Digital Microtube and Microplate shaker, Labnet) set at 800 ± 50rpm. The plate was washed 3x with 100 µl Wash Buffer. Fifty microliters of the diluted Streptavidin-PE were added to each well. The plate was covered with foil and incubated for 30 min at RT on shaker set at 800 ± 50 rpm. The plate was washed 3X with 100 µl wash buffer. Microparticles were resuspended by adding 100 µl of Wash Buffer to each well, incubated for 2 min on shaker (Orbit^{TM} Digital Microtube and Microplate shaker, Labnet) set at 800 ± 50 rpm and read on a Bio-Plex® MAGPIX™ Multiplex reader (MAGPIX13046704, BioRad Laboratories, Inc., California, USA).

3.2.5 Flow Cytometry

Cryopreserved lymphocytes from the WBA and LPA were washed in 10 ml PBS and centrifuged (Eppendorf 5810) for 10 min at 400 x g. The pellet was resuspended in 200 µl 1X permeabilization buffer (Biolegend), incubated at RT for 10 min and centrifuged (Eppendorf 5810) for 10 min at 400 x g. The cells were stained with 20 µl antibody cocktail: CD3; CD4 CD8; CD19; IFN-g; TNF-a; IL-2; IL-10 (Table: 3.4) and incubated at 4˚C (in the dark) for 1 hr. Cells were washed 2X with 1X permeabilization buffer and resuspended in 200 µl PBS and acquired on the BD FACS CANTO II Flow cytometer (BD Bioscences). We collected a total of 10^5 to 10^6 cells per tube.

Table: 3.4: Antibodies and its conjugated fluorophores used for flow cytometry

Antibody	Fluorophore	Company
CD3	PerCP	Biocom Africa
CD4	APC/H7	BD Bioscience
CD8	BV510	Biocom Africa
CD19	FITC	Biocom Africa
IFN-g	BV421	Biocom Africa
TNF-a	PE	Biocom Africa
IL-2	PE/Cy7	Biocom Africa
IL-10	APC	Biocom Africa

3.2.6 Statistical and Data analysis

GraphPad Prism 8 software was used for the statistical analysis of the molecular biology protein concentrations and expression analysis. Multiple t-test was done without assuming equal standard deviation among samples and without correction for multiple comparisons. A *p*-value of smaller than 0.05 was considered statistically significant. Analysis of the immunogenicity of Rv1460 was performed by a qualified statistician (Prof Martin Kidd) using the Statistica 13 software. For all analysis and comparisons, a *p*-value of smaller than 0.05 was considered statistically significant.

Chapter 4: Results

4.1 Molecular Biology

4.1.1 Construction of *Mycobacterium tuberculosis* reporter strains

In this study we aimed to investigate the regulation of Rv1460 protein levels in the Mtb laboratory strain H37Rv by evaluating both *Rv1460* expression and Rv1460 protein levels. To measure expression of *Rv1460*, we constructed reporter constructs based on the fluorescent protein mCherry and sought to validate them under standard culture conditions.

Two fluorescence reporter vectors were constructed by cloning two *Rv1460* promoter regions (123 bp and 211 bp) upstream of a promoterless *mCherry* gene. Figure 4.1 A-C show the stepwise PCR results for the construction of the mCherry fluorescent reporter. In Figure 4.1 A, lane 2 shows the PCR amplified 211 bp Rv1460 promoter region including 138 bp upstream of the original start site, while and lane 4 the 123 bp promoter region of the new start site. The promoterless mCherry fluorescent gene was amplified with a forward primer containing 20 bp of the 3' end of *Rv1460* promoter region (Figure 4.1 B). The overlap PCR was then performed with each promoter region to generate a fusion product as shown in Figure 4.1 C, lane 2 and 4 shows Rv1460_123mCherry and Rv1460_211mCherry, respectively. The resulting products were cloned into the pJET1.2 sequencing vector and the presence of the insert confirmed by restriction enzyme digestion (Figure D and E, lane 2 and 3). The sequence of the fused products was confirmed by Sanger sequencing and cloned into pMV306H.

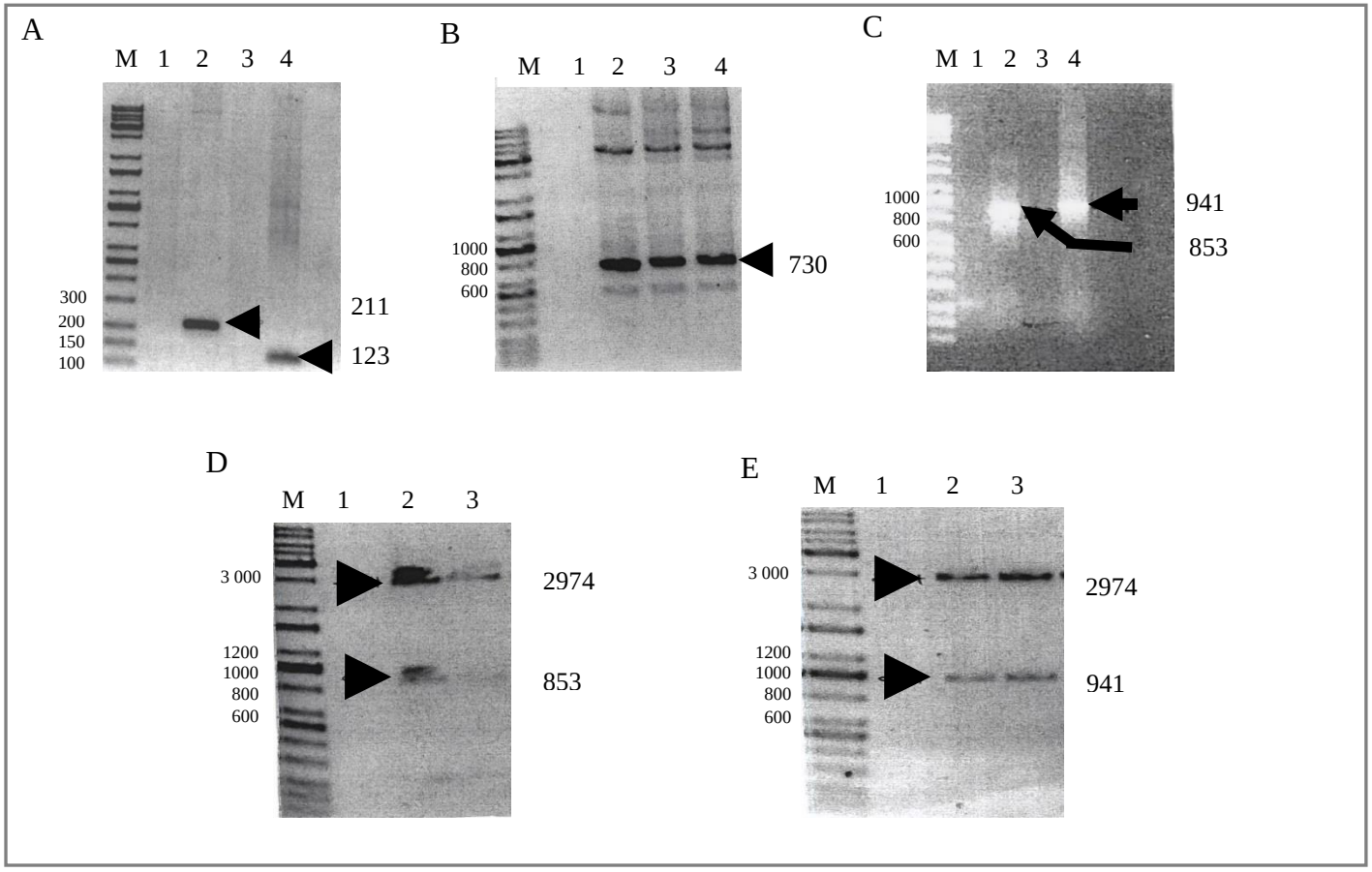

Figure 4.1: Generation of a fluorescent reporter construct: PCR amplification of (A) *Rv1460* promotor regions, lane 2 and 4 is the 211 bp and 123 bp promoter regions. (B) Overlap mCherry DNA, lane 2-3 is the promoterless *mcherry* gene containing 20 bp of the *Rv1460* promoter region. (C) Overlap PCR with mCherry overlap DNA and Rv1460 promoter regions, lane 2 and 4 is the fluorescent constructs of Rv1460_123mCherry and Rv1460_211mCherry, respectively. (D) 123mCherry fragment cloned into pMV306 plasmid and (E) 211mCherry fragment cloned into pMV306 plasmid.

4.1.2 Effect of fluorescent protein on the growth of fluorescent reporter strains

The two reporter constructs, and an empty vector (pMV306H) were transformed into the Mtb strain H37Rv (wild type, wt) and the growth of the strains was monitored under standard growth conditions by measuring the OD_{600nm} over 22 days. Growth was compared to the wt strain without the reporter to determine if the expression of the reporter protein altered the growth rate in any way. The expression of the reporter protein had no effect on the growth of the reporter strains when compared to wt (Figure 4.2).

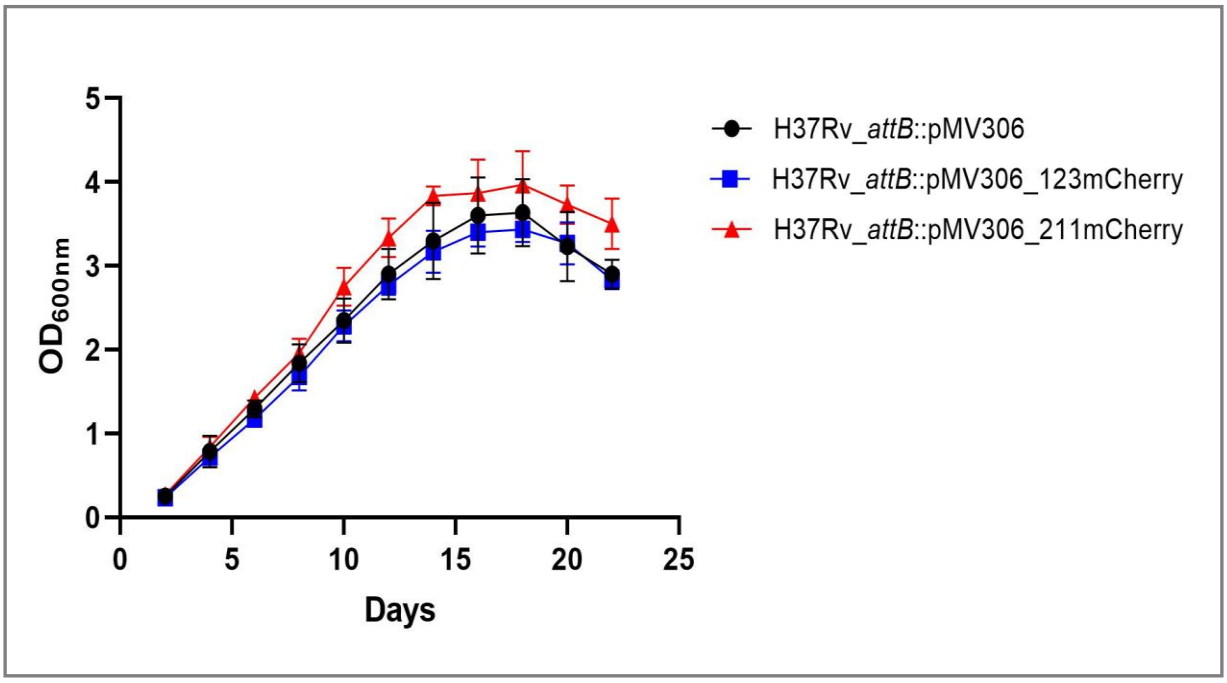

Figure 4.2: Growth curves of Mtb H37Rv_*attB*::pMV306 strain (wild type control) and two fluorescent reporter strains, H37Rv_*attB*::pMV306_123mCherry and H37Rv_*attB*::pMV306_211mCherry measuring the OD_{600nm} over the course of 22 days. Each point is the average and standard deviation of three biological replicates.

4.1.3 *In vitro* analysis of fluorescent reporter strains using a spectrophotometer

The expression of mCherry in the reporter strains, as a measure of the promoter activity of *Rv1460*, was then determined by measuring the relative fluorescence units (RFU) over time and expressed relative to CFU/well determined at each time point.

RFU showed an increase over time during exponential growth, apart from a slight dip at day 8 in both fluorescent reporter strains and the wt strain. Once the strains reached stationary phase (~ 15 days), the RFU plateaued for all the strains. Higher RFU was measured in both H37Rv_*attB*::pMV306_123mCherry and H37Rv_*attB*::pMV306_211mCherry when compared to the wt control H37Rv_*attB*::pMV306 with the highest FI measured in H37Rv_*attB*::pMV306_211mCherry (Figure 4.3 A). To estimate the RFU per cell at days 4, 10 and 14, the RFU was divided by the CFU/well (Figure 4.3 B). This revealed a large increase in RFU per cell when comparing day 10 (mid-exponential phase) and day 4 (early exponential phase), while no further increase was observed between day 10 and day 14 (early stationary phase).

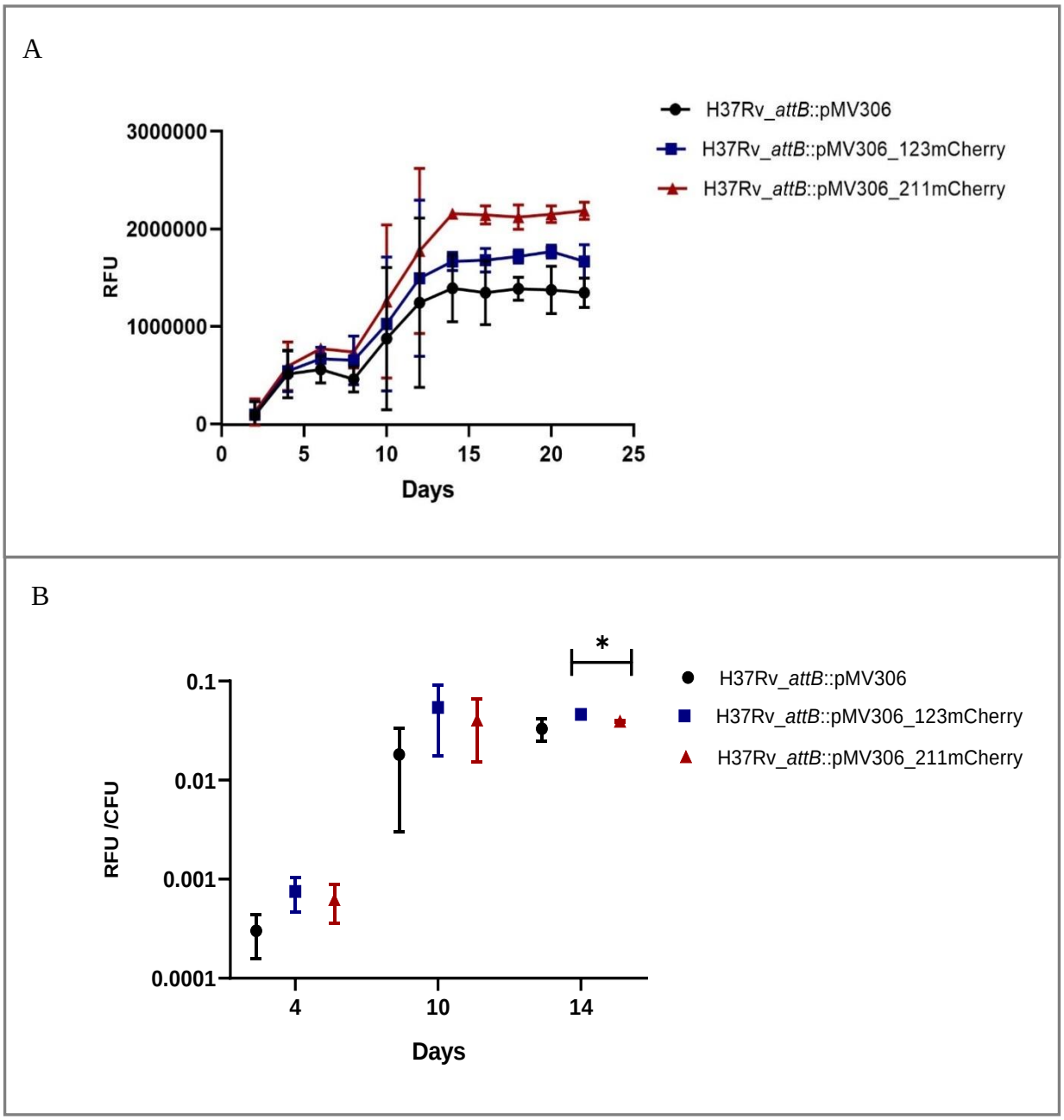

Figure 4.3: RFU and RFU over CFU of Mtb H37Rv_*attB*::pMV306 strain(wt) and fluorescent reporter strains, H37Rv_*attB*::pMV306_123mCherry and H37Rv_*attB*::pMV306_211mCherry. (A) Shows the RFU over the course of 22 days and (B) RFU over CFU at various time points: day 4, day 10 and day 14. RFU of mCherry (emission and excitation 587 and 610 nm) was measured in a POLARstar Omega, BMG LABTECH spectrophotometer. The average of the RFU readings was divided by the CFU/well count for the 3 strains at the various time points. Each point is representative of three biological replicates and two technical duplicates. The star indicates the significant difference and levels of significance between RFU of the different strains as determined by multiple unpaired *t*-test. $p \leq 0.05$ *.

4.1.4 *In vitro* analysis of fluorescent reporter strains using flow cytometry

The fluorescence per cell was also measured at day 4, 10 and 14 using flow cytometry. Figure 4.4 shows the overlayed histograms of negative control H37Rv*attB*::pMV306 (black) and fluorescent strains H37Rv_*attB*::pMV306_123mCherry (blue), H37Rv_*attB*::pMV306_211mCherry (red) and a *Mycobacterium smegmatis* strain containing a plasmid expressing mCherry was included as positive control (pink). A significant increase in the median fluorescent intensity (MFI) in both fluorescent reporter strains when compared to the negative control (pMV306 empty vector) is seen in the overlay histograms at day 4, 10 and 14, represented by a shift to the right on the x-axis (Figure 4.4 A, B and C). At day 14 a higher MFI for H37Rv_*attB*::pMV306_211mCherry (red) when compared H37Rv_*attB*::pMV306_123mCherry (blue) was observed.

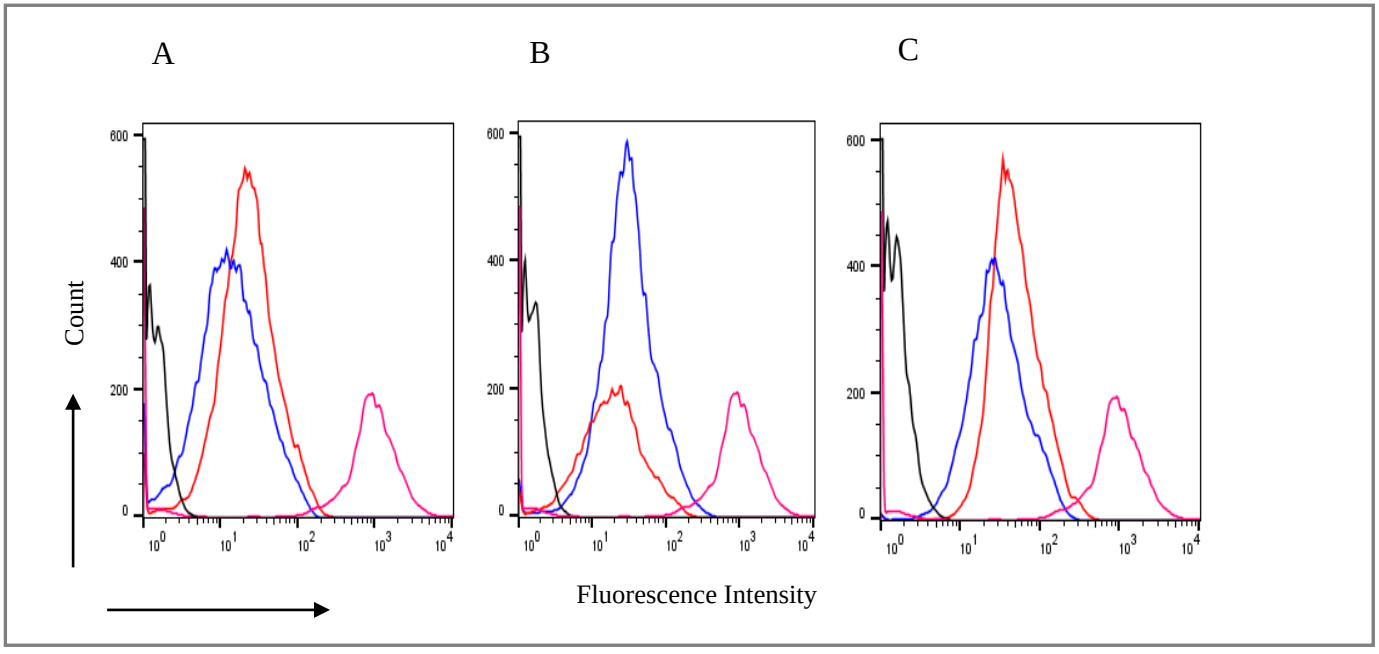

Figure 4.4: Overlayed histograms of Mtb H37Rv_*attB*::pMV306 strain (black), two fluorescent reporter strains, H37Rv_*attB*::pMV306_123mCherry (blue) and H37Rv_*attB*::pMV306_211mCherry (red) and *Mycobacterium smegmatis* strain containing a plasmid expressing mCherry as positive control (pink). The relative fluorescence intensity of the three strains was measured in a BD FACSJazz at 510 nm using a 610/20 filter overtime at day 4 (A), day 10 (B) and day 14 (C). The increase in fluorescence is a measure the increase in *Rv1460* expression overtime.

Figure 4.5 indicates the median fluorescent intensity (MFI) for the three strains at each time point. A significant difference in the MFI is seen in both H37Rv_*attB*::pMV306_123mCherry ($p < 0.006$, $p < 0.001$ and $p < 0.001$) and H37Rv_*attB*::pMV306_211mCherry ($p < 0.004$, $p < 0.001$ and $p < 0.001$) when compared to wt control at day 4, 10 and 14, respectively. At day 14, a significant difference in the MFI of H37Rv_*attB*::pMV306_211mCherry ($p < 0.001$) was observed when compared to H37Rv_*attB*::pMV306_123mCherry. This correlates with the significant difference in the RFU/CFU in Figure 4.3 B between the two fluorescent reporters at day 14 ($p < 0.008$).

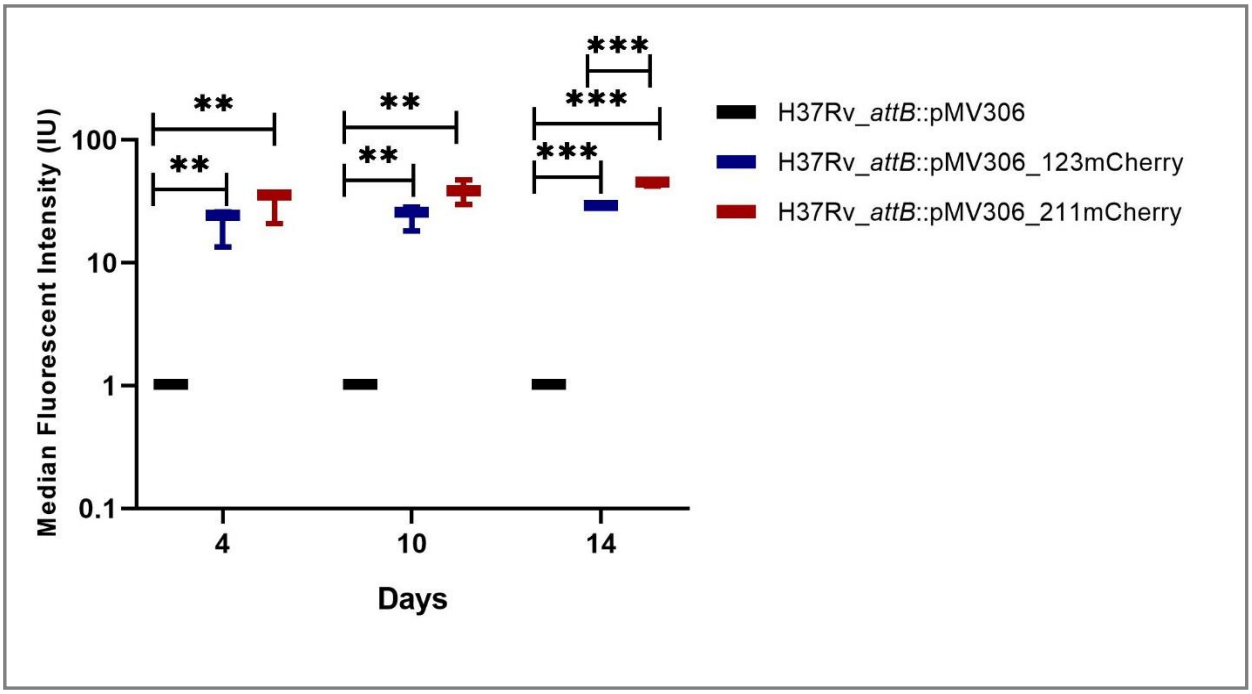

Figure 4.5: MFI of Mtb H37Rv_*attB*::pMV306 strain (wt) and two fluorescent reporter strains, H37Rv_a*ttB*::pMV306_123mCherry and H37Rv_*attB*::pMV306_211mCherry measuring the expression (MFI) of mCherry overtime at day 4, day 10 and day 14. Each point is representative of three biological and technical replicates. The star indicates the significant difference and levels of significance between MFI of the different strains as determined by multiple unpaired *t*-test. $p \leq 0.05$ *, $p \leq 0.01$ **, $p \leq 0.001$ ***

4.1.5 Quantification of *Rv1460 and mCherry* transcript levels using RT-qPCR

In order to validate the use of fluorescence reporter strains as tool for the quantification of gene expression using flow cytometry or fluorescence spectrophotometry, we need to show that expression of *Rv1460* correlates with expression of *mCherry* and with fluorescence in the reporter strains. To do this, the transcript levels of *mCherry* and *Rv1460* were determined in

the 3 strains at day 4, 10 and 14. Transcript levels of *mCherry* and *Rv1460* were quantified by RT-qPCR and expressed relative to an appropriate reference gene (*sigA*). Table 4.1 shows the relative expression of the reporter gene *mCherry* and our protein of interest *Rv1460*, and the ratio of the two at the three time points. The *Rv1460* transcript levels for H37Rv_*attB*::pMV306, H37Rv_*attB*::pMV306_123mCherry and H37Rv_*attB*::pMV306_211mCherry strains increased between day 4 and day 10, while decrease in transcript levels is observed between day 10 and 14. Higher transcript levels is observed for H37Rv_*attB*::pMV306_211mCherry strain at day 4 and 10, when compared to H37Rv_*attB*::pMV306_123mCherry strain. A sharp decrease in transcript levels was seen at day 14 for both fluorescent reporter strains. The *mCherry* transcript levels for H37Rv_*attB*::pMV306_123mCherry and H37Rv_*attB*::pMV306_211mCherry strains decreased between day 4 and day 10 (1.8fold and 1.23fold) respectively. A further sharp decrease is observed in H37Rv_*attB*::pMV306_123mCherry and H37Rv_*attB*::pMV306_211 mCherry strains between day 10 and 14 (3.4fold and 3.7fold) respectively. As expected, no *mCherry* expression was observed in the control strain. For *Rv1460* transcript levels an increase was observed between day 4 and day 10, while a decrease was observed between day 10 and day 14, for all strains, although the magnitude of the change differed between the strains. When comparing the ratio of *mCherry* transcript to *Rv1460* transcript, we observed the same trend for the *Rv1460* transcript levels with an increase between day 4 and 10 and a decrease between day 10 and 14 for both reporter strains. The *mCherry* transcript levels do not reflect the *Rv1460* transcript levels.

Table 4.1 Ratios of the relative expression of *Rv1460* and *mCherry*

	Mean ± SD		
	Day 4	**Day 10**	**Day 14**
Rv1460/sigA			
H37Rv_*attB*::pMV306	77.96 ± 17.78	99.32 ± 51.23	12.42 ± 4.01
H37Rv_*attB*::pMV306_123mCherry	23.32 ± 24.38	82.90 ± 35.59	7.24 ± 2.28
H37Rv_*attB*::pMV306_211mCherry	68.73 ± 52.98	105.06 ± 106.67	7.6 ± 1.53
mCherry/sigA			
H37Rv_*attB*::pMV306	0.00 ± 0.00	0.00 ± 0.00	0.00 ± 0.00
H37Rv_*attB*::pMV306_123mCherry	0.56 ± 0.19	0.31 ± 0.08	0.09 ± 0.06
H37Rv_*attB*::pMV306_211mCherry	0.96 ± 0.23	0.78 ± 0.51	0.21 ± 0.16
Rv1460/mCherry			
H37Rv_*attB*::pMV306_123mCherry	56.06 ± 40.66	319.73 ± 227.83	102.21 ± 38.18
H37Rv_*attB*::pMV306_211mCherry	62.20 ± 40.73	91.63 ± 86.72	55.70 ± 27.76

4.1.6 Quantification of Rv1460 levels using western blot analysis

To determine the protein levels of Rv1460 within the fluorescent and wt strains, WCL was prepared by lysing bacteria by bead beating on day 10 and 14. The level of Rv1460 protein was quantified by western blotting with anti-Rv1460 antibody and standardised against total protein per well. Figure 4.6 (A) shows the SDS Page gel electrophoreses and Figure 4.6 (B) shows the western blot analysis, where the only band detected is that of the positive control, the purified recombinant Rv1460 protein. After several attempts we were unable to detect Rv1460 protein in the WCL of our reporter and wt strains. Lane 10 contained a Rv1460 truncated mutant, we did not expect to see a band since the Rv1460 protein was not made. However, we expected a band in the lane 11 where the mutant strain was complemented. This suggests that the level of Rv1460 protein in the samples was lower than the limit of detection of the antibody and prevented us quantifying the protein level by western blotting.

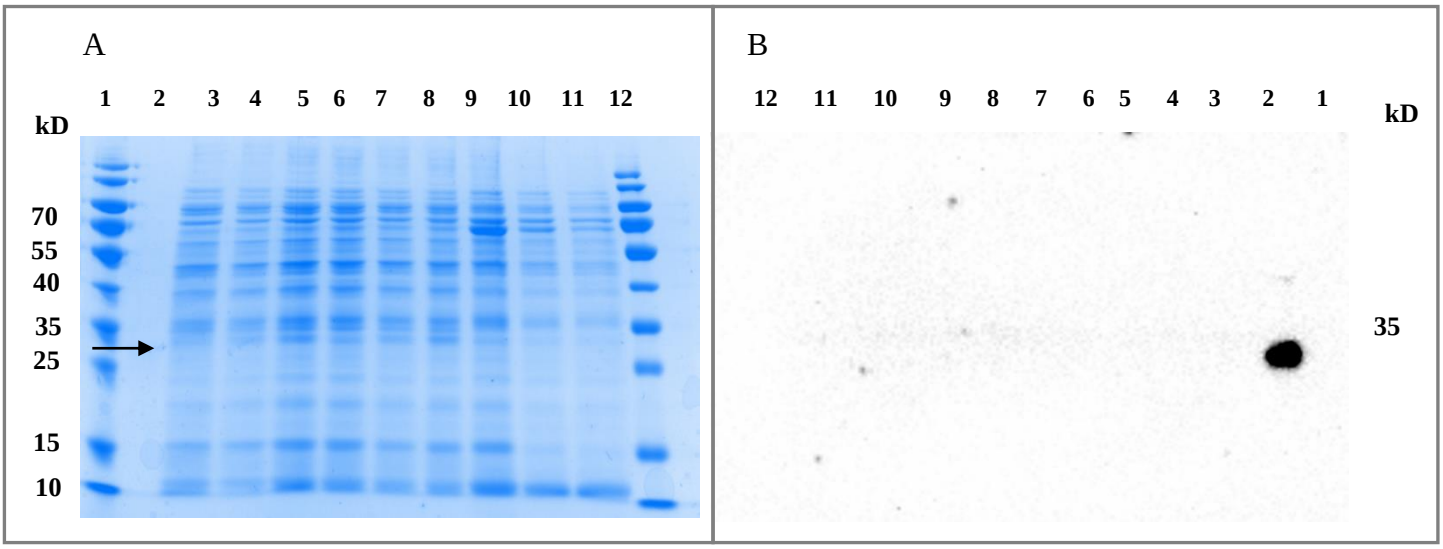

Figure 4.6: SDS PAGE gel (A) and Western Blot (B) of Mtb whole cell lysates: lane 1 Marker; lane 2 purified recombinant Rv1460 protein; lane 3 H37Rv_*attB*::pMV306 strain day 10 ; lane 4 H37Rv_*attB*::pMV306 strain day 14; lane 5 H37Rv_*attB*::pMV306_123mCherry day 10, lane 6H37Rv_*attB*::pMV306_123mCherryday 14; lane 7 H37Rv_*attB*::pMV306_211mCherry day 10; lane 8 H37Rv_*attB*::pMV306_211mCherry day 14; lane 9 H37Rv no plasmid; lane 10 H37Rv Rv1460stop mutant: 1ane 11 H37Rv Rv1460stop mutant-complementation and lane 12 marker. (A) SDS Page gel and (B) Western blot, where only the purified Rv1460 protein was detected at 34 kDa.

4.1.7 THP-1 infection with fluorescent reporter strains for quantification of Rv1460 protein levels

4.1.7.1 Fluorescent reporter strains survival within THP-1 cells

To determine level of Rv1460 expression during intracellular growth we used an ex vivo THP-1 macrophage model, by infecting differentiated THP-1 macrophages with H37Rv_*attB*::pMV306 strain as our wt control and two fluorescence reporter strains H37Rv_*attB*::pMV306_123mCherry and H37Rv_*attB*::pMV306_211mCherry to measure the expression of *Rv1460* during intracellular growth. A MOI of 2:1 and 5:1 was used. The Mtb infected THP-1 cells were lysed at 24, 48 and 72 hours and serial dilutions were plated to determine colony forming units (CFUs)/well. Bacterial cells from triplicate wells were pooled and analysed by flow cytometry. There was no significant difference in the number of Mtb (H37Rv_*attB*::pMV306, H37Rv_*attB*::pMV306_123mCherry and H37Rv_*attB*::pMV306_211mCherry) being phagocytosed by the THP-1 cells for MOI of 2:1 and 5:1, although lower numbers of H37Rv_*attB*::pMV306_211mCherry were taken up, but these differences were not significant (Figure 4.7). Less survival of the bacteria within the

host cells was observed for the higher MOI (Figure 4.8), which is due to increased death of the THP-1 cells because of the high bacterial burden.

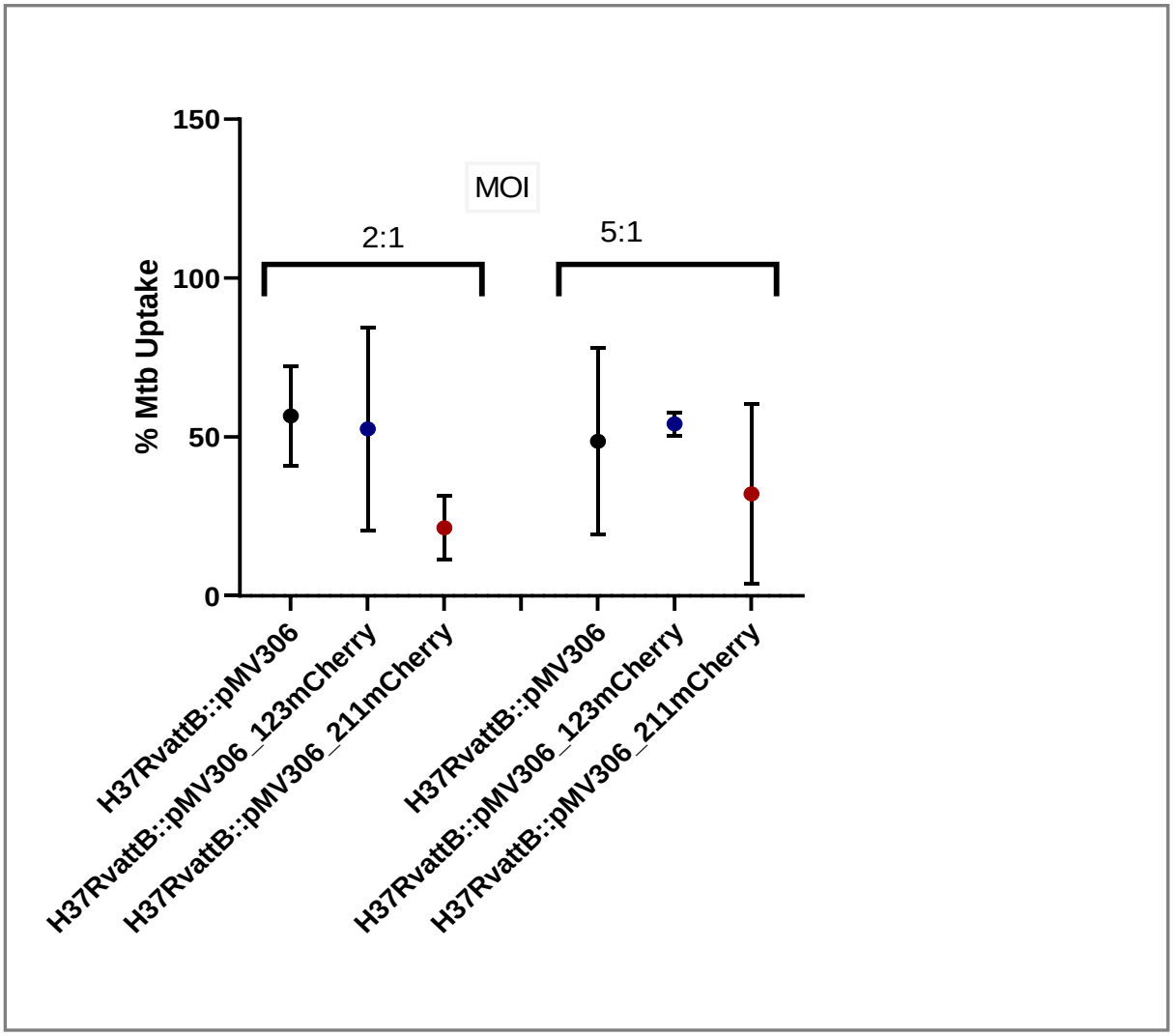

Figure 4.7: Mtb H37Rv control and fluorescent reporter strains uptake within differentiated THP-1 macrophages. THP-1 macrophages were infected with H37Rv_*attB*::pMV306 strain as wt control and two fluorescent reporter strainsH37Rv_*attB*::pMV306_123mCherry and H37Rv_*attB*::pMV306_211mCherry at a MOI of 2:1 and 5:1 for 3 hrs. The number of bacterial cells internalized was determined by dividing CFU/ml count of the original cultures (MOI: 2:1 and 5:1) by the CFU/mL count of the bacterial culture at time 0 (3hrs after infection). Each point is representative of three biological and three technical replicates.

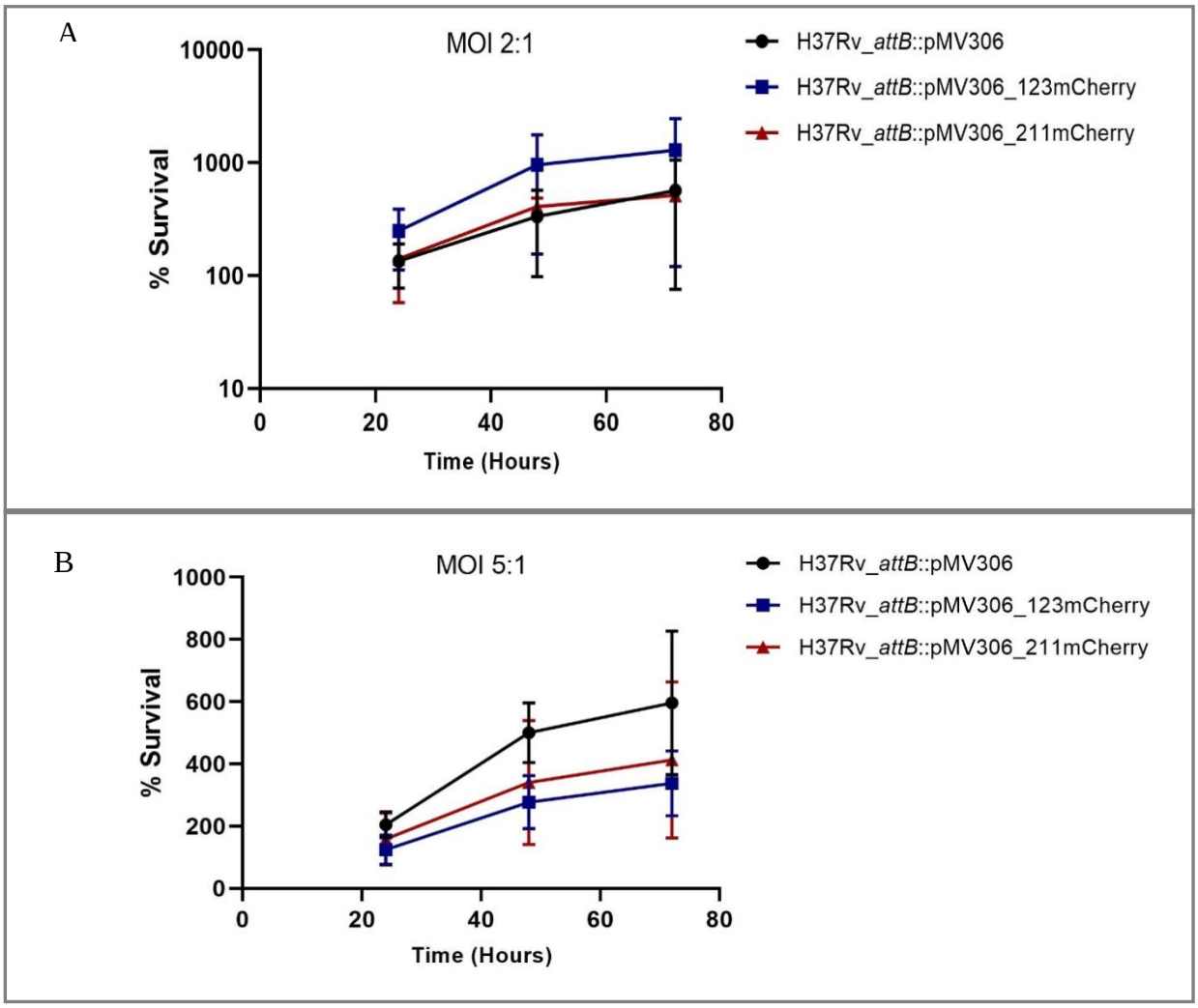

Figure 4.8: Mtb H37Rv control and fluorescent reporter strains survival within differentiated THP-1 macrophages. THP-1 macrophages were infected with H37Rv_*attB*::pMV306 strain as wt control and two fluorescent reporter strainsH37Rv_*attB*::pMV306_123mCherry and H37Rv_*attB*::pMV306_211mCherry at a MOI of (A) 2:1 and (B) 5:1 for 3 hrs. THP-1 cells were lysed and bacterial cells were harvested, and serial dilutions plated on solid media at 24, 48 and 72 hours post infection, to determine CFU/ml. Each point is representative of three biological and three technical replicates.

4.1.7.2 Flow cytometry analysis of *in vivo* expression of Rv1460 overtime represented by the mCherry protein levels

Fluorescent reporters and flow cytometry are excellent tools to study host-pathogen interactions. This allows researchers to study gene expression in real time. We aimed to investigate the expression of Rv1460 within macrophages over time using mCherry as a fluorescent reporter. As expected we saw no shift in the histogram for the negative control at the 4 time points for both MOIs. For the MOI of 2:1 (Figure 4.9) at 0 hrs, the histogram for both the H37Rv_*attB*::pMV306_123mCherry and H37Rv_*attB*::pMV306_211mCherry

strains coincided with the empty vector control (H37Rv_*attB*::pMV306). At 24 hrs, a small shoulder appears to the right of the negative population for both strains, and this shoulder continued to grow at 48 and 72 hours. This suggests that a subset of the population of bacteria within the macrophages has higher expression of the reporter gene. For the MOI of 5:1 (Figure 4.10), the H37Rv_*attB*::pMV306_211mCherry strain shows a shoulder to the right of the negative population at time zero, which is not seen for the H37Rv_*attB*::pMV306_123mCherry strain. This sub-population with higher reporter gene expression is not observed for the H37Rv_*attB*::pMV306_211mCherry strain at 24 and 48 hours. At 72 hours, both strains resemble the 72-hour time point for MOI 2:1, with the greatest shift seen in the H37Rv_*attB*::pMV306_211mCherry strain. Taken together, these results suggest that *Rv1460* expression is induced in a subset of bacteria within macrophages, and this population increases over the course of a 72-hour infection.

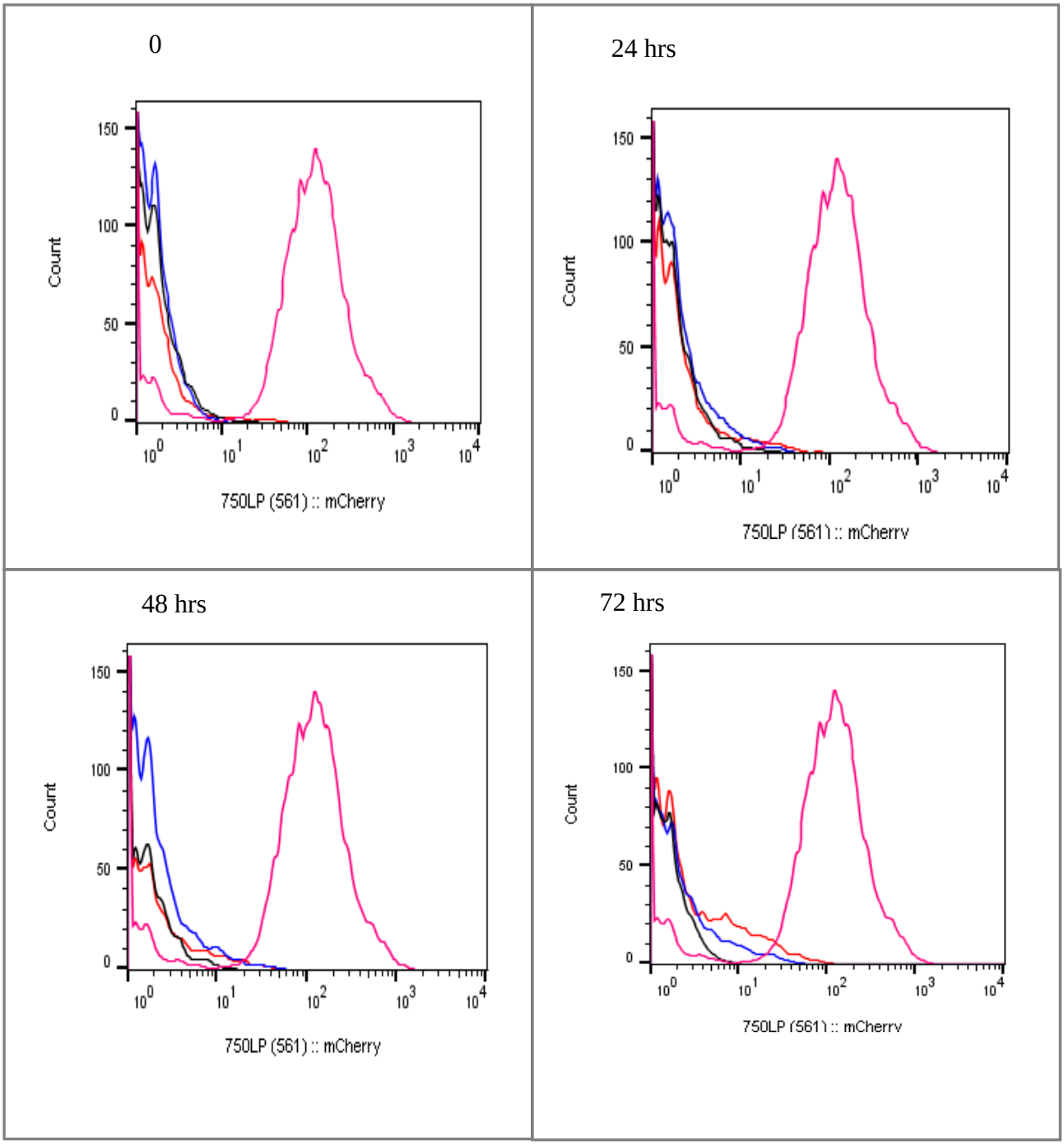

Figure 4.9: Mtb THP-1 infection with a MOI of 2:1. Mtb H37Rv_*attB*::pMV306 strain as wt control (black) and two fluorescent reporter strains, H37Rv_*attB*::pMV306_123mCherry (blue) and H37Rv_*attB*::pMV306_211mCherry (red) was used to infect THP-1 macrophage like cells, lysed at various time points 0, 24, 48, and 72 hrs. *Mycobacterium smegmatis* strain containing a plasmid expressing mCherry was used as positive control (pink).The bacterial culture was harvested and fixed with 4% formaldehyde and run on FACSjazz flow cytometer to measure the mCherry fluorescence (510 nm with a 610/20 filter) which is a measure of *Rv1460* gene expression.

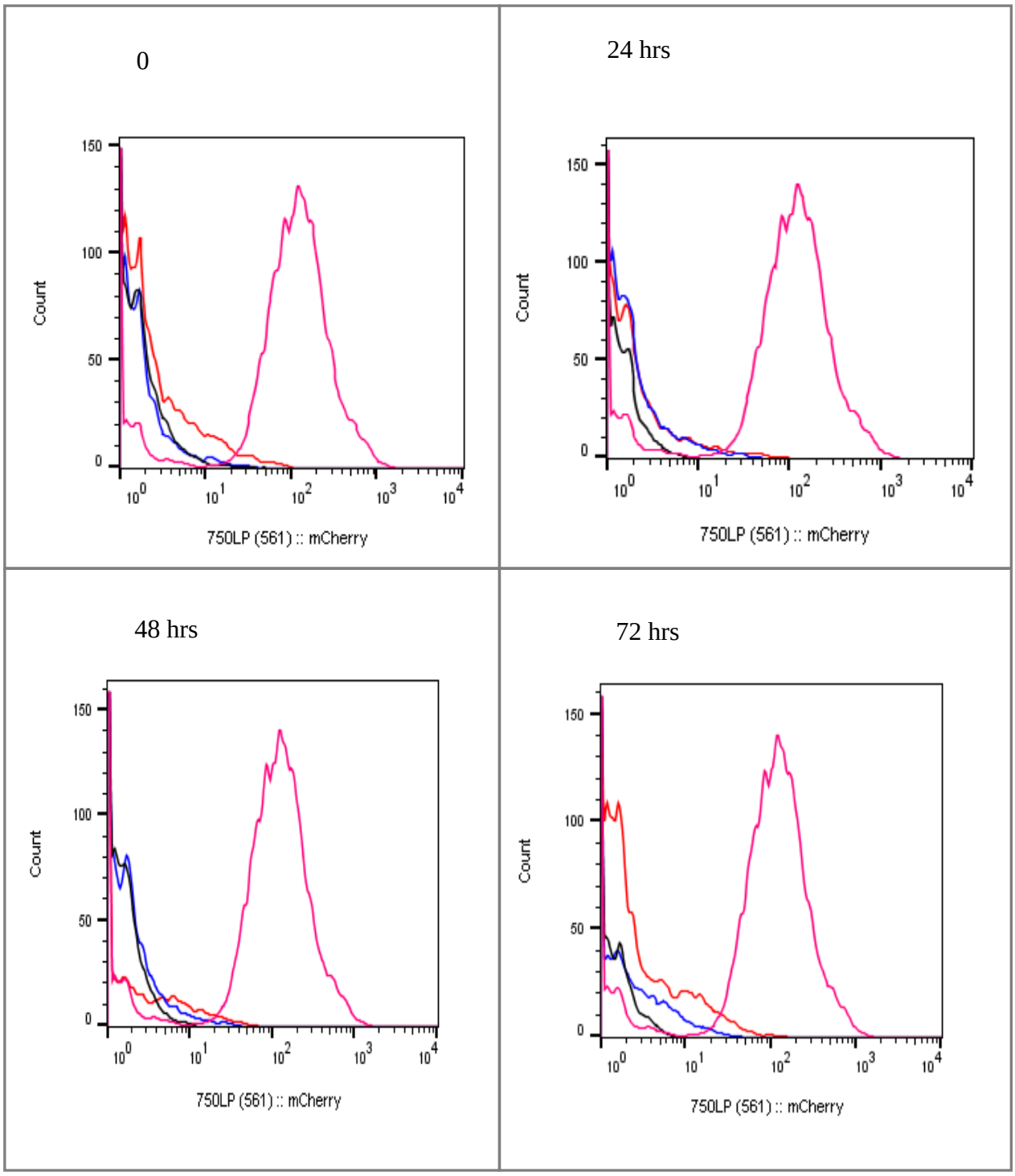

Figure 4.10*:* Mtb THP-1 infection with a MOI of 5:1. MtbH37Rv_*attB*::pMV306 strain as wt control (black) and two fluorescent reporter strains, H37Rv*attB*::pMV306_123mCherry (blue) and H37Rv_*attB*::pMV306_211mCherry (red) was used to infect THP-1 macrophage like cells, lysed at various time points 0, 24, 48, and 72 hrs. *Mycobacterium smegmatis* strain containing a plasmid expressing mCherry was used as positive control (pink). The bacterial culture was harvested and fixed with 4% formaldehyde and run-on BD FACSjazz flow cytometer to measure the mCherry fluorescence (510 nm with 610/20 filter) which is a measure of *Rv1460* gene expression.

4.2 Immunology

4.2.1 Analysis of selected analytes by multiplex cytokine array

We assessed the immunogenicity of the transcription regulator Rv1460 by direct *ex vivo* stimulation of whole blood samples from newly diagnosed and untreated active TB, QFN pos and QFN neg participants. Two different assays were performed: 1) a short term 12-hour stimulation to characterise the production of IFN-g and other cytokines/growth factors suggestive of an effector response and 2) a longer term 7-day stimulation to see if Rv1460 is able to induce a memory type immune response.

To assess the immunogenicity of Rv1460 the levels of 8 whole blood supernatant analytes MCP-1, RANTES, IL-1b, IL-8, MIP-1b, IFN-g, IL-6 and MMP-9 were measured in the clinical groups: active TB, QFN pos and QFN neg. Stimulation with Rv1460 was performed with a concentration of 1 µg/ml for both the 12-hour and 7-day assays, respectively. Two control conditions, unstimulated and BCG stimulated conditions were added to the experiments.

Within the active TB, QFN pos and QFN neg groups we observed low levels of MCP-1, IL-1b, MIP-1b, IFN-g and IL-6 following 12 hours in the unstimulated and Rv1460 stimulation conditions (Figure 4.11). Lower levels of IL-8 although not significant is seen in the QFN neg group when compared to QFN pos ($p = 0.06$) and active TB ($p = 0.08$) groups following 12 hours for both unstimulated and Rv1460 stimulation, respectively. Significantly lower levels of MMP-9 were seen in the QFN neg group when compared to QFN pos ($p = 0.00$) and active TB ($p = 0.01$) groups after 12 hours of being unstimulated and Rv1460 stimulated, respectively. *Ex vivo,* 12-hour stimulation of whole blood of active TB, QFN pos and QFN neg groups with Rv1460 does elicit a good even though not significant, immune response for the chosen analytes. Significantly lower levels of RANTES were measured in the active TB group for the 12-hour unstimulated ($p = 0.00$ and $p = 0.00$), Rv1460 stimulated ($p = 0.00$ and $p = 0.00$) or BCG stimulated ($p = 0.00$ and $p = 0.00$) when compared to QFN pos and QFN neg groups, respectively. BCG 12-hour stimulation gave significantly higher levels for all analytes except RANTES in all three groups when compared to the unstimulated and Rv1460 stimulated conditions. QFN neg group had the highest levels of MCP-1 compared to active TB ($p = 0.02$) and MMP-9 when compared to QFN pos ($p = 0.03$) following 12-hour BCG stimulation. Active TB group had the highest levels of IL-1b when compared to QFN pos ($p = 0.00$) and QFN neg ($p = 0.00$) following 12-hour BCG stimulation. QFN pos group had the

highest levels of IFN-g when compared to active TB (p = 0.00) and IL-6 when compared to active TB (p = 0.00) and QFN neg (p = 0.03) following 12-hour BCG stimulation.

Rv1460 induced very low levels of all analytes in the active TB, QFN pos and QFN neg groups following 7-day stimulation (Figure 4.11). BCG 7-day stimulation induced significantly higher levels for MCP-1, IL-8, IFN-g and MMP-9 in all groups when compared to the unstimulated and Rv1460 stimulated populations. Following 7-day BCG stimulation resulted in significantly higher levels in the QFN pos group when compared to unstimulated (p = 0.04) and Rv1460 stimulated (p = 0.04). Similar to the 12-hour BCG stimulation, the QFN neg group had the highest level of MCP-1 when compared to active TB (p = 0.00) and QFN pos (p = 0.00) groups and MMP-9 when compared QFN pos (p = 0.00) following 7-day BCG stimulation. QFN pos group had the highest level of IL-8 and IFN-g when compared to active TB group (p = 0.00 and p = 0.00) following 7-day BCG stimulation. IFN-g and MMP-9 levels showed similar patterns following 12-hour vs 7-day BCG stimulations (Figure 4.11).

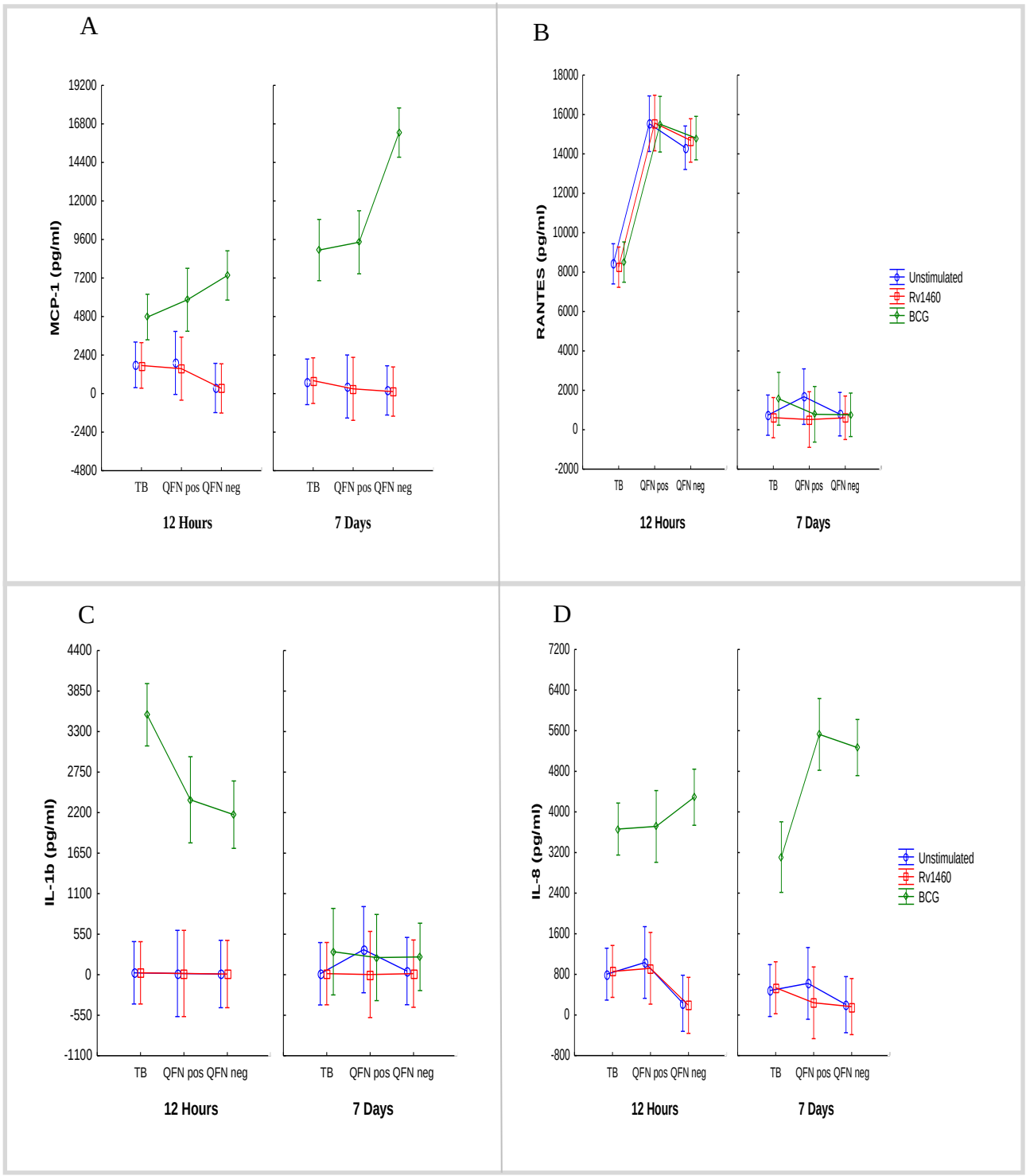

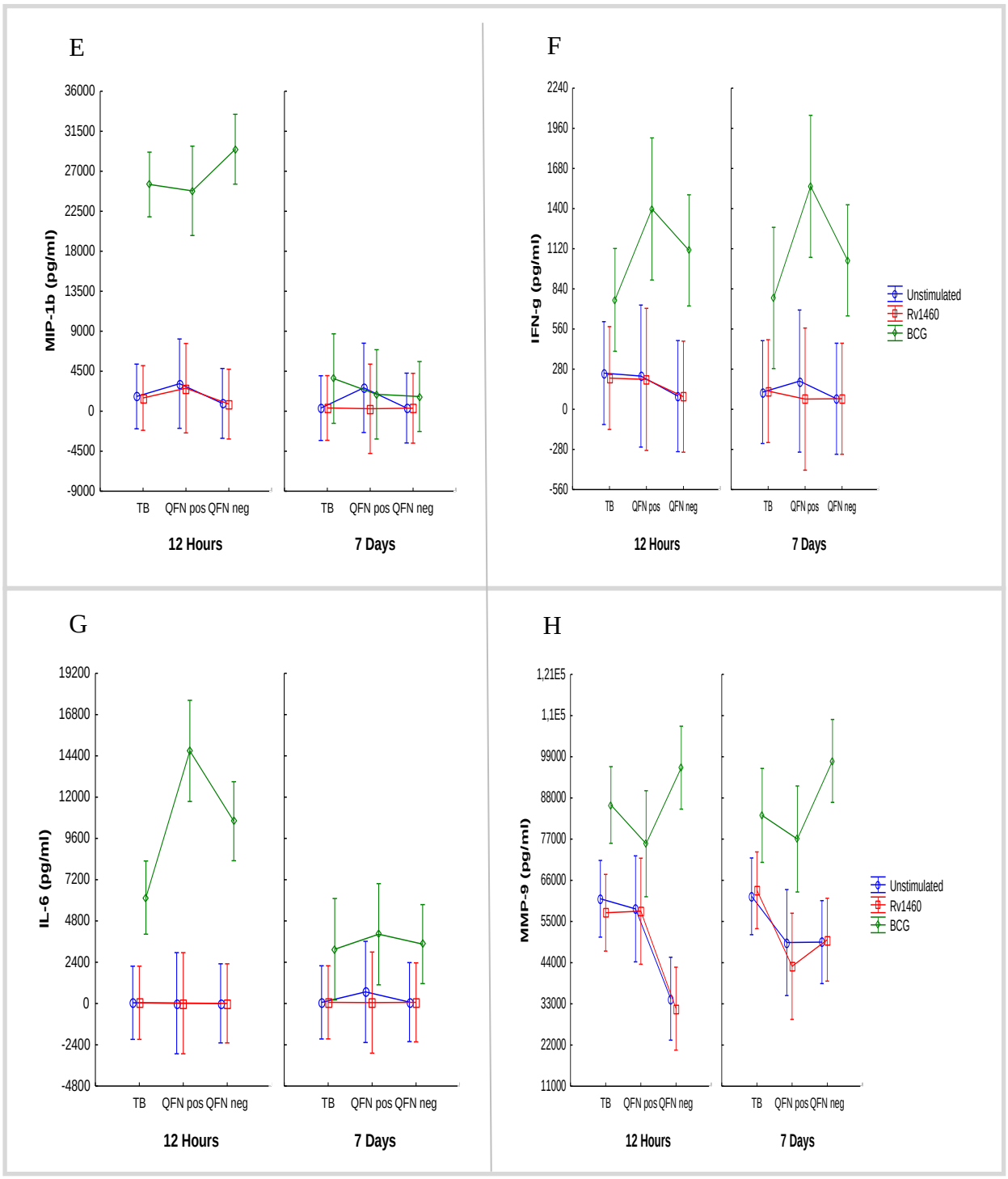

Figure 4.11: Luminex analysis of whole blood supernatant analyte concentrations measured in active TB (n = 20), QFN pos (n = 9) and QFN neg (n =17) groups. Whole blood from participants was left unstimulated or stimulated with Rv1460 and BCG for 12 hours and 7 days, respectively. Supernatant analytes (pg/ml) of (A) MCP-1, (B) RANTES, (C) IL-1b, (D) IL-8, (E) MIP-1b, (F) IFN-g, (G) IL-6 and (H) MMP-9 were measured. ANOVA test was performed to determine statistically significant differences between groups. Vertical bars denote 0.95 CI.

4.2.2 Analytes at recruitment (baseline) and month 6 of TB treatment

Table 4.2 list concentrations of the measured analytes at baseline (study enrolment) vs 6 months. No significant differences were observed in the levels of MCP-1, IFN-g and MMP-9 at baseline vs 6 months for all stimulated conditions following 12-hour stimulation. IL-1b (p = 0.00), MIP-1b (p = 0.00) and IL-6 (p = 0.00) showed significant differences following 12-hour BCG stimulation, while IL-8 showed significant difference following 12 hours of being unstimulated (p = 0.02) and Rv1460 (p = 0.01) stimulation. RANTES showed significant differences for all three stimulation conditions (p = 0.03, p = 0.00 and p = 0.00) respectively, following 12-hour stimulation. MCP-1 (p= 0.00), IL-8 (p = 0.00), IFN-g (p = 0.01) and IL-6 (p = 0.00) showed significant differences following 7-day BCG stimulation.

Table 4.2: List of the concentrations of measured analytes at Baseline (study enrolment) and Month 6

			MCP-1 (pg/ml)	RANTES (pg/ml)	IL-1b (pg/ml)	IL-8 (pg/ml)	MIP-1b (pg/ml)	IFN-g (pg/ml)	IL-6 (pg/ml)	MMP-9 (pg/ml)
Baseline	**12-hour**	**US**	1791.84	8421.98	25.95	804.66	1665.97	252.71	44.91	61074.43
		Rv1460	1755.37	8251.57	25.63	858.52	1497.77	187.09	42.17	57343.84
		BCG	4770.66	8511.06	3528.28	3662.99	25516.69	763.47	6158.53	86121.35
	7-day	**US**	731.53	741.11	13.40	481.49	350.48	120.03	65.61	61732.05
		Rv1460	809.32	613.50	14.86	37.02	371.87	127.05	68.94	63334.49
		BCG	8922.38	177.73	312.43	3101.51	3733.81	774.18	3169.22	83290.61
Month 6	**12-hour**	**US**	1695.84	11601.42	20.36	2163.87	1035.34	90.93	11.17	59141.73
		Rv1460	1639.38	14896.68	20.93	2441.32	1362.10	96.19	17.96	59710.41
		BCG	4049.66	15286.71	1111.75	4318.11	8151.35	740.41	2507.64	82267.88
	7-day	**US**	404.72	1268.28	20.36	235.01	1087.31	17.61	46.76	55609.35
		Rv1460	423.99	1129.24	5.76	228.35	455.09	17.61	31.21	54700.28
		BCG	927.58	1130.55	12.42	1229.93	516.48	38.67	7.109	63949.75

4.2.3 Flow cytometry analysis of lymphocyte receptors

4.2.3.1 CD4+ T cell subset- Baseline: 12-hour and 7-day assays

We performed phenotypic screening of CD4+, CD8+ and CD19+ cells after stimulating whole blood of active TB, QFN pos and QFN neg groups with Rv1460 (1 µg/ml) for 12

hours and 7 days, respectively. Three stimulation conditions, unstimulated, BCG and PHA stimulated were added to the experiments as controls.

The frequency of three pro-inflammatory cytokines IFN-g, TNF-a, and IL-2 and one anti-inflammatory cytokine IL-10 was measured in all the cell subtypes. Combinations of these four cytokines were also measured to determine the frequency of multifunctional T and B cells under the different stimulation conditions and the two timepoints**.**

Table 4.3 Shows the T cell subsets (CD4+, CD8+) and B cell (CD19+) cell count under the different stimulation conditions for the two timepoints. There were lower cell frequencies for all the subsets after 7-day stimulation when compared to the 12-hour assays. The number of cells in the unstimulated condition had also less cells when compared to the Rv1460, BCG and PHA stimulated populations. There was no significant difference in the percentages of the T cell and B cell subsets between the two timepoints.

Table 4.3: Lymphocyte subsets cell count by stimulation times and conditions

		Unstim			**Rv1460**			**BCG**			**PHA**		
		active TB	**QFN pos**	**QFN neg**	**active TB**	**QFN pos**	**QFN neg**	**active TB**	**QFN pos**	**QFN neg**	**active TB**	**QFN pos**	**QFN neg**
12-hour	**CD4+ (C)**	74918	76353	86340	70315	89549	90908	70796	86853	99021	62090	77245	68468
	CD4+	56.25	57.62	58.15	56.19	56.16	57.34	55.84	56.24	58	56.02	54.8	56.16
	CD8+(C)	50788	43417	57253	46060	53519	58813	51298	48951	62596	38670	47910	43589
	CD8+	37.25	34.28	34.51	37.36	35.08	35.18	37.45	35.54	34.75	37	36.79	34.41
	CD19+(C)	18191	13265	24046	16663	18421	24967	19124	17714	24247	15427	16017	18993
	CD19+	8.92	7.85	10.47	9.18	8.31	10.36	9.45	7.74	9.39	8.57	8.2	9.62
7-day	**CD4+ (C)**	6406	19209	25336	6590	21206	27346	5898	25876	27987	4467	20173	27096
	CD4+	64.94	65.24	64.42	56.51	58.34	59.62	51.99	65.32	57.88	55.95	52.87	57.21
	CD8+(C)	4242	9436	14608	5078	10824	16718	3825	11500	16970	2575	11627	16989
	CD8+	29.12	29.63	30.72	31.45	32.27	31.1	2.9.49	26.7	30.12	32.20	36.38	32.51
	CD19+(C)	903	3735	7754	1013	4929	7997	647	4644	7969	540	4995	7565
	CD19+	6.61	6.37	7.81	6.18	7.79	7.79	4.62	5.14	7.27	6.58	6.94	7.74

(C) represents count

The gating strategy of the phenotype screening and multifunction potential of the T and B cell are shown in Figure 4.12. There was no difference in the frequency of CD4+IFN-g+, CD4+TNF-a+, CD4+IL-2+, CD4+IL-10+ populations (Figure 4.13) in the active TB, QFN pos and QFN neg groups after 12 hours of being unstimulated and Rv1460 stimulation.

Significantly increased frequencies of CD4+IFN-g+ and CD4+IL-2+, was observed in the QFN neg ($p < 0.01$; $p < 0.01$) group when compared to active TB after 12-hour PHA stimulation. Significantly higher frequencies of CD4+TNF-a+ was measured in the QFN neg group ($p = 0.05$) compared to active TB after 12-hour BCG stimulation and QFN pos group ($p < 0.01$) and QFN neg group ($p < 0.01$) compared to active TB after 12-hour PHA stimulation. No differences were measured in the CD4+ cytokine frequencies following 12-hour Rv1460 stimulation (Figure 4.13).

For the 7-day stimulation assays, we also observed no significant difference in the frequencies of CD4+IFN-g+, CD+IL-2+, CD4+IL-10+ measured in the active TB, QFN pos and QFN neg groups in the unstimulated, Rv1460, BCG and PHA conditions. We did, however, observe significantly higher frequencies of CD4+TNF-a+ populations in the QFN pos group when compared to active TB ($p < 0.01$) and QFN neg groups ($p = 0.02$) after 7-day PHA stimulation. Also, significantly higher frequencies of CD4+TNF-a+ is measured in the active TB ($p < 0.01$), QFN pos ($p < 0.01$) and QFN neg groups ($p < 0.01$) after 7-day stimulation with Rv1460, BCG and PHA when compared the unstimulated populations (Figure 4.13).

Although not significant a higher frequency of CD4+IFNg+IL2+IL10-TNFa- multifunctional T cells can be seen in the QFN pos group when compared to active TB ($p = 0.28$) and QFN neg ($p = 0.13$) following 7-day stimulation with Rv1460. Twelve hours Rv1460 stimulation also showed significantly higher frequencies of CD4+IFNg-IL2+IL10-TNFa- multifunctional T cells in QFN neg group when compared to QFN pos ($p = 0.05$) group. Table 4.4 lists the frequencies of the CD4+ multifunctional subsets after 12-hour and 7-day stimulation with BCG and PHA. The greatest differences seem to be in the active TB vs QFN neg group after 12-hour BCG and PHA stimulation. Twelve hours and 7-day PHA stimulation showed significant differences in the CD4+IFNg-IL2+IL10-TNFa+ subsets of active TB vs QFN neg and QFN pos.

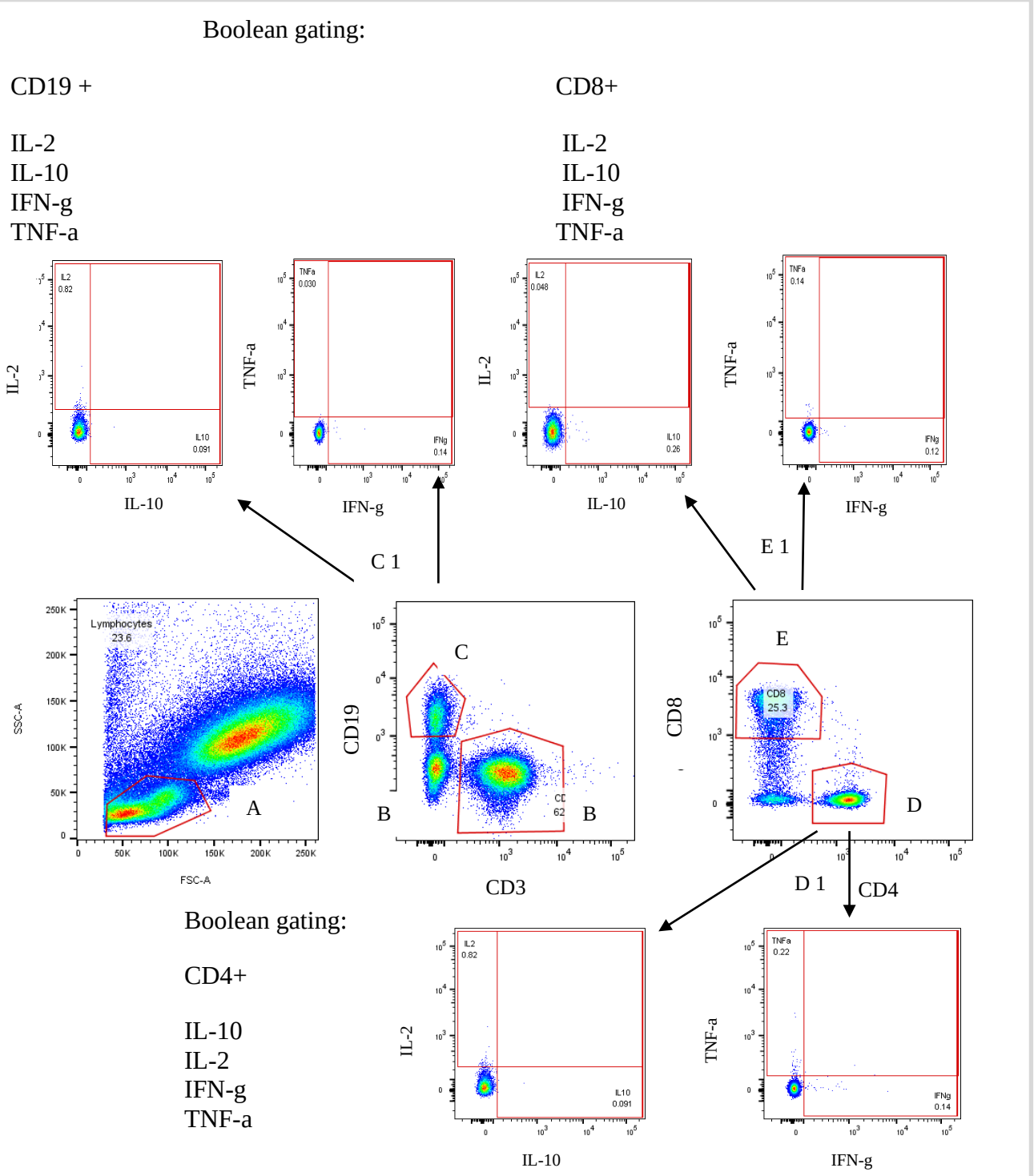

Figure 4.12: Gating strategy for analysis of phenotype screening of T and B cells. (A) Lymphocytes were gated on by plotting SSC-A vs FSC-A, followed by gating (B) CD3+ T cells and (C) CD19+ B cells (CD3-). T cells were further subdivided in (D) CD4+ and CD8+ T cells. Boolean gating strategy (C1, E1 and D1) was used to determine the frequencies of each potential combination cytokine produced by CD4+, CD8+ and CD19+.

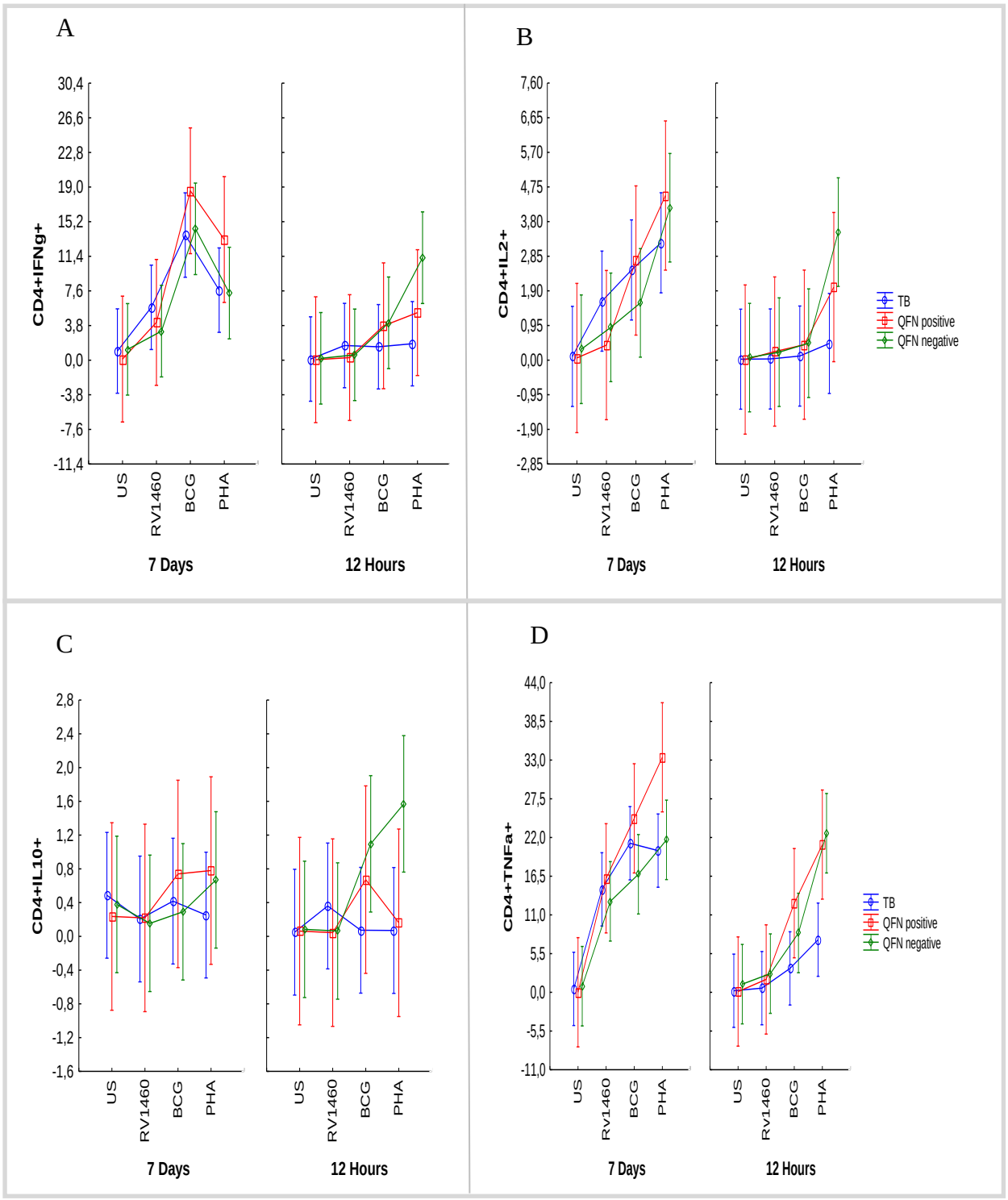

Figure 4.13: Flow cytometry phenotype screening of CD4+ T cell subsets in whole blood from active TB group (n=20), QFN pos group (n=9) and QFN neg group (n=17) after 12 hours and 7 days of being unstimulated and stimulated with Rv1460, BCG and PHA. The graph shows the CD4+ T cell subsets (A) CD4+IFN-g, (B) CD4+IL-2+, (C) CD4+IL-10+ and (D) CD4+TNF-a+. ANOVA test was performed to determine statistically significant differences between groups. Vertical bars denote 0.95 CI.

Table 4.4: List of multifunctional CD4+T cell subset frequencies of in active TB, QuantiFERON negative and QuantiFERON positive groups following BCG and PHA stimulation at 2 timepoints

		12-hour			7-day		
		Active TB VS QFN pos	Active TB VS QFN neg	QFN neg VS QFN pos	Active TB VS QFN pos	Active TB VS QFN neg	QFN neg VS QFN pos
CD4+IFNg+IL2+IL10+TNFa+	BCG	ns	Ns	ns	*p* = 0.01	ns	*P* = 0.00
	PHA	ns	*p* = 0.01	*p* = 0.05	ns	ns	ns
CD4+IFNg+IL2+IL10-TNFa+	BCG	ns	Ns	ns	ns	ns	ns
	PHA	ns	Ns	ns	ns	ns	ns
CD4+IFNg+IL2+IL10-TNFa-	BCG	ns	Ns	ns	ns	*p* = 0.00	*p* = 0.02
	PHA	ns	Ns	ns	ns	ns	ns
CD4+IFNg+IL2-IL10+TNFa+	BCG	ns	Ns	ns	ns	ns	*p* = 0.05
	PHA	ns	*p* = 0.00	*p* = 0.02	ns	ns	ns
CD4+IFNg+IL2-IL10-TNFa+	BCG	ns	Ns	ns	ns	ns	*P* = 0.03
	PHA	ns	Ns	ns	*p* = 0.05	ns	*p* = 0.04
CD4+IFNg+IL2-IL10-TNFa-	BCG	ns	Ns	ns	ns	*p* = 0.01	*p* = 0.02
	PHA	ns	*p* = 0.01	ns	ns	ns	ns
CD4+IFNg-IL2+IL10-TNFa+	BCG	ns	Ns	ns	ns	ns	ns
	PHA	*p* = 0.04	*p* = 0.00	ns	*p* = 0.03	*p* = 0.01	ns
CD4+IFNg-IL2+IL10-TNFa-	BCG	ns	Ns	ns	ns	ns	ns
	PHA	ns	*p* = 0.00	ns	ns	*p* = 0.00	P = 0.00
CD4+IFNg-IL2-IL10+TNFa+	BCG	ns	Ns	ns	ns	ns	ns
	PHA	ns	*p* = 0.01	ns	*p* = 0.02	ns	ns
CD4+IFNg-IL2-IL10+TNFa-	BCG	ns	*p* = 0.04	ns	ns	ns	ns
	PHA	ns	Ns	ns	ns	ns	ns
CD4+IFNg-IL2-IL10-TNFa+	BCG	*p* = 0.00	Ns	ns	ns	ns	ns
	PHA	*p* = 0.00	*p* = 0.00	ns	ns	*p* = 0.01	*p* = 0.00
CD4+IFNg-IL2-IL10-TNFa-	BCG	ns	Ns	ns	ns	ns	ns
	PHA	ns	*p* = 0.00	ns	*p* = 0.05	ns	ns

4.2.3.2 CD4+ T cell subset- Baseline vs Month 6

Table 4.5 summarizes the change in the CD4+ subsets and multifunctional CD4+ T cell subsets at baseline and month 6 over 2 stimulation timepoints and 4 stimulation conditions. We are merely discussing our findings; however, no conclusion can be made as the results of only four participants are being analysed. No change in the frequency of the subsets for baseline vs month 6 after 12-hour stimulation for all the stimulation conditions. For the naïve CD4+IFNg-IL2-IL10-TNFa- multifunctional T cell subset, we see an increase at month 6 after stimulation with Rv1460 (p = 0.08) and BCG (p = 0.08). These changes are not significant. Long term stimulation with BCG shows the greatest effects in the levels of the CD4+ subsets. The IFN-g+ (p = 0.02) and TNF-a+ (p = 0.00) levels are significantly decreased at month 6 vs baseline. A decrease is seen in the levels of CD4+IFNg+IL2-IL10+TNFa+ (p = 0.06) and CD4+IFNg+IL2-IL10-TNFa+ (p = 0.02) at month 6 vs baseline following 7-day BCG stimulation and CD4+IFNg-IL2+IL10-TNFa- (p = 0.03) following PHA stimulation.

Table 4.5: Summary of CD4+ subset: Baseline vs Month 6

	Baseline vs Month 6							
	12-hour				**7-days**			
	US	**Rv1460**	**BCG**	**PHA**	**US**	**Rv1460**	**BCG**	**PHA**
CD4+IFNg+	ns	ns	ns	ns	ns	ns	p = 0.02	ns
CD4+IL2+	ns	ns	ns	ns	ns	ns	ns	ns
CD4+IL10+	ns	ns	ns	ns	ns	ns	ns	ns
CD4+TNFa+	ns	ns	ns	ns	ns	ns	p = 0.00	ns
CD4+IFNg+IL2+IL10+TNFa+	ns	ns	ns	ns	ns	ns	ns	ns
CD4+IFNg+IL2+IL10-TNFa+	ns	ns	ns	ns	ns	ns	ns	ns
CD4+IFNg+IL2+IL10-TNFa-	ns	ns	ns	ns	ns	ns	ns	ns
CD4+IFNg+IL2-IL10+TNFa+	ns	ns	ns	ns	ns	ns	p=0.06*	ns
CD4+IFNg+IL2-IL10+TNFa-	ns	ns	ns	ns	ns	ns	ns	ns
CD4+IFNg+IL2-IL10-TNFa+	ns	ns	ns	ns	ns	ns	p = 0.02	ns
CD4+IFNg+IL2-IL10-TNFa-	ns	ns	ns	ns	ns	ns	ns	ns
CD4+IFNg-IL2+IL10-TNFa+	ns	ns	ns	ns	ns	ns	ns	ns
CD4+IFNg-IL2+IL10-TNFa-	ns	ns	ns	ns	ns	ns	ns	p= 0.03
CD4+IFNg-IL2-IL10+TNFa+	ns	ns	ns	ns	ns	ns	ns	ns
CD4+IFNg-IL2-IL10+TNFa-	ns	ns	ns	ns	ns	ns	ns	ns
CD4+IFNg-IL2-IL10-TNFa+	ns	ns	ns	ns	ns	ns	ns	ns
CD4+IFNg-IL2-IL10-TNFa-	ns	p=0.08*	p=0.08*	ns	ns	ns	p = 0.00	p= 0.02

ns = not significant; * not significant

4.2.3.3 CD8+ T cell subset - Baseline: 12-hour and 7-day assays

In the CD8+ subset there was no significant difference between active TB, QFN pos and QFN neg groups following 12 hours of being unstimulated, Rv1460 and BCG stimulated. Following 12-hour PHA stimulation significantly higher frequencies of CD8+IFN-g+ ($p < 0.01$), CD8+IL-2+ ($p = 0.05$) and CD8+TNF-a+ ($p < 0.01$) was seen in the QFN neg group ($p < 0.01$; $p = 0.05$ and $p < 0.01$) vs active TB after 12-hour PHA stimulation (Figure 4.14).

Significantly higher frequencies of CD8+IL-10+ ($p < 0.01$) and CD8+TNF-a+ ($p = 0.01$) were observed in the QFN pos respectively vs QFN neg following 7-day PHA stimulation (Figure 4.14). There was however no significant difference in the frequency of CD+IFN-g+ and CD+IL-2+ between active TB, QFN pos and QFN neg groups following 7-day Rv1460, BCG and PHA stimulation.

We observed significantly higher frequencies for CD8+IFN-g+ and CD8+TNF-a+ in the active TB, QFN pos and QFN neg group following 7-day Rv1460 stimulation compared to the unstimulated condition (Figure 4.14).

Higher frequencies (not significant) of the CD8+IFNg+IL2+IL10-TNFa- multifunctional T-cell subset in the active TB ($p = 0.09$) compared to the QFN pos group following 7-day Rv1460 stimulation. Increased frequencies of CD8+IFNg+IL2-IL10-TNFa+, CD8+IFNg+IL2-IL10-TNFa-, CD8+IFNg-IL2-IL10-TNFa+ multifunctional T cells were measured in all three groups after 7-day Rv1460 stimulation when compared to the unstimulated condition (Table 4.6).

Significantly higher frequencies were observed in the multifunction T cell subset CD8+IFNg+IL2-IL10+TNFa+ in QFN neg group compared to active TB ($p = 0.03$) and QFN pos group ($p = 0.01$) following 7-day PHA stimulation. Also, significantly higher frequencies were observed in the multifunction T cell subset CD8+IFNg-IL2-IL10+TNFa+ in the QFN pos group vs active TB ($p = 0.00$) and QFN neg group ($p = 0.01$) and in the QFN neg group vs active TB ($p = 0.02$) following 7-day PHA stimulation. Overall, we observed significantly higher frequencies of the multifunctional T cells following 7-day stimulation compared to 12-hour stimulation (Table 4.6).

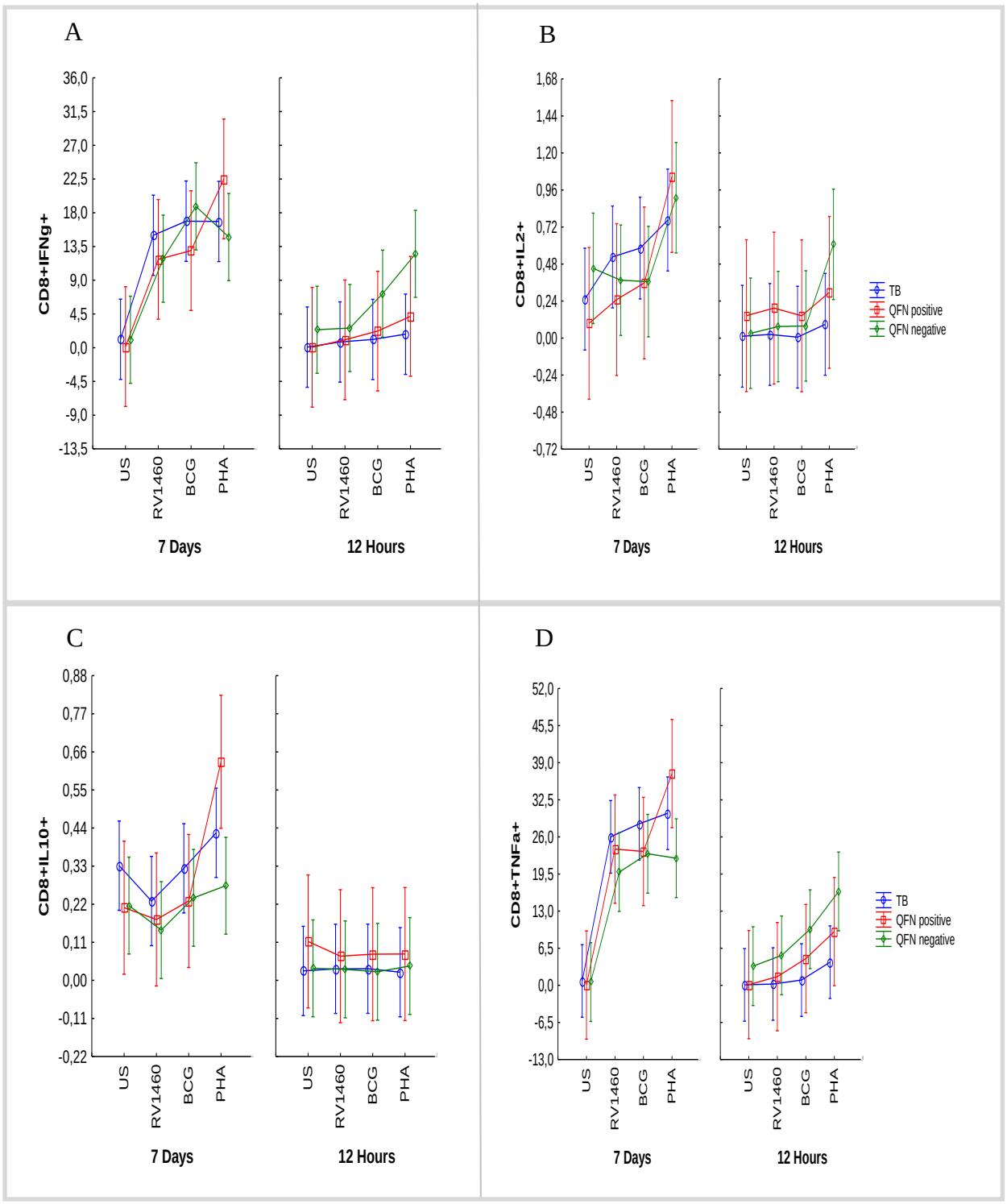

Figure 4.14: Flow cytometry phenotype screening of CD8+ T cell subset in whole blood from active TB group (n=20), QFN pos group (n=9) and QFN neg group (n=17) after 12 hours and 7 days of being unstimulated and stimulated with Rv1460, BCG and PHA. We measured the frequency of CD8+ T cell subsets (A) CD8+IFN-g, (B) CD8+IL-2+, (C) CD8+IL-10+ and (D) CD8TNF-a+ cells. ANOVA test was performed to determine statistically significant differences between groups. ANOVA test was performed to determine statistically significant differences between groups. Vertical bars denote 0.95 CI.

Table 4.6: List of multifunctional CD8+T cell subset frequencies of in active TB, QuantiFERON negative and QuantiFERON positive groups following BCG and PHA stimulation at 2 timepoints

		12-hour			7-day		
		Active TB VS QFN pos	Active TB VS QFN neg	QFN neg VS QFN pos	Active TB VS QFN pos	Active TB VS QFN neg	QFN neg VS QFN pos
CD8+IFNg+IL2+IL10+TNFa+	BCG	ns	ns	ns	ns	ns	ns
	PHA	ns	ns	ns	ns	ns	ns
CD8+IFNg+IL2+IL10-TNFa-	BCG	ns	ns	ns	ns	ns	ns
	PHA	ns	ns	ns	ns	ns	ns
CD8+IFNg+IL2-IL10+TNFa+	BCG	ns	ns	ns	ns	ns	ns
	PHA	ns	ns	ns	ns	$p = 0.03$	$p = 0.01$
CD8+IFNg+IL2-IL10+TNFa-	BCG	ns	ns	ns	$p = 0.03$	ns	ns
	PHA	ns	ns	ns	ns	ns	ns
CD8+IFNg+IL2-IL10-TNFa+	BCG	ns	$p = 0.03$	ns	ns	ns	ns
	PHA	ns	$p = 0.04$	ns	ns	$p = 0.04$	ns
CD8+IFNg-IL2+IL10-TNFa-	BCG	ns	ns	ns	ns	ns	ns
	PHA	ns	$p = 0.01$	ns	ns	ns	ns
CD8+IFNg-IL2+IL10-TNFa-	BCG	ns	ns	ns	ns	ns	ns
	PHA	ns	$p = 0.01$	ns	ns	ns	ns
CD8+IFNg-IL2+IL10-TNFa+	BCG	ns	ns	ns	ns	ns	ns
	PHA	ns	$p = 0.01$	ns	$p = 0.03$	ns	ns
CD8+IFNg-IL2+IL10-TNFa-	BCG	ns	ns	ns	ns	ns	ns
	PHA	ns	ns	ns	ns	ns	ns
CD8+IFNg-IL2-IL10+TNFa+	BCG	ns	ns	ns	ns	$p = 0.01$	ns
	PHA	ns	ns	ns	$p = 0.00$	$p = 0.02$	$p = 0.01$
CD8+IFNg-IL2-IL10+TNFa-	BCG	ns	ns	ns	ns	ns	ns
	PHA	ns	ns	ns	ns	ns	ns
CD8+IFNg-IL2-IL10-TNFa+	BCG	ns	ns	ns	ns	$p = 0.02$	ns
	PHA	ns	ns	ns	ns	ns	ns
CD8+IFNg-IL2-IL10-TNFa-	BCG	ns	ns	ns	ns	ns	ns
	PHA	ns	$p = 0.00$	ns	ns	ns	$p = 0.03$

4.2.3.4 CD8+ T cell subset - Baseline vs Month 6

Table 4.7 summarizes the change in the CD8+ subsets and multifunctional CD8+ T cell subsets at baseline and month 6 over 2 stimulation timepoints and 4 stimulation conditions. No change in the frequency of the subsets for baseline vs month 6 following 12-hour stimulation for all the stimulation conditions. Long term stimulation with Rv1460 showed a decrease in CD8+IFN-g+ (p = 0.08), CD8+IL-10+ (p = 0.06) and CD8+TNF-a+ (p = 0.00) levels at month 6 vs baseline. A decrease in the levels of CD8+IFNg-IL2-IL10-TNFa+ (p = 0.02) and increase in the levels of CD8+IFNg-IL2-IL10-TNFa- (p = 0.02) at month 6 vs baseline following 7-day Rv1460 stimulation. Long term stimulation with Rv1460, BCG and PHA had a greater effect on the CD8+ subsets when compared to the CD4+ subsets.

Table 4.7 Summary of CD8+ subset: Baseline vs Month 6

	Baseline vs Month 6							
	12-hour				**7-day**			
	US	**Rv1460**	**BCG**	**PHA**	**US**	**Rv1460**	**BCG**	**PHA**
CD8+IFNg+	ns	ns	ns	ns	ns	*p*=0.08*	*p*=0.03	*p*=0.05
CD8+IL2+	ns	ns	ns	ns	ns	ns	*p*=0.00	*p*=0.00
CD8+IL10+	ns	ns	ns	ns	*p*=0.02	*p*=0.06*	ns	*p*=0.09*
CD8+TNFa+	ns	ns	ns	ns	*p*=0.00	*p*=0.00	*p*=0.00	ns
CD8+IFNg+IL2+IL10+TNFa+	ND	ND	ND	ND	ND	ND	ND	ND
CD8+IFNg+IL2+IL10-TNFa+	ns	ns	ns	ns	ns	ns	ns	ns
CD8+IFNg+IL2+IL10-TNFa-	ns	ns	ns	ns	ns	ns	ns	ns
CD8+IFNg+IL2-IL10+TNFa+	ns	ns	ns	ns	ns	ns	ns	ns
CD8+IFNg+IL2-IL10+TNFa-	ns	ns	ns	ns	ns	ns	*p*=0.06*	ns
CD8+IFNg+IL2-IL10-TNFa+	ns	ns	ns	ns	ns	ns	*p*=0.06*	*p*=0.04
CD8+IFNg+IL2-IL10-TNFa-	ns	ns	ns	ns	ns	ns	*p*=0.04	ns
CD8+IFNg-IL2+IL10-TNFa+	ns	ns	ns	ns	ns	ns	ns	ns
CD8+IFNg-IL2+IL10-TNFa-	ns	ns	ns	ns	ns	ns	ns	ns
CD8+IFNg-IL2-IL10+TNFa+	ns	ns	ns	ns	ns	ns	*p*=0.01	ns
CD8+IFNg-IL2-IL10+TNFa-	ns	ns	ns	ns	*p*=0.03	ns	ns	ns
CD8+IFNg-IL2-IL10-TNFa+	ns	ns	ns	ns	ns	*p*=0.02	*p*=0.00	*p*=0.02
CD8+IFNg-IL2-IL10-TNFa-	ns	ns	ns	ns	ns	*p*=0.00	*p*=0.00	*p*=0.00

ns = not significant; * not significant; ND = not determined

4.2.3.5 CD19+ B cell subsets - Baseline: 12-hour and 7-day assays

For the B cell analysis, we saw no significant differences in the frequency of CD19+IFN-g+ and CD19+IL-10+ cells in the active TB, QFN pos and QFN neg groups after 12-hour stimulation with Rv1460, BCG and PHA. Higher frequencies of CD19+IL-2+ although not significant was measured in the QFN pos group (p = 0.07) when compared to active TB after 12-hour Rv1460 stimulation. There were also significantly higher levels of CD19+TNF-a+

measured in QFN neg group ($p < 0.01$) when compared to active TB group following 12-hour PHA stimulation (Figure 4.15).

No significant differences were observed in the CD19+IL-2+ levels in the three groups following 7-day Rv1460, PHA stimulation and the unstimulated conditions. Significantly higher levels of CD19+IFN-g+ cells in the QFN neg group when compared active TB (p = 0.03) and QFN pos (p = 0.02) following 7-day BCG stimulation. Significantly higher frequency of CD19+IL-10+ in the active TB group when compared to QFN pos (p = 0.01) and QFN neg (p =0.01) following 7-day BCG stimulation. Inversely, significantly lower frequencies of CD19+TNF-a+ in the active TB group when compared to QFN pos (p = 0.02) and QFN neg (p = 0.03) following 7-day PHA stimulation (Figure 4.15)

The CD19+IFNg-IL2+IL10-TNFa- multifunctional B cells were significantly increased in the QFN pos group (p = 0.02) when compared to active TB following 12-hour Rv1460 stimulation. We also observed significantly higher levels of CD19+IFNg-IL2-IL10-TNFa+ cells in the QFN neg group (p = 0.02) when compared to active TB following 7-days Rv1460 stimulation. Table 4.8 summarizes the multifunctional B cell frequencies in the three groups, following BCG and PHA stimulation.

4.2.3.6 CD19+ B cell subset- Baseline vs Month 6

Table 4.9 summarizes the change in the CD19+ subsets and multifunctional CD19+ T cell subsets at baseline and month 6 over 2 stimulation timepoints and 4 stimulation conditions. No significant change in the frequency of the subsets for baseline vs month 6 after 12-hour stimulation for all the stimulation conditions. Long term stimulation with Rv1460 show decrease in CD19+IFN-g+ (p = 0.05), CD19+IL-2+ and CD19+TNF-a+ (p = 0.02) levels at month 6 vs baseline. A decrease in the levels of CD19+IFNg+IL2-IL10+TNFa+ (p = 0.07), CD19+IFNg+IL2-IL10-TNFa+ (p = 0.05) and increase in the levels of CD19+IFNg-IL2-IL10-TNFa- (p = 0.01) at month 6 vs baseline following 7-day Rv1460 stimulation.

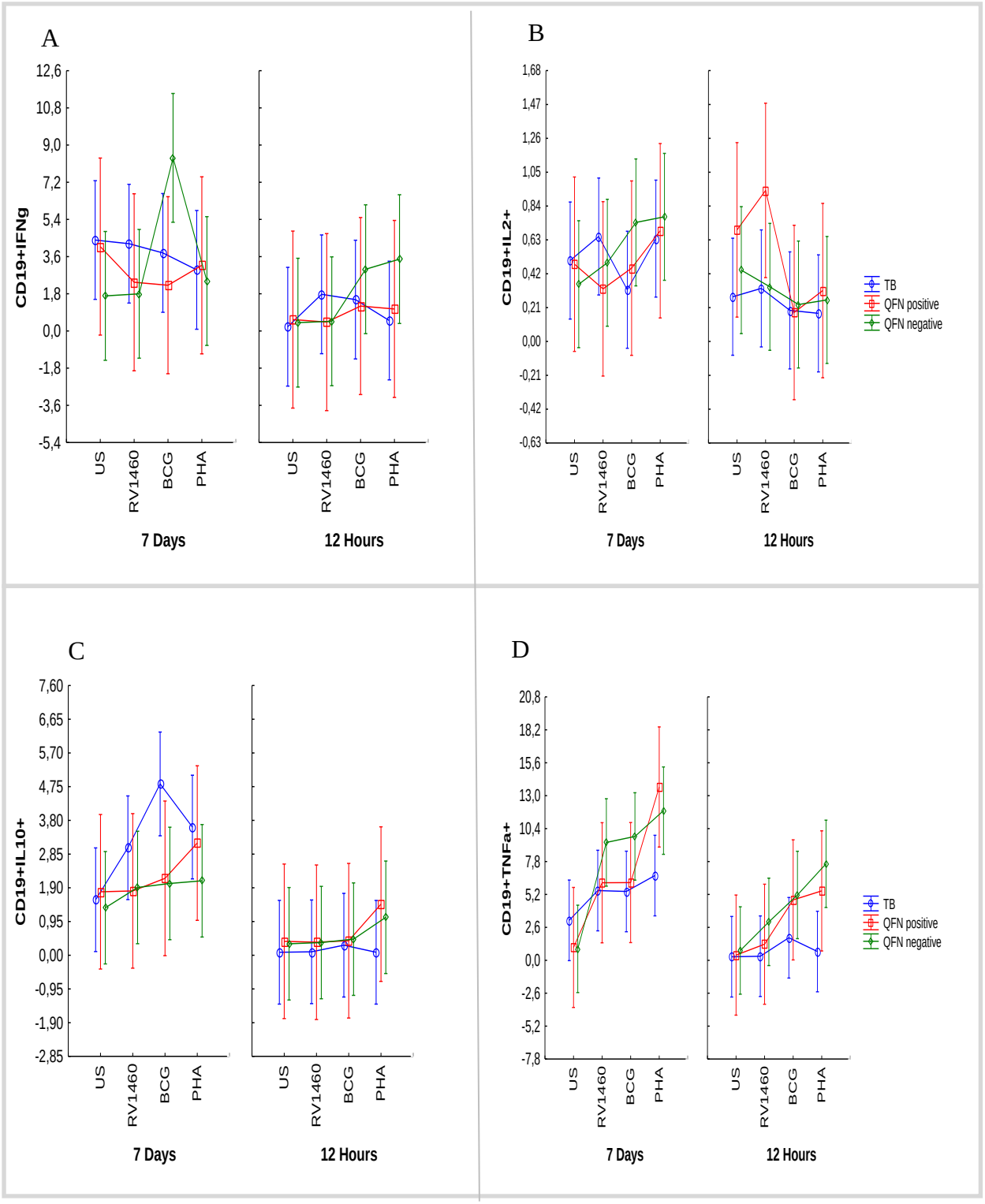

Figure 4.15: Flow cytometry phenotype screening of CD19+ B cell subset in whole blood from active TB group (n = 20), QFN pos group (n = 9) and QFN neg group (n = 17) after 12 hours and 7 days of being unstimulated (US) and stimulated with Rv1460, BCG and PHA. The CD19+ B cell subsets (A) CD19+IFN-g, (B) CD19+IL-2+, (C) CD19+IL-10+ and (D) CD19+TNF-a+. ANOVA test was performed to determine statistically significant differences between groups. ANOVA test was performed to determine statistically significant differences between groups. Vertical bars denote 0.95 CI.

Table 4.8: List of multifunctional CD19+ B cell subset frequencies of in active TB, QuantiFERON negative and QuantiFERON positive groups following BCG and PHA stimulation at 2 timepoints

		12-hour			7-day		
		Active TB VS QFN pos	ActiveTB VS QFN neg	QFN neg VS QFN pos	ActiveTB VS QFN pos	ActiveTB VS QFN neg	QFN neg VS QFN pos
CD19+IFNg+IL2-IL10+ TNFa+	BCG	ns	ns	ns	ns	$p = 0.01$	ns
	PHA	ns	ns	ns	ns	ns	ns
CD19+IFNg+IL2-IL10+ TNFa-	BCG	ns	ns	ns	ns	ns	ns
	PHA	ns	$p = 0.05$	ns	ns	ns	ns
CD19+IFNg+IL2-IL10- TNFa+	BCG	ns	ns	ns	ns	$p = 0.01$	$p = 0.02$
	PHA	ns	ns	ns	ns	ns	ns
CD19+IFNg+IL2-IL10- TNFa-	BCG	ns	ns	ns	ns	ns	$p = 0.04$
	PHA	ns	ns	ns	ns	ns	ns
CD19+IFNg-IL2-+IL10- TNFa-	BCG	ns	ns	ns	ns	ns	ns
	PHA	ns	ns	ns	ns	ns	ns
CD19+IFNg-IL2+IL10- TNFa+	BCG	ns	ns	ns	ns	ns	ns
	PHA	ns	ns	ns	ns	ns	ns
CD19+IFNg-IL2-IL10+ TNFa+	BCG	ns	$p = 0.01$	ns	ns	ns	ns
	PHA	$p = 0.03$	ns	ns	$p = 0.03$	ns	ns
CD19+IFNg-IL2-IL10+ TNFa-	BCG	ns	ns	ns	$p = 0.00$	$p = 0.01$	ns
	PHA	ns	ns	ns	ns	ns	ns
CD19+IFNg-IL2-IL10- TNFa+	BCG	ns	ns	ns	ns	ns	ns
	PHA	ns	$p = 0.01$	ns	$p = 0.02$	$p = 0.04$	ns
CD19+IFNg-IL2-IL10- TNFa-	BCG	ns	ns	ns	ns	ns	ns
	PHA	ns	$p = 0.01$	ns	ns	ns	ns

Table 4.9: Summary of CD19+ B cell subset: Baseline vs Month 6

	Baseline vs Month 6							
	12-hour				**7-day**			
	US	**Rv1460**	**BCG**	**PHA**	**US**	**Rv1460**	**BCG**	**PHA**
CD19+IFNg+	ns	ns	ns	ns	ns	*p*=0.05	ns	ns
CD19+IL2+	ns	ns	ns	ns	ns	*p*=0.08*	ns	ns
CD19+IL10+	ns	ns	ns	ns	ns	ns	*p*=0.07*	ns
CD19+TNFa+	ns	ns	ns	ns	ns	*p*=0.02	ns	*p*=0.04
CD19+IFNg+IL2+IL10+TNFa+	ND	ND	ND	ND	ND	ND	ND	ND
CD19+IFNg+IL2+IL10-TNFa+	ND	ND	ND	ND	ND	ND	ND	ND
CD19+IFNg+IL2+IL10-TNFa-	ND	ND	ND	ND	ND	ND	ND	ND
CD19+IFNg+IL2-IL10+TNFa+	ns	ns	ns	ns	ns	*p*=0.07*	ns	*p*=0.08*
CD19+IFNg+IL2-IL10+TNFa-	ns	ns	ns	ns	ns	ns	ns	ns
CD19+IFNg+IL2-IL10-TNFa+	ns	ns	ns	ns	ns	*p*=0.05	ns	ns
CD19+IFNg+IL2-IL10-TNFa-	ns	ns	ns	ns	ns	ns	ns	ns
CD19+IFNg-IL2+IL10-TNFa+	ns	ns	ns	ns	ns	ns	ns	ns
CD19+IFNg-IL2+IL10-TNFa-	ND	ND	ND	ND	ND	ND	ND	ND
CD19+IFNg-IL2-IL10+TNFa+	ns	ns	ns	ns	ns	ns	ns	ns
CD19+IFNg-IL2-IL10+TNFa-	ns	ns	ns	ns	ns	ns	ns	ns
CD19+IFNg-IL2-IL10-TNFa+	ns	ns	ns	ns	ns	ns	ns	*p*=0.01
CD19+IFNg-IL2-IL10-TNFa-	ns	ns	ns	ns	ns	*p*=0.01	*p*=0.05	ns

ns = not significant; * not significant; ND = not determined

Chapter 5: Discussion

Mtb a human adapted pathogen has found multiple ways to manipulate the host immune response during and after infection (113). The human immune response to Mtb infection is a highly complex cascade of reactions (114), with macrophages as preferred intracellular location (115). Within the alveolar macrophages several mechanisms take place to kill the bacilli such as vacuole acidification, proteases, antimicrobial peptides, reactive oxygen, nitrogen species and changes in ion flux (116). Interaction with the host through infection gives rise to expression of specific gene products for survival and multiplication within the host. The signals that the pathogens encounter during infection cause them to selectively express genes in response to signals (117).

The regulation of iron levels by the host plays a crucial role in the susceptibility and outcome of Mtb infection (91). Of interest is one of nature's most versatile biological prosthetic group, Fe-S clusters biosynthesis which is of major importance for mycobacterial survival (102). Iron-sulphur clusters are polynuclear combinations of iron and sulphur atoms, required by enzymes involved in multiple important cellular processes (118, 119). Mtb SUF system likely plays a fundamental role in the pathogen's intracellular survival, due to the fact that Fe-S cluster biosynthesis and repair are a crucial step for Mtb survival inside the macrophage (102).

Traditionally, investigation of Mtb genes that is specifically induced in infected macrophages requires the lysis of the macrophages and enumerating colony forming units and RNA extraction for RT-qPCR. This presents several challenges, including the low bacterial transcript levels relative to host RNA, and the inability to measure differential expression in individual bacterial cells. Reporter strains are powerful tools used to study Mtb physiology during infection studies using high throughput techniques like flow cytometry, microtiter plate assays and high-content microscopy (120).

A fluorescence reporter was constructed by cloning two regions (123 bp and 211 bp) upstream of a promoterless *mCherry* gene, to enable us to monitor *Rv1460* expression by fluorescence. We showed that the expression of the mCherry protein in the fluorescent strains had no effect on the growth of the fluorescent strains when compared to the wt control. This is in agreement with a study done by Carroll *et al* (2010) which showed that fluorescent reporter strains expressing mCherry showed no fitness defects *in vitro* and in macrophages and that FI signals are stable (121).

Flow cytometry is a tool used for the quantification of gene expression of fluorescent reporters on a single cell level (122) whereas fluorescence plate readers report on the mean response of a population (123). We used both a fluorescence spectrometer and flow cytometer to quantify mCherry expression by measuring the FI overtime. The optical density and FI measurements show a strong correlation. A study Bugalhão (2013) showed a linear correlation between optical density and fluorescent plate readouts (124). Fluorescent spectrometric analysis of the mean fluorescence intensity overtime showed a sigmoidal curve similar to the growth curves (OD_{600nm}).

We observed a fluorescent signal as early as day 4 (Figure 4.2 B) which increased by day 10 and plateauing between day 10 and 14. A statistically significant difference was observed in the fluorescent signal at day 14 for H37Rv_*attB*::pMV306_123mCherry (p = 0.008) (0.15fold) when compared to H37Rv_*attB*::pMV306_211mCherry. High background fluorescence was seen in the wt control, which increased overtime. However, the background fluorescence signal in the wt control was lower than the signal measured for fluorescent reporter strains. The high back ground fluorescence could be explained by autofluorescence of the plate, the media and the bacterial cells; the autofluorescence can dominate the signal from the fluorescent reporter (123). Culture medium that contains cellular extracts may also be a contributing factor to the high background fluorescence. One method in overcoming the autofluorescence in media is to wash the cultures with a washing agent like PBS, which has low background fluorescence (125). The bacterial cultures in Figure 4.4 and 4.5 showed less background fluorescence. These bacterial cultures were stored in PBS - 0.05% Tween-80 and washed and resuspended in PBS before flow cytometry analysis. Another contributing factor for the background fluorescence could be the intrinsic fluorescence of the cells. Cellular and structural components and metabolites within most organisms exhibit an intrinsic natural fluorescence (autofluorescence) (125, 126). The sigmoidal increase in the fluorescence observed for the control strain suggests that the autofluorescence of the cells are the major contributor to the background. The lower background signal seen with the flow cytometry analysis could also be attributed to a gate being set around the control cells without the reporter strain, showing only the fluorescent signals coming from the reporter strains.

As with the fluorescence spectrometry results we also observed a fluorescence signal as early as day 4 for the flow cytometric analysis (Figure 4.4). A statistically significant difference was observed for H37Rv_*attB*::pMV306_123mCherry ($p < 0.006$, $p < 0.001$ and $p < 0.001$) and H37Rv_*attB*::pMV306_211mCherry ($p < 0.004$, $p < 0.001$ and $p < 0.001$) at day 4, 10

and 14 when compared to wt control however no difference was observed overtime. Similar to the fluorescent spectrometry results a statistically significant difference was demonstrated between strains at day 14 with higher MFI signals for H37Rv_*attB*::pMV306_211mCherry (p = 0.000) (0.58fold) when compared to H37Rv_*attB*::pMV306_123mCherry.

The conditions for the bacterial cell preparation before analysis could also impact the results. Fresh growing bacterial cultures were analysed on the plate reader, whereas the bacterial cultures for flow cytometry analysis were fixed and stored in the dark at 4 ˚C prior to analysis. Fluorescence proteins maturation are affected by their environmental pH, and O_2 which is required for complete maturation. Proteins from DsRed can remain in an intermediate state until post translational maturation. Exposure to O_2 can take up to 1 – 2 hours for maturation (127). However according to Shaner *et al* (2005) the time for mCherry maturation is 15 min and 68 s to bleach (128). These experimental conditions could have an influence in the difference in the fluorescence signal observed between day 4 and 10 for the two techniques. The magnitude of the fold change for the two fluorescent reporters for both techniques are not significant. For the day 14 fluorescent analysis a fold change of less than 1 is seen between fluorescent reporter strains for both techniques. Both flow cytometry and fluorescent spectrometry have advantages and disadvantages although flow cytometry is sensitive in detecting smaller differences in expression and lower levels of background fluorescence.

RT-qPCR is another tool for quantification of gene expression generating reliable, reproducible, and biologically meaningful results. However, the quality of the RNA template is an important factor affecting the reproducibility and biological relevance of the results (129). In order to validate the use of fluorescence reporter strains as tool for the quantification of gene expression using flow cytometry or fluorescence spectrometry, we need to show that expression of *Rv1460* correlates with expression of *mCherry* and with fluorescence in the reporter strains. The *mCherry* transcript levels were much lower than *Rv1460* transcript levels, and the ratio of *Rv1460/mCherry* transcript did not remain constant over time in the different strains. A possible explanation for this is differences in the transcript stability for *mCherry* and *Rv1460*. A study analysing transcript stability in Mtb showed that the mean transcript stability was 9.5 min, which is significantly longer than most other prokaryotes (130). Although *Rv1460* was not measured in this study, the half-life of other genes in the same operon were calculated to be between 9 and 9.4 min. A lower transcript stability for *mCherry* mRNA could account for the lower transcript levels observed at all time points, and

result in an increase in the ratio of *Rv1460*/*mCherry* when *Rv1460* transcript levels rise in mid-log phase.

Our results showed an increase in the *Rv1460* transcript levels for both fluorescent reporters between day 4 and 10 similar to the fluorescent spectrometry. However, a decrease in transcript levels is seen between day 10 and 14, while the fluorescent signal for the fluorescent spectrometry plateaued. The median fluorescent intensity (flow cytometry) showed no difference over the three time points.

The FI signal seem to be stable at day 14 for both fluorescent quantification techniques but the day 14 RT-qPCR results show a decrease in the transcript levels for both *Rv1460* and *mCherry*. One suggestion can be an accumulation of the mCherry protein at day 14. Carroll *et al* (2010) demonstrated that mCherry is very stable since fluorescence was not diminished over 12 days after protein synthesis was inhibited by chloramphenicol. mCherry is therefore not subjected to high turnover rates by endogenous proteases. The authors showed a stable fluorescence signal from mCherry reporter even after long-term excitation (121). mCherry is therefore useful for measuring induction of a promoter but is unable to detect subsequent repression because of its long half-life.

Quantification of protein levels of Rv1460 within the WCL's of the fluorescent and wt strains was attempted by western blotting with custom made anti-Rv1460 antibody. However, we could not detect the levels of Rv1460 protein in the WCL, suggesting that the level of Rv1460 protein in the samples was lower than the limit of detection of the antibody and this prevented us quantifying the protein level by western blotting. It is important to quantify protein levels as mRNA transcript levels do not always correlate directly to protein levels, due to factors such as transcript stability, post-transcriptional and post-translational regulation (131). A more sensitive method, such as mass spectrometry, would therefore be required to investigate Rv1460 protein levels.

To evaluate *Rv1460* expression during intracellular growth, we infected a THP-1 macrophage like cell with H37Rv fluorescent reporter strains and an empty vector control. Our CFU results show no statistically significant differences in number of bacteria that were phagocytosed for either of the MOI's (2:1 and 5:1), however lower levels of H37Rv_*attB*::pMV306_211mCherry is being phagocytosed for both MOIs when compared to H37Rv_*attB*::pMV306_123mCherry and wt control (Figure 4.7). Lower survival of the bacteria within the host cells was observed for the higher MOI, which might be due to

increased death of the THP-1 cells because of the high bacterial burden (Figure 4.8 A and B). In the first 24 hours post infection bacterial numbers are relatively stable, while an increase in CFU between 24 and 48 hours was observed, indicative of replication. Raffetseder *et al* (2014) found that infection of human monocyte-derived macrophages (hMDMs) with Mtb H37Rv at a lower MOI of 1 showed no significant increase in replication for atleast 10 days, a period during which the viability of infected and uninfected cells was similar. The higher MOI of 10 showed significant increase in bacterial growth by day 7, followed by extensive cell death and increasing numbers of Mtb in the extracellular fraction. (132).

In vivo flow cytometric analysis (Figure 4.9 and 4.10) of the fluorescent reporters showed similar results as the *in vitro* flow cytometric analysis (Figure 4.4 and 4.5), with low fluorescent background observed for the wt control. We saw a lower fluorescent signal for the fluorescent strains for the flow cytometric analysis of these bacterial cultures which might be due to longer storage (> 3 weeks at 4˚C). We also see some variation in the fluorescent signal between the fluorescent strains overtime for fluorescent reporters. However, we see the greatest shift for both fluorescent reporters and both MOIs at the 72-hour time point, with the greatest shift seen in the H37Rv_*attB*::pMV306_211mCherry strain. Our results suggest that *Rv1460* expression is induced in a subset of bacteria within macrophages, and this population increases over the course of a 72-hour infection. Rhode *et al* (2007) investigated the Mtb global gene expression dynamics and cues during macrophage invasion. Delayed kinetics was exhibited by 76 genes that showed no increase in expression 2 hr post infection but were upregulated in the 24-hr phagosome. They found that extended periods of exposure to intracellular stressors led to up regulation of genes that were also induced *in vitro* by oxidative stress, including the *Rv1460-Rv1466* operon (107,108). Population heterogeneity for intracellular Mtb was demonstrated in a study by Mouton *et al* (2016), where they saw relatively homogeneous replication rates at early time points, very similar to those of *in vitro*-cultured bacteria. However, the emergence of a more slowly replicating population was noticed, suggesting a programmed adaptation to the intracellular environment (133). This highlights the need to investigate gene expression at a single cell level, as measuring changes in average expression may be unable to detect differences in these sub-populations.

Diagnosing TB is no simple matter. This is highlighted by the shortcomings of current immunodiagnostics for the detection of progression from LTBI to active TB and treatment monitoring of TB (29). It is important to stop the spread of infection by treating those who are likely to progress to disease. Currently our diagnostic toolbox is inadequate to achieve

these goals (134). The development of next-generation vaccines requires new antigens with the ability to safeguard against primary or reactivation TB disease (135).

We hypothesized that Rv1460 is expressed during intracellular growth and human infection and induces an immune response that confers diagnostic potential. Therefore, we assessed the immunogenicity of Rv1460 by direct *ex vivo* stimulation of whole blood samples from newly diagnosed and untreated active TB and QFN pos and QFN neg participants.

We assessed the immunogenicity of Rv1460 by measuring the levels of 8 whole blood supernatant analytes MCP-1, RANTES, IL-1b, IL-8, MIP-1b, IFN-g, IL-6, and MMP-9. Higher levels of IL-8 ($p = 0.08$) although not significant and significantly higher levels of MMP-9 ($p = 0.00$) in the active TB group when compared to the QFN neg group for the short-term stimulation (12 hours) with Rv1460 is suggestive of an effector or memory. However, this response was not unique to Rv1460 stimulation, similar results was shown for the unstimulated population. Monocytes and macrophages are primary producers of IL-8 when infected with Mtb however, neutrophils as well as respiratory epithelial cells also can secrete this chemokine. It has been shown that IL-8 is essential for granuloma formation (136). It is a strong neutrophil, monocyte, and T-cells chemoattractant. Increased levels of IL-8 are seen in the plasma and bronchoalveolar lavage (BAL) fluids of TB patients (137). Krupa *et al* 2015 has shown significantly higher IL-8 levels in BAL Fluids ($p < 0.001$) and plasma ($p < 0.02$) from TB patients than in normal subjects (136). MMP's are not expressed under normal circumstances but their overexpression is observed during inflammation. An increase in MMP-8 and MMP-9 are seen in pulmonary TB and reflects the severity of the destructive process (138). Preliminary findings in study by Araujo *et al* (2019) showed that MMP-9 differentiated between indigenous LTBI individuals from not infected controls (NIC) indigenous individuals. The authors concluded that MMP-9 may be useful as a potential biomarker in diagnosing LTBI and new infected Warao indigenous individuals who are progressing to active TB disease. (139). These gene expression results resemble our results where higher levels of MMP-9 are measured in the QFN pos and active TB group when compared to QFN neg group. The elevated IL-8 and MMP-9 in the active TB group seem to correlate with similar findings in literature. IL-8 stimulates the release of MMP-9 (gelatinase B) from neutrophils. A study by Van Den Steen *et al* (2000) demonstrated that MMP-9 processes IL-8 and other CXC chemokines and alters the specific activities and receptor usage. They showed activated neutrophil MMP-9 can convert natural and recombinant IL-8 (1-77) to IL-8 (7-77). The converted IL-8 (7-77) has been recovered from leukocytes and

fibroblasts being able to induce degranulation of the specific and MMP-9 containing granules from neutrophils (140). RANTES is involved in the selective attraction of memory T cells (141), a signalling molecule that is produced by T cells, macrophages, and a variety of cell types. It selectively attracts monocyte or macrophage in the airways inducing recruitment of memory T cells (142). Lee *et al* (2008) shown downregulation of RANTES in PBMCs from active TB when compared to healthy tuberculin reactors following stimulation with 30-kDa or TSP antigen. The authors suggest that altered RANTES production might play a valuable role in immunopathogenesis during TB (142). We showed significantly lower levels of RANTES in the active TB group after 12 hours when left unstimulated (p = 0.00 and p = 0.00), Rv1460 stimulated (p = 0.00 and p = 0.00) or BCG stimulated (p = 0.00 and p = 0.00) when compared to QFN pos and QFN neg groups respectively. A study done by Teklu *et al* (2018) showed quantitative changes for RANTES, both antigen stimulated and unstimulated blood plasma supernatants, with p values of 0.013 and 0.012, respectively, in active TB vs LTBI cases and 0.001 and 0.002, respectively, in active TB versus healthy controls (141). Our results for stimulated and unstimulated is similar, except that the levels of RANTES in our active TB group is significantly decreased when compared with LTBI and uninfected control group. No difference in the levels of MCP-1, IL-1b, MIP-1b, IFN-g and IL-6 in the active TB, QFN pos and QFN neg groups was observed following 12 hours unstimulated and Rv1460 stimulated conditions. As expected BCG stimulation showed increased levels for all analytes except for IL-1b and RANTES (following 7 days) for both time points when compared to the unstimulated and Rv1460 stimulated populations. IFN-g and MMP-9 levels showed similar patterns for 12-hour vs 7-day BCG stimulations.

T cells are pivotal in the host immune response against Mtb infection (143). Flow cytometry allows us to evaluate T and B cells that simultaneously produce two (bifunctional) or three (multifunctional) cytokines. In chronic viral infections such as HIV and hepatitis C virus multifunctional T cells have shown to play a crucial role associated with protection against infections (144). We evaluated conventional T cell subsets, CD4 and CD8 T cells whose roles correlate with protection and control of the intracellular Mtb (145).

Mono- and multifunctional specific CD4+ and CD8+ T-cell and CD19+ B cell responses were evaluated using flow cytometry analysis to see if these phenotypes can distinguish between active TB, LTBI and healthy controls. A study done by Lichtner *et al* (2015) showed slightly higher frequency of both “all IFN-g+” and “all IL-2+” CD4+ T cells in LTBI patients with respect to active TB patients (146). Short term stimulation with PHA shows higher

frequencies of CD4+IFN-g+, CD4+IL-2+ and CD4+TNF-a+ populations in QFN neg group ($p < 0.01$, $p < 0.01$ and $p < 0.01$) when compared to active TB. Higher frequencies of CD4+TNF-a+ was also seen in the QFN pos ($p < 0.01$) compared to active TB. BCG stimulation gives higher frequencies of CD4+TNF-a+ in QFN neg ($p < 0.01$) when compared to active TB. Our long term PHA stimulation showed significantly higher frequencies of CD4+TNF-a+ populations in the QFN pos group when compared to active TB ($p < 0.01$) and QFN neg groups ($p = 0.02$). Stimulation with Rv1460 did not alter the CD4+IFN-g+, CD4+IL-2+, CD4+TNF-a+ and CD4+IL-10+ frequencies in a way that would enable us to distinguish between groups. Although not significant, long term stimulation with of Rv1460 showed higher frequencies of CD4+IFNg+IL2+IL10-TNFa- multifunctional T cells in active TB group when compared to QFN neg ($p = 0.15$) and QFN pos ($p = 0.021$) group, while short term stimulation showed higher frequencies in CD4+IFNg-IL2+IL10-TNFa- subset in QFN neg group when compared to QFN pos ($p = 0.05$) group. Similar to our finding, Caccamo *et al* (2010) showed (short term stimulation) the percentage of CD4+ cells producing both IFN-g+ and IL-2+ was significantly increased in TB patients compared to LTBI subjects (147). The greatest differences were observed in the active TB vs QFN neg group following 12-hour BCG and PHA stimulation. Twelve hours and 7-day PHA stimulation showed significant differences in the CD4+IFNg-IL2+IL10-TNFa+ subset in active TB vs QFN neg and QFN pos groups.

Short term PHA stimulation showed higher frequencies of CD8+IFN-g+ ($p < 0.01$), CD8+IL-2+ ($p = 0.05$) and CD8+TNF-a+ ($p < 0.01$) in the QFN neg group compared to those with active TB (Figure 4.13). Lichtner *et al* (2015) showed higher frequency of CD8+IFN-g+ ($p = 0.0045$), CD8+IL-2+ ($p = 0.0033$) and TNF-a+ ($p = 0.0078$) in active TB vs healthy controls. Although no studies on IL-2 production by CD8 T cells in TB has been performed, it is thought that is important for T cell proliferation (146). Long term PHA stimulation gave significantly higher frequencies in CD8+IL-10+ and CD8+TNF-a+ in the QFN pos group ($p < 0.01$ and $p = 0.01$) when compared to QFN neg group (Figure 4.13). Stimulation with Rv1460 did not alter the CD8+IFN-g+, CD8+IL-2+, CD8+TNF-a+ and CD8+IL-10+ frequencies in a way that would enable us to distinguish between groups.

Multifunctional T-cell subset CD8+IFNg+IL2+IL10-TNFa- showed increase frequencies (not significant) in the active TB group ($p = 0.09$) compared to the QFN pos group following 7-day Rv1460 stimulation. Overall, there was a significantly higher frequency of the

multifunctional T cells after 7-day stimulation compared to 12- stimulation in the active TB group (Figure 4.13).

B-cells or B lymphocytes are a subtype of lymphocytes which have the primary role of secreting antibodies. When B cells are stimulated with whole organisms (like Mtb) or Toll-like receptors (TLR) antigens they develop the ability to produce pro- and anti-inflammatory cytokines. When activated by an Mtb antigen naïve B cells can develop into activated plasma cells which have the ability to secrete TB-specific antibodies and produce cytokines (148).

Analysis of B cells shows higher frequency of CD19+IL-2+ (not significant) in the QFN pos group (p = 0.07) when compared to active TB following 12-hour Rv1460 stimulation. There were also significantly higher levels of CD19+TNF-a+ in QFN neg group (p < 0.01) when compared to active TB following 12-hour PHA stimulation (Figure 4.14).

Long term stimulation with BCG gave significantly higher frequencies of CD19+IFN-g+ cells in the QFN neg group when compared to active TB (p = 0.03) and QFN pos (p = 0.02) and CD19+IL-10+ in the active TB group when compared to QFN pos (p = 0 .01) and QFN neg (p = 0.01). Inversely, significantly lower frequencies of CD19+TNF-a+ were seen in the active TB group when compared to QFN pos (p = 0.02) and QFN neg (p = 0.03) following stimulation with PHA (Figure 4.14). A statistically significantly higher frequency of CD19+IFNg-IL2+IL10-TNFa- multifunctional B cells in the QFN pos group (p = 0.02) when compared to active TB was observed following 12-hour Rv1460 stimulation. We also observed significantly higher levels of CD19+IFNg-IL2-IL10-TNFa+ cells in the QFN neg group (p = 0.02) when compared to active TB following 7-day Rv1460 stimulation.

Short term stimulation with Rv1460 gave higher frequency of CD19+IL-2+ subtypes and multifunctional subtype CD19+IFNg-IL2+IL10-TNFa- in QFN pos group when compared to active TB.

We wanted to assess the change if any in the analyte profile in the active TB patients after 6 months of being on TB treatment. No conclusion can be made from our results as the number of participants were only 4. However, we will discuss our findings. The frequencies of the CD4+ subsets did not change overtime, except for the BCG 7-day stimulation. CD4+IFN-g+ (p = 0.02), TNF-a+ (p = 0.00) CD4+ subsets and of CD4+IFNg+IL2-IL10+TNFa+ (p = 0.06) and CD4+IFNg+IL2-IL10-TNFa+ (p = 0.02) multifunctional subsets frequencies were lower at 6 months vs baseline. CD8+ subsets showed the greatest effect between baseline and 6 months following stimulation with, Rv1460, BCG and PHA. Stimulation with Rv1460 seems

to have a greater effect on the CD8+ and CD19+ subsets. Stimulation with Rv1460 show lowered frequencies in CD8+IFN-g+ (p = 0.08), CD8+IL-2+ and CD8+TNF-a+ (p = 0.00) levels at month 6 vs baseline. Decreased frequencies were seen the levels of CD8+IFNg-IL2-IL10-TNFa+ (p = 0.02) and increase in the levels of CD8+IFNg-IL2-IL10-TNFa- (p = 0.02) at month 6 vs baseline following 7-day Rv1460 stimulation. Stimulation with Rv1460 show decreased frequencies in CD19+IFN-g+ *(*p = 0.05), CD19+IL-2+ and CD19+TNF-a+ (p = 0.02) levels at month 6 vs baseline. A decrease in the levels of CD19+IFNg+IL2-IL10+TNFa+ (p = 0.07), CD19+IFNg+IL2-IL10-TNFa+ (p = 0.05) and increase in the levels of CD19+IFNg-IL2-IL10-TNFa- (p = 0.02) was seen at month 6 vs baseline following 7-day Rv1460 stimulation.

The immune response elicited by Rv1460 for both WBA and LPA were low. Rv1460 did not show a strong immune response for the Luminex analytes tested and did not seem to have strong discriminatory potential according to the flow cytometry, phenotypic screening. The Rv1460 concentration (1 µg/ml) we used might have been too low and therefore failed to elicit a strong immune response. Peptides instead of whole protein might also have elicited a better immune response.

Conclusion:

This study was undertaken to investigate the regulation of Rv1460 protein levels under standard conditions *in vitro* and intracellular growth within macrophages. Several studies have demonstrated that *Rv1460* is induced during intracellular growth in macrophage models. It was however unclear what the Rv1460 protein level is under these conditions, as well as the mechanisms involved in the regulation of these protein's levels. We therefore aimed to investigate the regulation of the level of Rv1460 protein by comparing the amount of *Rv1460* transcript and Rv1460 protein under standard culture conditions and determining protein levels within a macrophage infection model.

A fluorescent reporter was constructed by cloning two regions (123 bp and 211 bp) upstream of a promoterless *mCherry* gene, to enable us to monitor *Rv1460* expression by fluorescence. We showed that the expression of the mCherry protein in the fluorescent strains had no effect on the growth of the fluorescent strains when compared to the wt control.

Fluorescence spectrometry and flow cytometry was used to quantify the mCherry gene expression by measuring FI overtime. Florescence per cell was determined either by dividing fluorescence determined in a plate reader by colony forming units per well (RFU/CFU) or by flow cytometry. RFU/CFU measurements showed more than a 10X increase between day 4 and 10 for all three strains, while values remained constant between day10 and 14. Flow cytometry showed no increase in fluorescence between day 4, 10 and 14 for the two reporter strains with a 10-fold higher fluorescent signal in the reporter strains compared to wt-control. The plate reader results showed high background fluorescence in the wt control, which increased overtime. The high background fluorescence could be explained by autofluorescence of the plate, the media, and the bacterial cells. Flow cytometry was more sensitive in detecting smaller differences in expression and showed lower levels of background fluorescence.

To validate the use of fluorescence reporter strains as tool for the quantification of gene expression using flow cytometry or fluorescence spectrometry, we need to show that expression of *Rv1460* correlates with expression of *mCherry* and with fluorescence in the reporter strains. The *mCherry* transcript levels were much lower than *Rv1460* transcript levels and decreased between day 4 to 14 and the ratio of the two transcripts was not constant. Furthermore, while the increase in the *Rv1460* transcript levels for both fluorescent reporters between day 4 and 10 corresponded to an increase in the fluorescent spectrometry

measurement, the fluorescent signal plateaued between day 10 and 14 despite a decrease in transcript levels. The median fluorescent intensity (flow cytometry) showed no difference over the three time points. We concluded mCherry is useful for measuring induction of a promoter but is unable to detect subsequent repression because of its long half-life.

Measurement of Rv1460 protein levels in this study relied on the use of a custom generated antibody raised against purified recombinant Rv1460. This antibody was unable to detect Rv1460 protein in *M. tuberculosis* protein lysates, and therefore this objective could therefore not be achieved. Mass spectrometry-based methods, which are more sensitive, could be used to investigate this question in future.

To evaluate *Rv1460* expression during intracellular growth, we infected a THP-1 macrophage like cell with H37Rv fluorescent reporter strains and an empty vector control. We saw some variation in the fluorescent signal between the fluorescent strains over time. However, we saw the greatest shift for both fluorescent reporters and both MOIs at the 72-hour time point, with the greatest shift seen in the H37Rv_*attB*::pMV306_211mCherry strain. Our results suggest that *Rv1460* expression is induced in a subset of bacteria within macrophages, and this population increases over the course of a 72-hour infection.

Since Rv1460 levels are predicted to be elevated during intracellular growth and infection, we hypothesized that it is immunogenic and may induce an immune response in individuals infected with Mtb and might have a diagnostic potential. Of the 8 whole blood supernatant analytes assessed by Luminex technology, higher levels of IL-8 (not statistically significant) and MMP-9 was measured in the active TB group when compared to the QFN neg after short term stimulation with Rv1460. RANTES, a signalling molecule involved in the chemoattraction of memory T cells showed significantly lower levels in the active TB group when compared to the QFN neg and QFN pos group, for both time points. No difference in the levels of MCP-1, IL-1b, MIP-1b, IFN-g and IL-6 in the active TB, QFN pos and QFN neg groups following 12 hours unstimulated and Rv1460 stimulation conditions. Rv1460 did not seem to be highly immunogenic for the analytes measured.

Phenotype screening showed higher frequencies of CD4+IFNg+IL2+IL10-TNFa- multifunctional T cells in active TB group when compared to QFN neg (p = 0.15) and QFN pos (p = 0.021) group after 7-day Rv1460 stimulation, while short term stimulation showed higher frequencies in CD4+IFNg-IL2+IL10-TNFa- subset in QFN neg group when compared to QFN pos (p = 0.05) group. Multifunctional T-cell subset CD8+IFNg+IL2+IL10-TNFa-

showed increase frequencies (not significant) in the active TB group (p = 0.09) compared to the QFN pos group following 7-day Rv1460 stimulation. B cells analysis shows higher frequency of CD19+IL-2+ (not significant) in the QFN pos group (p = 0.07) when compared to active TB following 12-hour Rv1460 stimulation. A statistically significant higher frequency of CD19+IFNg-IL2+IL10-TNFa- multifunctional B cells in the QFN pos group (p = 0.02) when compared to active TB was observed following 12-hour Rv1460 stimulation. Higher frequencies of IL-2 in combination with IFN-g and TNF-a is seen in all three cell subsets. Increase frequencies of CD4+IFNg+IL2+IL10-TNFa- in QFN pos vs active TB and QFN neg respectively and CD4+IFNg-IL2+IL10-TNFa- showed increase frequencies in QFN neg groups vs QFN pos. The presence of Mtb infection may be demonstrated by the higher frequencies IL-2 through its participation in the initiation of the immune response against Mtb. It is also known to stimulate proliferation of T cells. Higher frequencies of IL-2 cytokine are also seen in the multifunctional CD8+ T and CD19+ B cells CD8+IFNg+IL2+IL10-TNFa- and CD19+IFNg-IL2+IL10-TNFa-. Higher frequencies of IL-2 and IFN-g, which plays an essential role in macrophage activation in combination with TNF-a which also play a role in Mtb control in the different subsets may demonstrate protective activity within the LTBI population. The discriminatory role of IL-2, TNF-a and IFN-g may be explored further with higher stimulation concentrations of Rv1460.

Limitations and future studies

The results in this study are predominantly negative but has highlighted the need for future studies addressing the shortcomings of this study.

The first objective was to investigate regulation of Rv1460 protein levels by comparing the amount of *Rv1460* transcript and Rv1460 protein under standard culture conditions, however this could not be achieved because of the low sensitivity of the antibody. The antibody used in this study was generated by immunisation of rabbits with recombinant Rv1460 protein that was produced and purified from *E. coli*. The *E. coli* expression system is a simple system, with short generation time and generating a high yield. However, the system may lack enzymes needed for post-translational modification, resulting in protein products that are not properly folded. Improperly folded Rv1460 protein might be one of the reasons that the protein could not be detected within the H37Rv WCL's since the native epitopes may not be present in the recombinantly produced protein. Mass spectrometry-based methods, which are more sensitive, could be used to investigate this question in future.

Improperly folded Rv1460 protein might also be the reason for the low immunogenic activity of the protein due to the inability of the epitopes to stimulate an immune response in the whole blood of study participants. It would be beneficial to express the protein in a mycobacterial expression system and repeat all the experiments.

However, it would be interesting to see the regulation of Rv1460's transcript and protein levels during oxidative stress and iron limiting conditions, since these conditions mimic the intracellular environment the bacilli experience within the host.

It would also be beneficial to have a dual reporter system with *Rv1460* as our gene of interest and normalizing with *sigA* as a reference gene. This study may further benefit by constructing a second dual reporter construct with one of the downstream genes of the SUF operon as a control.

The plate reader results showed high background fluorescence in the wt control, which increased overtime. Background fluorescence can be decreased by washing and resuspending the bacterial cultures in PBS before analysis. Background fluorescence can also be decreased by using spectral or linear unmixing to remove autofluorescence (Lichten *et al*, 2014). They use a single excitation wavelength, but measure emission at two wavelengths rather than one. The emission spectrum of autofluorescence is broader than that of the enhanced GFP and

they can infer the extent of the autofluorescence emission in the wavelengths used for the fluorescent reporter from the autofluorescence emission measured at a higher wavelength

Due to financial constraints only a limited number of whole blood supernatant analytes could be investigated. It would be interesting to evaluate the immunogenicity of Rv1460 protein with a range of titrated concentrations of the recombinant protein in an unbiased fashion amongst the different diseased groups.

Finally, future studies may benefit from using fluorescent proteins with a faster maturation time as well as a shorter half-life.

References:

1. Sakula A. Robert Koch: centenary of the discovery of the tubercle bacillus, 1882. Thorax. 1982 Apr;37(4):246–51.

2. Cardona P-J. What We Have Learned and What We Have Missed in Tuberculosis Pathophysiology for a New Vaccine Design: Searching for the "Pink Swan." Front Immunol 2017 May 15;8:556

3. World Health Organization. Global tuberculosis report 2019. Geneva: World Health Organization; 2019.

4. Brighenti S, Lerm M. How Mycobacterium tuberculosis Manipulates Innate and Adaptive Immunity – New Views of an Old Topic. In: Understanding Tuberculosis – Analyzing the Origin of Mycobacterium Tuberculosis Pathogenicity. IntechOpen; 2012. 10.5772\29651

5. Sakamoto K. The Pathology of Mycobacterium tuberculosis Infection. Vet Pathol. 2012 May 1;49(3):423–39.

6. Cook GM, Berney M, Gebhard S, Heinemann M, Cox RA, Danilchanka O, et al. Physiology of Mycobacteria. Adv Microb Physiol. 2009; 55:81–319.

7. Abel L, El-Baghdadi J, Bousfiha AA, Casanova J-L, Schurr E. Human genetics of tuberculosis: a long and winding road. Philos Trans R Soc Lond B Biol Sci. 2014 Jun 19;369(1645).

8. Gideon HP, Flynn JL. Latent tuberculosis: what the host "sees"? Immunol Res. 2011 Aug;50(0):202–12.

9. Chaves AS, Rodrigues MF, Mattos AMM, Teixeira HC. Challenging Mycobacterium tuberculosis dormancy mechanisms and their immunodiagnostic potential. Braz. j. infect. dis. 2015 Nov 1;19(6):636–42.

10. Flynn JL, Chan J. Tuberculosis: Latency and Reactivation. Infect Immun. 2001 Jul;69(7):4195–201.

11. Kiazyk S, Ball T. Latent tuberculosis infection: An overview. Can Commun Dis Rep. 2017 Mar 2;43(3–4):62–6.

12. Ottenhoff THM. New pathways of protective and pathological host defense to mycobacteria. Trends Microbiol. 2012 Sep;20(9):419–28.

13. Raviglione M, Sulis G. Tuberculosis 2015: Burden, Challenges and Strategy for Control and Elimination. Infect Dis Rep. 2016 Jun 24;8(2):6570.

14. Kasprowicz VO, Churchyard G, Lawn SD, Squire SB, Lalvani A. Diagnosing Latent Tuberculosis in High-Risk Individuals: Rising to the Challenge in High-Burden Areas. J Infect Dis. 2011 Nov 15;204(Suppl 4):S1168–78.

15. Seung KJ, Keshavjee S, Rich ML. Multidrug-Resistant Tuberculosis and Extensively Drug-Resistant Tuberculosis. Cold Spring Harb Perspect Med. 2015 Sep;5(9):a017863.

16. Vekemans J, O'Brien KL, Farrar J. Tuberculosis vaccines: Rising opportunities. PLOS Med. 2019 Apr 23;16(4):e1002791.

17. TB-Strategy-WEB.pdf. Available from: https://www.finddx.org/wp-content/uploads/2016/02/TB-Strategy-WEB.pdf

18. Nahid P, Pai M, Hopewell PC. Advances in the Diagnosis and Treatment of Tuberculosis. Proc Am Thorac Soc. 2006 Mar;3(1):103–10.

19. Catanzaro A, Perry S, Clarridge JE, Dunbar S, Goodnight-White S, LoBue PA, et al. The Role of Clinical Suspicion in Evaluating a New Diagnostic Test for Active Tuberculosis: Results of a Multicenter Prospective Trial. JAMA. 2000 Feb 2;283(5):639–45.

20. Biya O, Gidado S, Abraham A, Waziri N, Nguku P, Nsubuga P, et al. Knowledge, care-seeking behavior, and factors associated with patient delay among newly-diagnosed pulmonary tuberculosis patients, Federal Capital Territory, Nigeria, 2010. Pan Afr Med J. 2014 Jul 21;18(Suppl 1).

21. Osei E, Akweongo P, Binka F. Factors associated with DELAY in diagnosis among tuberculosis patients in Hohoe Municipality, Ghana. BMC Public Health. 2015 Dec;15(1).

22. Ryu YJ. Diagnosis of Pulmonary Tuberculosis: Recent Advances and Diagnostic Algorithms. Tuberc Respir Dis (Seoul). 2015 Apr;78(2):64–71.

23. Rossato Silva D, Müller AM, de Tarso Roth Dalcin P. Factors associated with delayed diagnosis of tuberculosis in hospitalized patients in a high TB and HIV burden setting: a cross-sectional study. BMC Infect Dis. 2012 Mar 15;12:57.

24. Teixeira HC, Abramo C, Munk ME. Immunological diagnosis of tuberculosis: problems and strategies for success. J Bras Pneumol. May-Jun 2007;33(3):323-34.

25. Kaufmann, Stefan H.E., Parida, Shreemanta K. Tuberculosis in Africa: Learning from Pathogenesis for Biomarker Identification. Cell Host & Microbe. 2008 Sep 11;4(3):219–28.

26. Abraham PR, Devalraju KP, Jha V, Valluri VL, Mukhopadhyay S. PPE17 (Rv1168c) protein of Mycobacterium tuberculosis detects individuals with latent TB infection. PLoS ONE. 2018 Nov 28;13(11):e0207787

27. CAO Shu Hui, CHEN Yan Qing, SUN Yong, LIU Yang, ZHENG Su Hua, ZHANG Zhi Guo, et al. Screening of Serum Biomarkers for Distinguishing between Latent and Active Tuberculosis Using Proteome Microarray. Biomed Environ Sci. 2018;31(7):515–26.

28. Sharma SK, Vashishtha R, Chauhan LS, Sreenivas V, Seth D. Comparison of TST and IGRA in Diagnosis of Latent Tuberculosis Infection in a High TB-Burden Setting. PLoS One. 2017 Jan 6;12(1).

29. Chegou NN, Heyckendorf J, Walzl G, Lange C, Ruhwald M. Beyond the IFN-c horizon: biomarkers for immunodiagnosis of infection with Mycobacterium tuberculosis. Eur Respir J. 2014;43(5):1472–1486.

30. Ghiasi M, Pande T, Pai M. Advances in Tuberculosis Diagnostics. Curr Trop Med Rep. 2015 Jun;2(2):54–61.

31. Mulder C, Mgode G, Reid SE. Tuberculosis diagnostic technology: an African solution … think rats. Afr J Lab Med. 2017 Mar 31;6(2):420.

32. Boehme CC, Nabeta P, Hillemann D, Nicol MP, Shenai S, Krapp F, et al. Rapid Molecular Detection of Tuberculosis and Rifampin Resistance. N Engl J Med. 2010 Sep 9;363(11):1005–15.

33. Jurado LF, Palacios DM. Tuberculosis: A Risk Factor Approach. 10.5772/intechopen.73538 (2018)

34. Dutta NK, Karakousis PC. Latent Tuberculosis Infection: Myths, Models, and Molecular Mechanisms. Microbiol Mol Biol Rev. 2014 Sep;78(3):343–71.

35. Berkowitz N, Okorie A, Goliath R, Levitt N, Wilkinson RJ, Oni T. The prevalence and determinants of active tuberculosis among diabetes patients in Cape Town, South Africa, a high HIV/TB burden setting. Diabetes Res and Clin Pract. 2018 Apr;138:16–25.

36. Kirenga BJ, Ssengooba W, Muwonge C, Nakiyingi L, Kyaligonza S, Kasozi S, et al. Tuberculosis risk factors among tuberculosis patients in Kampala, Uganda: implications for tuberculosis control. BMC Public Health. 2015 Jan 21;15.

37. Brighenti S, Joosten SA. Friends and foes of tuberculosis: modulation of protective immunity. J Intern Med. 2018;284(2):125–44.

38. Marais BJ, Lönnroth K, Lawn SD, Migliori GB, Mwaba P, Glaziou P, et al. Tuberculosis comorbidity with communicable and non-communicable diseases: integrating health services and control efforts. Lancet Infect Dis. 2013 May;13(5):436–48.

39. Kumar NP, Banurekha VV, Nair D, Dolla C, Kumaran P, Babu S. Modulation of iron status biomarkers in tuberculosis-diabetes co-morbidity. Tuberculosis (Edinb). 2018 Jan;108:127–35.

40. Workneh MH, Bjune GA, Yimer SA. Prevalence and associated factors of tuberculosis and diabetes mellitus comorbidity: A systematic review. PLoS One. 2017 Apr 21;12(4).

41. Bastos HN, Osório NS, Gagneux S, Comas I, Saraiva M. The Troika Host–Pathogen–Extrinsic Factors in Tuberculosis: Modulating Inflammation and Clinical Outcomes. Front Immunol. 2018 Jan 9;8:1948

42. Verver S, Warren RM, Beyers N, Richardson M, van der Spuy GD, Borgdorff MW, et al. Rate of Reinfection Tuberculosis after Successful Treatment Is Higher than Rate of New Tuberculosis. Am J Respir Crit Care Med. 2005 Jun 15;171(12):1430–5.

43. Uys P, Brand H, Warren R, van der Spuy G, Hoal EG, van Helden PD. The Risk of Tuberculosis Reinfection Soon after Cure of a First Disease Episode Is Extremely High in a Hyperendemic Community. Mistry N, editor. PLOS ONE. 2015 Dec 9;10(12):e0144487.

44. Zignol M, Wright A, Jaramillo E, Nunn P, Raviglione MC. Patients with Previously Treated Tuberculosis No Longer Neglected. Clin Infect Dis. 2007 Jan;44(1):61–4.

45. Valencia DN. Brief Review on COVID-19: The 2020 Pandemic Caused by SARS-CoV-2. Cureus. 2020 March 12(3) e7386.

46. Coperchini F, Chiovato L, Croce L, Magri F, Rotondi M. The Cytokine storm in COVID-19: An overview of the involvement of the chemokine/chemokine-receptor system. Cytokine Growth Factor Rev. 2020 May 11; 53:25-32.

47. Liu Y, Bi L, Chen Y, Wang Y, Fleming J, Yu Y, et al. Active or latent tuberculosis increases susceptibility to COVID-19 and disease severity. Infectious Diseases (except HIV/AIDS); 2020 Mar. http://medrxiv.org/lookup/doi/10.1101/2020.03.10.20033795

48. Li X, Geng M, Peng Y, Meng L, Lu S. Molecular immune pathogenesis and diagnosis of COVID-19. J Pharm Anal. 2020 Apr;10(2):102-108.

49. Ye Z-W, Yuan S, Yuen K-S, Fung S-Y, Chan C-P, Jin D-Y. Zoonotic origins of human coronaviruses. Int J Biol Sci. 2020 Mar 15;16(10):1686–97.

50. Raoult D, Zumla A, Locatelli F, Ippolito G, Kroemer G. Coronavirus infections: Epidemiological, clinical and immunological features and hypotheses. Cell Stress. 2020 April;4(4):66-75.

51. Motta I, Centis R, D'Ambrosio L, García-García J-M, Goletti D, Gualano G, et al. Tuberculosis, COVID-19 and migrants: preliminary analysis of deaths occurring in 69 patients from two cohorts. Pulmonol. 2020 May 14;26(4):233-240.

52. Singh A, Gupta A, Das K. Severe Acute Respiratory Syndrome Coronavirus-2 and Pulmonary Tuberculosis Coinfection: Double Trouble. Resarch Square. 2020; doi:10.21203/rs.3.rs-22464/v4. PPR:PPR199906.

53. Togun T, Kampmann B, Stoker NG, Lipman M. Anticipating the impact of the COVID-19 pandemic on TB patients and TB control programmes. Ann Clin Microbiol Antimicrob. 2020 May 23;19(1).

54. Nema V. Tuberculosis diagnostics: Challenges and opportunities. Lung India. 2012;29(3):259–66.

55. Weiner J, Kaufmann SHE. Recent advances towards tuberculosis control: vaccines and biomarkers. J Intern Med. 2014 May;275(5):467–80.

56. Walzl G, McNerney R, Plessis N du, Bates M, McHugh TD, Chegou NN, et al. Tuberculosis: advances and challenges in development of new diagnostics and biomarkers. Lancet Infect Dis. 2018 Jul 1;18(7):e199–210.

57. Goletti D, Petruccioli E, Joosten SA, Ottenhoff THM. Tuberculosis Biomarkers: From Diagnosis to Protection. Infect Dis Rep. 2016 Jun 24;8(2):6568

58. Burel JG, Babor M, Pomaznoy M, Lindestam Arlehamn CS, Khan N, Sette A, et al. Host Transcriptomics as a Tool to Identify Diagnostic and Mechanistic Immune Signatures of Tuberculosis. Front Immunol. 2019 Feb 19;10:221

59. Mangtani P, Abubakar I, Ariti C, Beynon R, Pimpin L, Fine PEM, et al. Protection by BCG Vaccine Against Tuberculosis: A Systematic Review of Randomized Controlled Trials. Clin Infect Dis. 2014 Feb 15;58(4):470–80.

60. McShane H. Editorial Commentary: Understanding BCG Is the Key to Improving It. Clin Infect Dis. 2014 Feb 15;58(4):481–2.

61. Michelsen SW, Soborg B, Koch A, Carstensen L, Hoff ST, Agger EM, et al. The effectiveness of BCG vaccination in preventing *Mycobacterium tuberculosis* infection and disease in Greenland. Thorax. 2014 Sep;69(9):851–6.

62. Angelidou A, Diray-Arce J, Conti MG, Smolen KK, Haren SD van, Dowling DJ, et al. BCG as a Case Study for Precision Vaccine Development: Lessons From Vaccine Heterogeneity, Trained Immunity, and Immune Ontogeny. Front Microbiol. 2020;11:332

63. McShane H, Jacobs WR, Fine PE, Reed SG, McMurray DN, Behr M, et al. BCG: Myths, realities, and the need for alternative vaccine strategies. Tuberculosis (Edinb). 2012 May;92(3):283–8.

64. Zimmermann P, Finn A, Curtis N. Does BCG Vaccination Protect Against Nontuberculous Mycobacterial Infection? A Systematic Review and Meta-Analysis. J Infect Dis. 2018 Jul 24;218(5):679–87.

65. Poyntz HC, Stylianou E, Griffiths KL, Marsay L, Checkley AM, McShane H. Non-tuberculous mycobacteria have diverse effects on BCG efficacy against Mycobacterium tuberculosis. Tuberculosis (Edinb). 2014 May;94(3):226–37.

66. Pang Y, Tan Y, Chen J, Li Y, Zheng H, Song Y, et al. Diversity of nontuberculous mycobacteria in eastern and southern China: a cross-sectional study. Eur Respir J. 2017 Mar;49(3):1601429.

67. Baldwin SL, Larsen SE, Ordway D, Cassell G, Coler RN. The complexities and challenges of preventing and treating nontuberculous mycobacterial diseases. PLoS Negl Trop Dis. 2019 Feb 14;13(2).

68. Valadas E. Nontuberculous Mycobacteria: Clinical Importance and Relevance to Bacille Calmette-Guerin Vaccination. Clin Infect Dis. 2004 Aug 15;39(4):457–8.

69. Kak G, Raza M, Tiwari BK. Interferon-gamma (IFN-γ): Exploring its implications in infectious diseases. BioMol Concepts. 2018;9:64–79.

70. Thakur A, Mikkelsen H, Jungersen G. Intracellular Pathogens: Host Immunity and Microbial Persistence Strategies. J Immunol Res. 2019 Apr 14;2019:1–24.

71. Pai M, Denkinger CM, Kik SV, Rangaka MX, Zwerling A, Oxlade O, et al. Gamma Interferon Release Assays for Detection of Mycobacterium tuberculosis Infection. Clin Microbiol Rev. 2014 Jan 1;27(1):3–20.

72. Lu LL, Smith MT, Yu KKQ, Luedemann C, Suscovich TJ, Grace PS, et al. IFN-γ-independent immune markers of Mycobacterium tuberculosis exposure. Nat Med. 2019 Jun;25(6):977–87.

73. Chegou NN, Essone PN, Loxton AG, Stanley K, Black GF, van der Spuy GD, et al. Potential of Host Markers Produced by Infection Phase-Dependent Antigen-Stimulated Cells for the Diagnosis of Tuberculosis in a Highly Endemic Area. PLoS One. 2012 Jun 5;7(6).

74. Chegou NN, Sutherland JS, Malherbe S, Crampin AC, Corstjens PL, Geluk A, et al. Diagnostic performance of a seven-marker serum protein biosignature for the diagnosis of active TB disease in African primary healthcare clinic attendees with signs and symptoms suggestive of TB. Thorax. 2016 May 4;71:785–94.

75. Wang S, Li Y, Shen Y, Wu J, Gao Y, Zhang S, et al. Screening and identification of a six-cytokine biosignature for detecting TB infection and discriminating active from latent TB. J Transl Med. 2018 Jul 20;16.

76. Suliman S, Thompson EG., Sutherland J, Weiner J 3rd, Ota, MOC, Shankar S, et al. Four-Gene Pan-African Blood Signature Predicts Progression to Tuberculosis. Am J Respir Crit Care Med. 2018 May 1;197(9):1198–1208.

77. Zak DE, Penn-Nicholson A, Scriba TJ, Thompson E, Suliman S, Amon LM, et al. A prospective blood RNA signature for tuberculosis disease risk. Lancet. 2016 Jun 4;387(10035):2312–22.

78. Jacobs R, Tshehla E, Malherbe S, Kriel M, Loxton AG, Stanley K, et al. Host biomarkers detected in saliva show promise as markers for the diagnosis of pulmonary tuberculosis disease and monitoring of the response to tuberculosis treatment. Cytokine. 2016 May;81:50–6.

79. Day CL, Abrahams DA, Bunjun R, Stone L, Kock M de, Walzl G, et al. PD-1 Expression on Mycobacterium tuberculosis-Specific CD4 T Cells Is Associated With Bacterial Load in Human Tuberculosis. Front Immunol. 2018;9.

80. van Rensburg IC, Wagman C, Stanley K, Beltran C, Ronacher K, Walzl G, et al. Successful TB treatment induces B-cells expressing FASL and IL5RA mRNA. Oncotarget. 2016 Sep 22;8(2):2037–43.

81. Chegou NN, Black GF, Loxton AG, Stanley K, Essone PN, Klein MR, et al. Potential of novel Mycobacterium tuberculosis infection phase-dependent antigens in the diagnosis of TB disease in a high burden setting. BMC Infect Dis. 2012 Dec;12(1).

82. Kassa D, Ran L, Geberemeskel W, Tebeje M, Alemu A, Selase A, et al. Analysis of Immune Responses against a Wide Range of Mycobacterium tuberculosis Antigens in Patients with Active Pulmonary Tuberculosis. Clin Vaccine Immunol. 2012 Dec;19(12):1907–15.

83. Lindestam Arlehamn CS, Lewinsohn D, Sette A, Lewinsohn D. Antigens for CD4 and CD8 T Cells in Tuberculosis. Cold Spring Harb Perspect Med. 2014 Jul;4(7):a018465.

84. Ivanyi J, Ottenhoff THM. Significance of Antigen and Epitope Specificity in Tuberculosis. Front Immunol. 2014 Oct 23;5:524.

85. Wallis RS, Kim P, Cole S, Hanna D, Andrade BB, Maeurer M, et al. Tuberculosis biomarkers discovery: developments, needs, and challenges. Lancet Infect Dis. 2013 Apr 1;13(4):362–72.

86. Loxton AG, Black GF, Stanley K, Walzl G. Heparin-binding hemagglutinin induces IFN-γ(+) IL-2(+) IL-17(+) multifunctional CD4(+) T cells during latent but not active tuberculosis disease. Clin Vaccine Immunol. 2012 May;19(5):746–51.

87. Menozzi FD, Rouse JH, Alavi M, Laude-Sharp M, Muller J, Bischoff R, et al. Identification of a heparin-binding hemagglutinin present in mycobacteria. J Exp Med. 1996 Sep 1;184 (3):993–1001.

88. Raze D, Verwaerde C, Deloison G, Werkmeister E, Coupin B, Loyens M, et al. Heparin-Binding Hemagglutinin Adhesin (HBHA) Is Involved in Intracytosolic Lipid Inclusions Formation in Mycobacteria. Front Microbiol. 2018;9:2258.

89. Sritharan M. Iron Homeostasis in Mycobacterium tuberculosis: Mechanistic Insights into Siderophore-Mediated Iron Uptake. J Bacteriol. 2016 Aug 25;198 (18):2399–409.

90. Ratledge C. Iron, mycobacteria and tuberculosis. Tuberculosis. 2004 ;84:110–130.

91. Rodriguez GM, Voskuil MI, Gold B, Schoolnik GK, Smith I. ideR, an Essential Gene in Mycobacterium tuberculosis: Role of IdeR in Iron-Dependent Gene Expression, Iron Metabolism, and Oxidative Stress Response. Infect Immun. 2002 Jul;70(7):3371–81.

92. Kurthkoti K, Amin H, Marakalala MJ, Ghanny S, Subbian S, Sakatos A, et al. The Capacity of Mycobacterium tuberculosis To Survive Iron Starvation Might Enable It To Persist in Iron-Deprived Microenvironments of Human Granulomas. mBio. 2017 Aug 15;8(4).

93. Phelan JJ, Basdeo SA, Tazoll SC, McGivern S, Saborido JR, Keane J. Modulating Iron for Metabolic Support of TB Host Defense. Front Immunol. 2018 Oct 15;9:2296.

94. Kolloli A, Singh P, Rodriguez GM, Subbian S. Effect of Iron Supplementation on the Outcome of Non-Progressive Pulmonary Mycobacterium tuberculosis Infection. J Clin Med. 2019 Aug 2;8(8):1155.

95. Zondervan NA, van Dam JCJ., Schaap PJ, Martins dos Santos VAP, Suarez-Diez M. Regulation of Three Virulence Strategies of Mycobacterium tuberculosis: A Success Story. Int J Mol Sci. 2018 Jan 24;19(2):347.

96. Rodriguez GM. Control of iron metabolism in Mycobacterium tuberculosis. Trends Microbiol. 2006 Jul;14(7):320–7.

97. Pandey SD, Choudhury M, Yousuf S, Wheeler PR, Gordon SV, Ranjan A, et al. Iron-Regulated Protein HupB of Mycobacterium tuberculosis Positively Regulates

Siderophore Biosynthesis and Is Essential for Growth in Macrophages. J Bacteriol. 2014 May 15;196(10):1853–65.

98. De Voss JJ, Rutter K, Schroeder BG, Su H, Zhu Y, Barry CE. The Salicylate-Derived Mycobactin Siderophores of Mycobacterium Tuberculosis Are Essential for Growth in Macrophages. Proc Natl Acad Sci USA. 2000;97(3):1252–7.

99. Boelaert JR, Vandecasteele SJ, Appelberg R, Gordeuk VR. The Effect of the Host's Iron Status on Tuberculosis. J Infect Dis. 2007 Jun 15;195(12):1745–53.

100. Sritharan N, Choudhury M, Sivakolundu S, Chaurasia R, Chouhan N, Rao PP, et al. Highly immunoreactive antibodies against the rHup-F2 fragment (aa 63–161) of the iron-regulated HupB protein of Mycobacterium tuberculosis and its potential for the serodiagnosis of extrapulmonary and recurrent tuberculosis. Eur J Clin Microbiol Infect Dis. 2014;34(1):33–40.

101. Sivakolundu S, Mannela UD, Jain S, Srikantam A, Peri S, Pandeya SD, et al. Serum iron profile and ELISA-based detection of antibodies against the iron-regulated protein HupB of Mycobacterium tuberculosis in TB patients and household contacts in Hyderabad (Andhra Pradesh), India. Trans R Soc Trop Med Hyg. 2013 Jan;107(1):43-50.

102. Huet G, Daffé M, Saves I. Identification of the Mycobacterium tuberculosis SUF machinery as the exclusive mycobacterial system of [Fe-S] cluster assembly: evidence for its implication in the pathogen's survival. J Bacteriol. 2005 Sep;187(17):6137–46.

103. Griffin JE, Gawronski JD, Dejesus MA, Ioerger TR, Akerley BJ, Sassetti CM. High-resolution phenotypic profiling defines genes essential for mycobacterial growth and cholesterol catabolism. PLoS Pathog. 2011 Sep;7(9):e1002251.

104. Paritala H, Carroll KS. New targets and inhibitors of mycobacterial sulfur metabolism. Infect Disord Drug Targets. 2013 Apr;13(2):85–115.

105. Sassetti CM, Boyd DH, Rubin EJ. Genes required for mycobacterial growth defined by high density mutagenesis. Mol Microbiol. 2003 Apr;48(1):77–84.

106. Willemse D, Weber B, Masino L, Warren RM, Adinolfi S, Pastore A, et al. Rv1460, a SufR homologue, is a repressor of the suf operon in Mycobacterium tuberculosis. PLoS One. 2018 Jul 6;13(7).

107. Rohde KH, Veiga DFT, Caldwell S, Balázsi G, Russell DG. Linking the transcriptional profiles and the physiological states of Mycobacterium tuberculosis during an extended intracellular infection. PLoS Pathog. 2012;8(6):e1002769.

108. Rohde KH, Abramovitch RB, Russell DG. Mycobacterium tuberculosis invasion of macrophages: linking bacterial gene expression to environmental cues. Cell Host Microbe. 2007 Nov 15;2(5):352–64.

109. Kumar M, Khan FG, Sharma S, Kumar R, Faujdar J, Sharma R, et al. Identification of Mycobacterium tuberculosis genes preferentially expressed during human infection. Microb Pathog. 2011 Jan;50(1):31–8.

110. Grewal R, Swanepoel C, Snyders C, Isaacs S, Abayomi A. Biomarker discovery for diagnosis and treatment of tuberculosis: a role for biobanking? Journal of Biorepository Science for Applied Medicine. 2015;3(1):47-56.

111. Cadena AM, Flynn JL, Fortune SM. The Importance of First Impressions: Early Events in Mycobacterium tuberculosis Infection Influence Outcome. mBio. 2016 Apr 5;7(2):e00342-16.

112. Sanchez-Puelles JM, Ronda C, Garcia JL, Garcia P, Lopez R, Garcia E. Searching for autolysin functions. Eur J of Biochem. 1986;158(2):289–93.

113. Torrelles JB, Schlesinger LS. Integrating Lung Physiology, Immunology and Tuberculosis. Trends Microbiol. 2017 Aug;25(8):688–97.

114. Schluger NW, Rom WN. The Host Immune Response to Tuberculosis. Am J Respir Crit Care Med. 1998 Mar;157(3):679–91.

115. Warner DF, Mizrahi V. The survival kit of Mycobacterium tuberculosis. Nat Med. 2007 Mar;13(3):282–4.

116. Arranz-Trullén J, Lu L, Pulido D, Bhakta S, Boix E. Host Antimicrobial Peptides: The Promise of New Treatment Strategies against Tuberculosis. Front Immunol. 2017 Nov 7;8:1499

117. Triccas JA, Gicquel B. Life on the inside: Probing Mycobacterium tuberculosis gene expression during infection. Immunol and Cell Biol. 2000;78(4):311-7.

118. Fontecave M, Ollagnier-de-Choudens S. Iron-sulfur cluster biosynthesis in bacteria: Mechanisms of cluster assembly and transfer. Arch Biochem Biophys. 2008 Jun 15;474(2):226–37.

119. Saini V, Farhana A, Glasgow JN, Steyn AJC. Iron sulfur cluster proteins and microbial regulation: implications for understanding tuberculosis. Curr Opin Chem Biol. 2012 Apr;16(1–2):45–53.

120. Abramovitch RB. Mycobacterium tuberculosis Reporter Strains as Tools for Drug Discovery and Development. IUBMB Life. 2018;70(9):818–25.

121. Carroll P, Schreuder LJ, Muwanguzi-Karugaba J, Wiles S, Robertson BD, Ripoll J, et al. Sensitive Detection of Gene Expression in Mycobacteria under Replicating and Non-Replicating Conditions Using Optimized Far-Red Reporters. PLoS One. 2010 Mar 23;5(3):e9823.

122. Galbusera L, Bellement-Theroue G, Urchueguia A, Julou T, Nimwegen E van. Using fluorescence flow cytometry data for single-cell gene expression analysis in bacteria. 2020; PLoS ONE 15(10):e0240233.

123. Lichten CA, White R, Clark IB, Swain PS. Unmixing of fluorescence spectra to resolve quantitative time-series measurements of gene expression in plate readers. BMC Biotechnol. 2014;14(1):11.

124. Bugalhão JMN. Mycobacterium tuberculosis subversion of host vesicular traffic pathways. 2013;54.

125. Billinton N, Knight AW. Seeing the Wood through the Trees: A Review of Techniques for Distinguishing Green Fluorescent Protein from Endogenous Autofluorescence. Anal Biochem. 2001 Apr;291(2):175–97.

126. Surre J, Saint-Ruf C, Collin V, Orenga S, Ramjeet M, Matic I. Strong increase in the autofuorescence of cells signals struggle for survival. Sci Rep. 2018;8(12088).

127. Pinilla-Redondo R, Riber L, Sørensen SJ. Fluorescence Recovery Allows the Implementation of a Fluorescence Reporter Gene Platform Applicable for the Detection and Quantification of Horizontal Gene Transfer in Anoxic Environments. Kivisaar M, editor. Appl Environ Microbiol. 2018 Jan 12;84(6).

128. Shaner NC, Campbell RE, Steinbach PA, Giepmans BNG, Palmer AE, Tsien RY. Improved monomeric red, orange and yellow fluorescent proteins derived from Discosoma sp. red fluorescent protein. Nat Biotechnol. 2004 Dec;22(12).

129. Bustin SA, Nolan T. Pitfalls of Quantitative Real-Time Reverse-Transcription Polymerase Chain Reaction. J Biomol Tech. 2004 Sep;15(3):155–66.

130. Rustad TR, Minch KJ, Brabant W, Winkler JK, Reiss DJ, Baliga NS, et al. Global analysis of mRNA stability in Mycobacterium tuberculosis. Nucleic Acids Res. 2013 Jan;41(1):509–17.

131. Ragno S, Romano M, Howell S, Pappin DJC, Jenner PJ, Colston MJ. Changes in gene expression in macrophages infected with Mycobacterium tuberculosis: a combined transcriptomic and proteomic approach. Immunology. 2001 Sep;104(1):99–108.

132. Raffetseder J, Pienaar E, Blomgran R, Eklund D, Brodin VP, Andersson H, et al. Replication Rates of Mycobacterium tuberculosis in Human Macrophages Do Not Correlate with Mycobacterial Antibiotic Susceptibility. PLoS ONE. 2014;9(11).

133. Mouton JM, Helaine S, Holden DW, Sampson SL. Elucidating population-wide mycobacterial replication dynamics at the single-cell level. Microbiology (Reading). 2016 Jun;162(6):966–78.

134. Kunnath-Velayudhan S, Gennaro ML. Immunodiagnosis of Tuberculosis: a Dynamic View of Biomarker Discovery. Clin Microbiol Rev. 2011 Oct;24(4):792–805.

135. Sutherland JS, Lalor MK, Black GF, Ambrose LR, Loxton AG, Chegou NN, et al. Analysis of Host Responses to Mycobacterium tuberculosis Antigens in a Multi-Site Study of Subjects with Different TB and HIV Infection States in Sub-Saharan Africa. PLoS One. 2013 Sep 10 ;8(9).

136. Krupa A, Fol M, Dziadek BR, Kepka E, Wojciechowska D, Brzostek A, et al. Binding of CXCL8/IL-8 to *Mycobacterium tuberculosis* Modulates the Innate Immune Response. Mediators of Inflamm. 2015; 2015:1–11.

137. Romero-Adrian T, Leal-Montiel J, Fernández G, Valecillo A. Role of cytokines and other factors involved in the Mycobacterium tuberculosis infection. World J Immunol. 2015 Mar 27;5(1):16–50.

138. Lavrova AI, Esmedljaeva DS, Belik V, Postnikov EB. Matrix Metalloproteinases as Markers of Acute Inflammation Process in the Pulmonary Tuberculosis. Data. 2019 Oct;4(137).

139. Araujo Z, Palacios A, Enciso-Moreno L, Lopez-Ramos JE, Wide A, Waard JH de, et al. Evaluation of the transcriptional immune biomarkers in peripheral blood from Warao indigenous associate with the infection by Mycobacterium tuberculosis. Rev Soc Med Trop. 2019;52:e20180516

140. Van den Steen PE, Proost P, Wuyts A, Van Damme J, Opdenakker G. Neutrophil gelatinase B potentiates interleukin-8 tenfold by aminoterminal processing, whereas it degrades CTAP-III, PF-4, and GRO-α and leaves RANTES and MCP-2 intact. Blood. 2000 Oct 15;96(8):2673–81.

141. Teklu T, Kwon K, Wondale B, HaileMariam M, Zewude A, Medhin G, et al. Potential Immunological Biomarkers for Detection of Mycobacterium tuberculosis Infection in a Setting Where M. tuberculosis Is Endemic, Ethiopia. Infect Immun. 2018 Mar 22;86(4):e00759-17.

142. Lee, Ji-Sook, Kim, Ki, Lee, Da-Youn, Choi, Hong-Hee, Lee, Hye-Mi, Son, Ji, et al. Depressed CCL5 Expression in Human Pulmonary Tuberculosis. J Bacteriol Virol. 2008;38(3):97–107.

143. Lin PL, Flynn JL. CD8 T cells and Mycobacterium tuberculosis infection. Semin Immunopathol. 2015 May;37(3):239–49.

144. Arroyo L, Rojas M, Franken KLMC, Ottenhoff THM, Barrera LF. Multifunctional T Cell Response to DosR and Rpf Antigens Is Associated with Protection in Long-Term Mycobacterium tuberculosis-Infected Individuals in Colombia. Rosenberg HF, editor. Clin Vaccine Immunol. 2016 Oct;23(10):813–24.

145. Prezzemolo T, Guggino G, Manna MPL, Liberto DD, Dieli F, Caccamo N. Functional Signatures of Human CD4 and CD8 T Cell Responses to Mycobacterium tuberculosis. Front Immunol. 2014;5:80

146. Lichtner M, Mascia C, Sauzullo I, Mengoni F, Vita S, Marocco R, et al. Multifunctional Analysis of CD4 $^{+}$ T-Cell Response as Immune-Based Model for Tuberculosis Detection. J Immunol Res. 2015;2015:1–10.

147. Caccamo N, Guggino G, Joosten SA, Gelsomino G, Carlo PD, Titone L, et al. Multifunctional CD4+ T cells correlate with active Mycobacterium tuberculosis infection. Eur J Immunol. 2010;40(8):2211–20.

148. Loxton AG. Bcells and their regulatory functions during Tuberculosis: Latency and active disease. Mol Immunol. 2019 Jul;111:145–51.

Appendix 1:

Buffer composition

PBS: 80g NaCl, 2g KCl, 14.4g $Na_2HPO_4 \cdot 2H_2O$, 2.4g KH_2PO_4 in 1000 mL dH_2O, pH 7.4

TAE: 4.84 g Tris, 1,142 mL Acetic acid, 2 ml 0.5 M EDTA (pH8) in 1000 mL dH_2O

TBS-T: 20 mM Tris pH 7.6, 137 g Sodium chloride (NaCl) and 0.1% Tween 80

Blocking buffer: 10% fat free milk powder in TBS-T buffer

Transfer buffer: 25 mM Tris base, 192 mM Glycine and 20% Methanol

Tris: 20mM Tris, 500mM NaCl, pH8

12% stacking gel: Acrylamide, 1.5 mM Tris-HCl pH 8.8, 10% SDS, H_2O, TEMED and 10% ammonium persulphate

3% resolving gel: Acrylamide, 1mM Tris-HCl pH 6.8, 10% SDS, H_2O, TEMED and 10% ammonium persulphate